

秋田県立大学大学院博士学位論文

**Development of Tough Epoxidized Soybean Oil/Poly(lactic  
acid) Blends and Their Composites**

(強靱なエポキシ化大豆油/ポリ乳酸ブレンドおよびその  
複合材料の創製)

劉 文地

2019年3月



## Abstract

As a biobased and biodegradable polyester, poly(lactic acid) (PLA) has been extensively utilized in many areas including packaging materials. The brittle nature of PLA is the key barrier for its broader application. Efforts on using epoxidized soybean oil (ESO) to enhance the ductility of PLA have been done; however, ESO is immiscible with PLA and would leach or migrate to the surface of PLA products when in use; thus, sufficient toughening efficiency is not achievable for the products.

The present study aims at developing fully biobased, thermally remoldable, and highly tough ESO/PLA blends in a large-scale production via dynamic vulcanization technique. During the melt-compounding of ESO with PLA, two strategies were proposed to induce the crosslinking of ESO to simultaneously facilitate the formation of a stable crosslinked-ESO rubbery phase within PLA matrix and improve the interfacial compatibility between ESO and PLA. One is the self-polymerization of ESO initiated by cationic catalyst to activate the dynamic vulcanization of PLA with ESO. For another, a biobased monomer, i.e., tannic acid (TA), was used as a green crosslinking agent for ESO since the abundant phenolic hydroxyl groups of TA are reactive towards the epoxy groups of ESO. It was found that both methods significantly increased the toughening efficiency of ESO on PLA and hence the toughness of the obtained ESO/PLA blends, while the mechanical strength and modulus of the blends were dramatically decreased after the incorporation of ESO phase. The TA-crosslinked ESO (TA-ESO) phase exhibited a higher toughening efficiency on PLA than the cationically polymerized ESO (PESO) phase. A matrix plastic deformation mechanism was proposed for explaining the high toughness of the blends.

To broaden the application fields of PLA products, the completely biobased and highly tough TA-ESO/PLA blends were further utilized for the manufacture of conductive nanocomposites and fiber-reinforced biocomposites. For repairing the sacrificial strength of the TA-ESO/PLA blends and imparting the composites with electrical conductivity, different concentrations of carbon nanotubes (CNTs) were

incorporated into the blends to prepare CNT/TA-ESO/PLA nanocomposites. The added CNTs selectively localized within PLA matrix, leading to a reduced size of TA-ESO phase. The introduction of CNTs contributed to increased tensile strength and modulus, storage modulus, thermal stability, crystallinity, and reduced elongation at break and toughness for the nanocomposites while endowing the nanocomposites with favorable electrical conductivity. On the other hand, bamboo fibers (BFs) were selected as reinforcing fibers for the TA-ESO/PLA blends to produce BF-reinforced TA-ESO/PLA (BF/TA-ESO/PLA) biocomposites. When the surfaces of BFs were coated with a low content of TA-ESO (0.5 wt%), the TA-ESO could form strong interactions with BFs via natural polyphenol-inspired chemistry, hence generating a flexible interfacial layer at the interface between BFs and PLA matrix. This resulted in improved fiber-matrix interfacial adhesion and hence mechanical properties of the biocomposites. With the further increase of TA-ESO concentrations, the TA-ESO would diffuse into PLA matrix and thereby give a toughening effect on PLA matrix via forming a stable rubbery phase, which greatly increased the toughness of the biocomposites. The two effects can be regulated through adjusting the concentration of TA-ESO, which further tailors the performance of the BF/TA-ESO/PLA biocomposites.

# Contents

<b>Abstract.....</b>	<b>i</b>
<b>Chapter 1 Introduction.....</b>	<b>1</b>
1.1 Background.....	1
1.2 Reactive compatibilization strategies of PLA-based blends and composites..	4
1.2.1 Incorporation of reactive polymers.....	4
1.2.2 Incorporation of monomers.....	11
1.2.3 Dynamic vulcanization.....	19
1.2.4 Interchange reactions.....	26
1.3 Current issues and future trend.....	28
1.4 Contribution from this dissertation.....	29
Abbreviations.....	31
References.....	32
<b>Chapter 2 Materials, Experiment and Characterization.....</b>	<b>44</b>
2.1 Materials.....	44
2.2 Preparation of PLA-based blends and composites.....	44
2.3 Characterization.....	45
2.3.1 Measurement of gel fraction.....	45
2.3.2 Fourier transform infrared spectroscopy (FTIR).....	45
2.3.3 X-ray photoelectron spectroscopy (XPS).....	45
2.3.4 Nuclear magnetic resonance (NMR).....	45
2.3.5 Gel permeation chromatography (GPC).....	46
2.3.6 Differential scanning calorimetry (DSC).....	46
2.3.7 Dynamic mechanical analysis (DMA).....	46
2.3.8 Thermogravimetric (TG) analysis.....	47
2.3.9 Tensile testing.....	47
2.3.10 Impact testing.....	47
2.3.11 Electrical properties.....	47
2.3.12 Scanning electron microscope (SEM).....	47
2.3.13 Transmission electron microscopy (TEM).....	48
<b>Chapter 3 Cationic Polymerization of Epoxidized Soybean Oil for Toughening PLA via Dynamic Vulcanization.....</b>	<b>49</b>

3.1 Introduction.....	49
3.2 Experimental section.....	51
3.2.1 Materials.....	51
3.2.2 Preparation of PESO/PLA blends.....	51
3.2.3 Characterization.....	51
3.3 Results and discussion.....	53
3.3.1 Dynamic crosslinking of ESO in PLA matrix.....	53
3.3.2 Crystallization behavior of PESO/PLA blends.....	54
3.3.3 Rheological behavior of PESO/PLA blends.....	56
3.3.4 Dynamic mechanical properties of PESO/PLA blends.....	57
3.3.5 Thermal stability of PESO/PLA blends.....	59
3.3.6 Tensile properties of PESO/PLA blends.....	60
3.3.7 Toughening mechanism.....	62
3.4 Conclusion.....	64
References.....	65
<b>Chapter 4 Tannic Acid-Induced Crosslinking of Epoxidized Soybean Oil for Toughening PLA via Dynamic Vulcanization.....</b>	<b>69</b>
4.1 Introduction.....	69
4.2 Experimental section.....	72
4.2.1 Materials.....	72
4.2.2 Preparation of TA-ESO/PLA blends.....	72
4.2.3. Characterization.....	73
4.3 Results and discussion.....	75
4.3.1 Dynamic vulcanization mechanism of PLA with ESO and TA.....	75
4.3.2 Crystallization behavior of TA-ESO/PLA blends.....	78
4.3.3 Dynamic mechanical properties of TA-ESO/PLA blends.....	80
4.3.4 Thermal stability of TA-ESO/PLA blends.....	82
4.3.5 Tensile properties of TA-ESO/PLA blends.....	84
4.3.6 Toughening mechanism.....	87
4.4 Conclusion.....	88
References.....	89
<b>Chapter 5 Investigation on Carbon Nanotubes-Reinforced Epoxidized Soybean Oil /PLA Nanocomposites.....</b>	<b>93</b>

5.1 Introduction.....	93
5.2 Experimental section.....	96
5.2.1 Materials.....	96
5.2.2 Preparation of CNT/TA-ESO/PLA nanocomposites.....	97
5.2.3 Characterization.....	97
5.3 Results and discussion.....	99
5.3.1 Morphological analysis.....	99
5.3.2 Crystallization behavior of CNT/TA-ESO/PLA nanocomposites....	101
5.3.3 Dynamic mechanical properties of CNT/TA-ESO/PLA nanocomposites.....	103
5.3.4 Thermal stability of CNT/TA-ESO/PLA nanocomposites.....	105
5.3.5 Tensile properties of CNT/TA-ESO/PLA nanocomposites.....	106
5.3.6 Reinforcing and toughening mechanism.....	108
5.3.7 Electrical properties of CNT/TA-ESO/PLA nanocomposites.....	109
5.4 Conclusion.....	110
References.....	111
<b>Chapter 6 Modification of Bamboo Fibers-Reinforced PLA Biocomposites with Tannic Acid-Crosslinked Epoxidized Soybean Oil.....</b>	<b>115</b>
6.1 Introduction.....	115
6.2 Experimental section.....	118
6.2.1 Materials.....	118
6.2.2 Preparation of BF/TA-ESO/PLA biocomposites.....	118
6.2.3 Characterization.....	120
6.3 Results and discussion.....	121
6.3.1 Reaction mechanism of TA-ESO in BF/PLA biocomposites.....	121
6.3.2 Morphological analysis of BF/TA-ESO/PLA biocomposites.....	124
6.3.3 Crystallization behavior of BF/TA-ESO/PLA biocomposites.....	126
6.3.4 Dynamic mechanical properties of BF/TA-ESO/PLA biocomposites .....	128
6.3.5 Mechanical properties of BF/TA-ESO/PLA biocomposites.....	129
6.3.6 Reinforcing and toughening mechanism.....	132
6.4 Conclusion.....	135
References.....	135

<b>Chapter 7 Summary.....</b>	<b>139</b>
<b>Publications.....</b>	<b>142</b>
<b>Acknowledgements.....</b>	<b>145</b>

# Chapter 1 Introduction

## 1.1 Background

Poly(lactic acid) (PLA) is a biobased and biodegradable polyester that is derived from renewable feedstocks via fermentation of starch-rich materials such as corn and wheat. PLA has been widely utilized to replace petroleum-based and non-degradable counterparts in some cases because of its merits including renewability, biodegradability, good processability, and high strength [1]. Unfortunately, there are a few drawbacks of PLA that inhibit its practical application. High brittleness, i.e., low elongation at break and impact strength, is the biggest challenge for PLA, especially when being used as structural materials. Another disadvantage of PLA is the relatively slow crystallization rate, which is associated with its low degree of crystallinity and heat deflection temperature (HDT). To deal with these issues, development of PLA-based blends and composites has been commonly conducted to broaden the application areas of PLA products.

As for the toughening of PLA, many strategies including copolymerization, plasticization, and polymer blending have been widely used [2,3]. Chemical copolymerization is a feasible method to modify and toughen PLA via introducing comonomers during the preparation of PLA, while it usually sacrifices some advantages of PLA such as high strength. Addition of plasticizers is capable of significantly increasing the toughness of PLA; however, the added plasticizers with small molecular weight are immiscible with PLA and is easy to leach or migrate to the surface of PLA products. Polymer blending is an efficient and convenient way to toughen PLA through introducing flexible polymers into PLA system; however, sufficient toughening efficiency is not accessible for the PLA-based blends due to the incompatibility between PLA and the incorporated polymers. Therefore, development of compatibilization strategies is highly desired for the PLA-based blends with improved properties. Copolymers that have one constituent block miscible with PLA and a second block miscible with the introduced polymers can be designed and

incorporated into the PLA-based blends [4]. The regulation of the copolymers localized at the interface of the immiscible blends could effectively reduce the interfacial tension between the blended components and hence increase the toughening efficiency of the introduced polymers on PLA. For instance, Ding et al. [5,6] recently synthesized two tri-block copolymers, i.e., PLA-poly(butylene adipate-co-terephthalate)-PLA (PLA-PBAT-PLA) and PLA-polyethylene glycol-PLA (PLA-PEG-PLA). These copolymers were then used for PLA/PBAT blends to emulsify their interfacial layer and thus reduce the particle size of the dispersed PBAT phase. On the other hand, the formation of chemical bonding between components is very effective in reducing the interfacial tension of PLA-based blends, which refers to the addition of reactive compatibilizers or grafting of functional groups onto the blended polymers. The reaction between the blended polymers with compatibilizers or functionalized polymers normally occurs during the processing of the blends; hence, the process is usually defined as a reactive or in-situ compatibilization process. For the blends compatibilized by a reactive compatibilization process, the copolymer is automatically generated at the interface between two immiscible components, which could avoid the formation of micelles as a separated phase of the added copolymer [7]. Therefore, the reactive compatibilization strategies are extensively developed and applied in PLA-based blends, which will be the focus of this chapter.

The incorporation of reinforcing fibers, micro- and/or nanofillers into PLA matrix to manufacture PLA-based composites is a powerful method to endow PLA products with specific use characteristics and improved properties. Reinforcing fibers such as glass, carbon, and natural fibers have been incorporated into PLA to develop engineering materials [8]. Natural fibers (NFs) are particularly attractive for their utilization in the production of NF-reinforced PLA biocomposites due to the benefits of NFs such as low-cost, renewability, and high specific strength and stiffness [9]. However, the most intractable issue for the NF-reinforced PLA biocomposites is the weak interfacial adhesion resulted from the highly hydrophilic NFs in contrast to the hydrophobic PLA matrix. Moreover, various microfillers such as talc, hydroxyapatite and inorganic carbonates, and nanofillers including cellulose nanocrystals (CNCs),

carbon nanotubes (CNTs) and graphite derivatives have been utilized in the fabrication of PLA-based composites with the purposes of increasing crystallinity degree, reducing costs, and improving mechanical properties of PLA products [8,10]. The main challenges for the particle-filled PLA composites are the poor dispersion of the fillers inside PLA matrix and the formed weak interfacial adhesion between filler and matrix. Therefore, interfacial compatibility is the key bottleneck for the development of PLA-based composites with high performance, whether the composites is prepared from reinforcing fibers or fillers. Surface chemical modification is a commonly used route for altering the surface characteristics of fibers/fillers into more intimate with PLA matrix, and hence improving the interfacial bonding of composites [11]. However, the modification for fibers/fillers is usually a rigorous reaction process that requires organic solvents, evaluated temperature, and/or organometal catalysts, which would dramatically increase the production cost of PLA-based composites. Similar to PLA-based blends, reactive compatibilization is an easy and low-cost method to compatibilize PLA-based composites by addition of compatibilizers. But this method for PLA-based composites seems to be not as effective as that for PLA-based blends. The reason might be that the reaction between solid fibers/fillers and compatibilizers is a heterogeneous reaction and thus is not easy to occur even at high temperature. Nevertheless, there still are some literatures related to reactive compatibilization for PLA-based composites, which will be also outlined in this chapter.

Recent advances in PLA-based blends and composites have previously been reviewed. Current developments in the preparation, compatibilization strategies, and characterization of PLA-based polymer blends were comprehensively reviewed by Hamad et al [12]. Murariu and Dubois [8] reported the main developments of PLA-based composites using traditional reinforcements, micro- and/or nanofillers, and specific additives. The relationship among composition, preparation, and properties of the composites was discussed. Research trends in NF-reinforced PLA composites have also been outlined by Siakeng et al [9]. Regarding the toughening of PLA, many authors have reviewed the toughening strategies and mechanism along

with their effects on properties of the toughened PLA products [13-15]. However, less interest has been focused on reviewing the reactive compatibilization of PLA-based blends and composites. As the development in this area moves very quickly and a great number of achievements have been obtained recently, it is necessary to review this topic in time and give a future recommendation. Accordingly, the present chapter will describe the principle and methods of reactive compatibilization for PLA-based blends and composites in relation to their morphologies, mechanical properties, crystallization behavior, and thermal properties.

## 1.2 Reactive compatibilization strategies of PLA-based blends and composites

### 1.2.1 Incorporation of reactive polymers

Concerning PLA-based blends, a reactive polymer is usually miscible with one polymer, i.e., PLA or the incorporated component, and reactive towards the functional groups of the other polymer. PLA is an aliphatic polyester that contains terminal  $-COOH$  and  $-OH$  groups, which provides the reactive sites for the introduced reactive polymers, i.e., compatibilizers, such as anhydride- or epoxy-grafted polymers.

#### 1.2.1.1 Anhydride-grafted polymers

Maleic anhydride (MA)-grafted polymer is one of the commonly used compatibilizers for PLA-based blends because the reaction between the anhydride groups of compatibilizers and the terminal  $-OH$  groups of PLA could occur during the melting processing of the blends (Figure 1-1). The grafting of MA onto polymers usually refers to a free-radical polymerization of the  $C=C$  bonds from MA and polymers, hence retaining the anhydride functionality on the MA-grafted polymers for

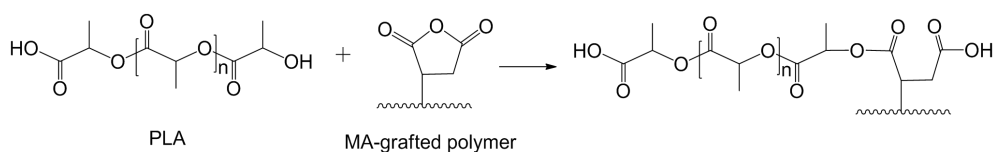


**Figure 1-1** Proposed reaction between PLA and MA-grafted polymer

further reaction. The selection of the grafted components depends on the characteristic of the incorporated polymer or reinforcing agents in the PLA-based products. Two MA-functionalized terpolymers, i.e., ethylene methyle acrylate (EMA)-MA and ethylene butyl acrylate (EBA)-MA, were synthesized for compatibilizing the blends of PLA with thermoplastic copolyester elastomer, which resulted in significantly increased impact strength of the blends [16]. Carrasco et al. [17] studied the blends of a multifunctional epoxide-type oligomer-extended PLA and acrylonitrile-butadiene-styrene (ABS) by using MA-grafted ABS as a compatibilizer. Ghozali et al. [18] synthesized a MA-grafted linear low density polyethylene (LLDPE) polymer using benzoyl peroxide as an initiator for use in LLDPE/PLA blends; however, the effect of the compatibilizer on the properties of the blends was not reported. To alleviate the interphase immiscibility of PLA and polypropylene (PP), MA-grafted PP was added into PP/PLA blends, which demonstrated that the addition of MA-grated PP increased the miscibility and hence tensile and impact toughness of the blends [19,20]. Rajan et al. [21] reported that 3 wt% MA-grafted PP was the optimum concentration for PP/PLA blend in terms of the rheological behavior and mechanical properties of the blends. The homogeneity of ternary blends from Nylon 6, PP and PLA were also improved by adding MA-grafted PP as a compatibilizing agent [22,23]. The radiation grafting of MA onto natural rubber (NR) in latex state was successfully performed to synthesize MA-grafted NR for improving the interfacial compatibility and increasing impact strength of NR/PLA blends [24]. In another work by Mohammad et al. [25], MA-grafted PLA and MA-grafted NR were respectively used as compatibilizers for NR/PLA blends, and results indicated that both compatibilizers are effective in increasing the interfacial compatibility of the blends. The MA-grafted polymers mentioned above were designed to react with the –OH groups of PLA and the grafted polymers are usually the blended components of PLA or are miscible with the components. For some of the blended components with functional groups, MA-grafted PLA was also used as a compatibilizer for the resulting blends. MA-grafted PLA could be synthesized from PLA and MA with the presence of free-radical initiator via a reactive melt-grafting process; the reaction

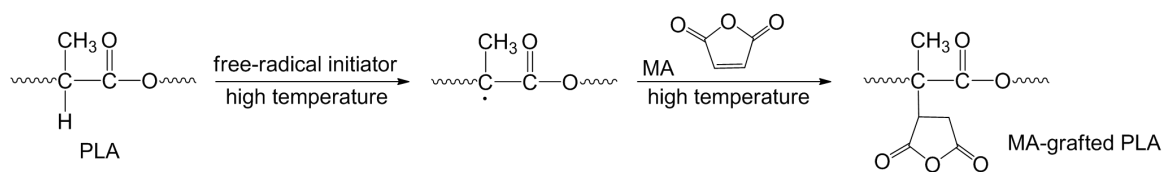


**Figure 1-2** Reaction mechanism on the grafting of PLA with MA

route was schemed in [Figure 1-2](#) [26-28]. Similar to PLA, both PBS and PBAT are fully biodegradable polyester that contains terminal  $-\text{COOH}$  and  $-\text{OH}$  groups. Therefore, MA-grafted PLA was introduced into PBS/PLA blends to increase their interfacial compatibility and hence tensile-impact toughness [29]. Teamsinsungvon et al. [26] reported that the incorporation of 2 wt% MA-grafted PLA into PBAT/PLA blends led to improved interfacial adhesion and hence increased tensile properties and thermal stability of the blends. In another work by Phetwarotai et al. [30], MA-grafted PLA was incorporated into PBAT/PLA blends with the presence of  $\text{TiO}_2$  as a nucleating agent; the synergistic effects of the  $\text{TiO}_2$  and MA-grafted PLA contributed to improved interfacial bonding and crystallinity degree of the composites. For thermoplastic starch (TPS)/PLA blends, MA-grafted PLA was employed as a compatibilizer due to the possible reaction between the  $-\text{OH}$  groups from TPS and the anhydride groups from MA; the addition of 4 wt% MA-grafted PLA into the blends achieved better morphological and rheological performance with improved tensile strength and elongation at break [31].

MA-grated PLA polymer is more suitable for PLA-based composites because most of incorporated fibers has reactive groups towards the anhydride groups of MA. For instance, NFs mainly consist of cellulose that has a large number of  $-\text{OH}$  groups for the reaction with MA. Accordingly, wood fibers (WFs)-reinforced PLA biocomposites were incorporated with MA-grafted PLA to improve their interfacial compatibility; the highest tensile and flexural strength of the composites were achieved when 30 wt% PLA was replaced with MA-grafted PLA [27]. The WFs/PLA biocomposites were also effectively compatibilized by a styrene-assisted MA-grafted PLA [32]. In the work of Dogu and Kaynak [33], microcrystalline cellulose (MCC) was used as reinforcing agent for PLA, and the obtained MCC/PLA composites with

3 wt% MA-grafted PLA exhibited a very uniform distribution of MCC within PLA matrix as well as improved ductility and toughness. More uniform dispersion of cellulose nanofibers (CNFs) within PLA matrix was also observed after the addition of MA-grafted PLA into CNFs/PLA nanocomposites, resulting in the composites with improved mechanical properties [34,35]. Significant enhancements of thermal stability, tensile strength and elongation at break were observed for the CNCs/poly(ethylene oxide)/PLA composites compatibilized with MA-grafted PLA; this was likely due to the improved dispersion of CNCs and interfacial adhesion between CNCs and matrix [36]. The synergetic effects of MA-grafted PLA and epoxy-functionalized graphene (EFG) on the properties of the obtained nanocomposites were studied by Issaadi et al. [37]; it was found that 5 wt% MA-grafted PLA was sufficient to increase the thermal, rheological, mechanical and barrier properties of the nanocomposite containing 7 wt% EFG. The graphite nanoplatelets (GNPs)/PLA composites with MA-grafted PLA as a compatibilizer showed much higher mechanical and thermomechanical properties compared to the composites without compatibilizer, although the MA-grafted PLA seems to have no covalent bonding with GNPs [38]. Similarly, the addition of MA-grafted PLA into carbon fibers (CFs)/PLA composites not only increased the tensile, flexural and impact strength of the composites, but also contributed to higher electrical conductivity and electromagnetic interference shielding effectiveness, which was probably because that the MA-grafted PLA might completely enwrap the CFs [28].

Itaconic anhydride (IA) is a biobased monomer that has a C=C bond and an anhydride functionality. Hence, IA can be used to graft PLA via free-radical polymerization to generate a IA-grafted PLA polymer. Based on the possible reaction between the anhydride groups of IA with protein, IA-grafted PLA was used to compatibilize thermoplastic protein/PLA blends during a reactive extrusion process, which caused the transformation of a sea-island structure of the blends to a cocontinuous morphology [39].

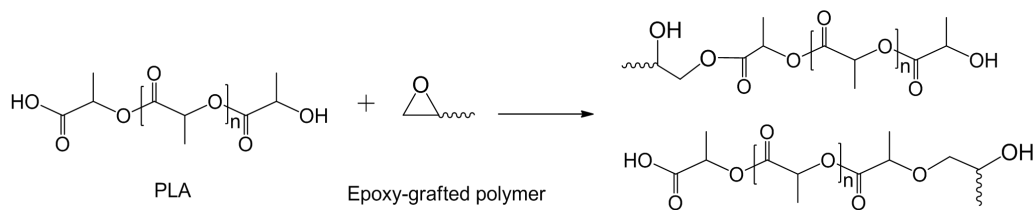


**Figure 1-3** Proposed reaction between PLA and epoxy-grafted polymer

### 1.2.1.2 Epoxy-grafted polymers

As schemed in [Figure 1-3](#), the epoxy functionality of the grafted polymer is able to react with the terminal  $-\text{COOH}$  and  $-\text{OH}$  groups of PLA. Glycidyl methacrylate (GMA) is a difunctional monomer with epoxy group and  $\text{C}=\text{C}$  bond. The  $\text{C}=\text{C}$  site of GMA gives the opportunity for polymerizing with other monomers to generate the polymers with epoxy functionality. GMA-grafted polymers thus could be used as compatibilizers for PLA-based blends and composites. Poly(butylene terephthalate) (PBT)/PLA blends were compatibilized with ethylene-GMA copolymer, and the reactive epoxy groups of the compatibilizer induced decrease in the interfacial tension of the blends and the particle size of PBT phase [40]. GMA-functionalized polyolefin elastomers were used as compatibilizers in poly(propylene carbonate) (PPC)/PLA and polyolefin elastomer/PLA blends, respectively; the results indicated that the introduction of the elastomers significantly increased the compatibility of the blends [41,42]. The toughness of LLDPE/PLA blends were greatly improved by adding GMA-grafted polyethylene as a compatibilizer, and the toughening efficiency of the compatibilizer was further improved by using cobalt octoate catalyst [43]. PBAT/PLA containing varying amounts of EMA-GMA copolymer were produced through reactive melt-blending to improve the toughness of the blends; the blends with 15 wt% EMA-GMA exhibited a greatly improved impact strength [44]. Two GMA-functionalized terpolymers, i.e., EMA-GMA and EBA-GMA, showed higher compatibilizing ability in thermoplastic copolyester elastomer/PLA blends than their corresponding MA-grafted polymers [16]. The interfacial adhesion of sisal fibers/PLA biocomposites was improved by using EMA-GMA as a coupling agent, where the epoxy groups of EMA-GMA were evidenced to react with the fibers by

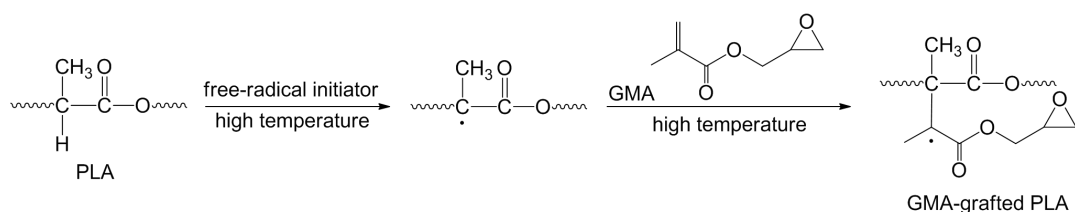


**Figure 1-4** Reaction mechanism on the grafting of PLA with GMA [52]

FTIR analysis [45]. Similarly, the incorporation of EBA-GMA into the composites from carboxylated carbon nanotubes (CNTs-COOH), PBAT and PLA considerably increased the interfacial interaction between the CNTs and PBAT/PLA matrix due to the formation of covalent linkages between epoxy and -COOH groups [46]. EMA-GMA and EBA-GMA were also employed as compatibilizers for poly(trimethylene terephthalate) (PTT)/PLA [47], biopolyethylene (bioPE)/PLA [48], bioPE/PLA/clay composites [49], and organoclay/PLA composites [50].

GMA-grafted PLA was synthesized by free radical copolymerization (Figure 1-4) and then used in silane treated banana fibers/PLA biocomposites to improve their compatibility as well as mechanical properties, water resistance, thermal properties and flame resistance [51,52]. Hemp hurd/PLA biocomposites were incorporated with GMA-grafted PLA to increase the interfacial bonding of the biocomposites [53]. The grafting of GMA onto PLA was conducted in an internal mixer and the generated GMA-grafted PLA was used to improve the dispersion and compatibility of CNFs with PLA matrix [54]. Poly(L-lactic acid) (PLLA)/PBS blends were prepared by melt blending with PLLA-based compatibilizer (PBS-PLLA) and a tri-arm block copolymer (PLLA-block-poly(GMA))<sub>3</sub> as a chain extender, showing significant improvements in mechanical properties [55].

The direct incorporation of PLA with GMA-functionalized polymers as toughening agents achieved a great toughening effect since the incorporated phase could form covalent bonding with PLA, leading to a superior interfacial adhesion between the polymers and PLA. A supertough flame-retardant PLA composite was prepared via reactive blending of PLA with ethylene-acrylic ester-GMA terpolymer with the presence of aluminum hypophosphite as a flame retardant [56]. Epoxidized

poly(styrene-*b*-butadiene-*b*-styrene) (ESBS) with different epoxidation degree was formulated by an in-situ peroxy-formic acid method; the melt blending of PLA with ESBS resulted in the formation of graft copolymer architecture at the interface, hence contributing to greatly improved impact strength of the blends [57].

Many works have been reported on other epoxy-functionalized polymers for compatibilizing the PLA-based products. Commercial grade multi-epoxy-functionalized oligomers (Joncryl ADR<sup>®</sup>-4368/4370s) have been widely used as compatibilizers for many PLA-based systems including PBT/PLA [58], PBAT/PLA [59], thermoplastic polyester elastomer/PLA [60], polycarbonate (PC)/PLA [61], polyamide 11/PLA [62], ABS/PLA [63], kraft pulps-talc/PLA hybrid composites [64], cotton/PLA [65] and sisal fibers/PLA biocomposites [66]. For example, it was revealed that the oligomer in sisal fibers/PLA biocomposites played a hinge-like role between the fibers and PLA matrix, resulting in simultaneously strengthening and toughening effects on the biocomposites [66]. Biodegradable PBAT/PLA blown films were produced using a epoxy-functionalized PLA as a modifier; the epoxy groups on the modifier would react with PBAT to form an in-situ copolymer at the interface of the blends, which resulted in improved melt strength and bubbled stability of the films [67]. In the work by Dong et al. [68], as shown in Figure 1-5, a reactive comb (RC) polymer consisting of one poly(methyl methacrylate) (PMMA) back, two PMMA side chains, and epoxy groups distributed on the backbone was developed to increase the compatibility of ABS/PLLA blends; the PMMA side of the compatibilizer was miscible with ABS, and the epoxy functionality could react with PLA, hence

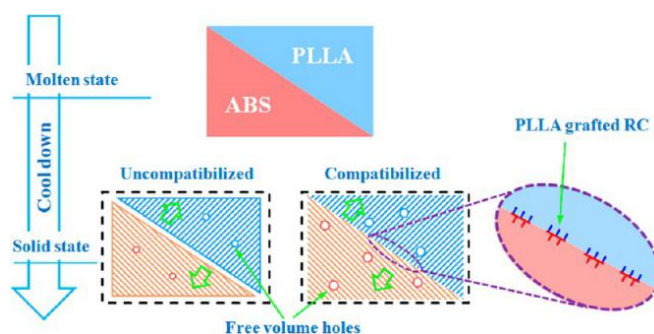


**Figure 1-5** Schematic mechanism of a reactive comb polymer in compatibilizing ABS/PLLA blends [68]

promoting the in-situ formation of PLLA-grafted RC polymers at the interface of the blends.

### *1.2.1.3 Other functionalized polymers*

Some works focused on the development of the polymers containing both anhydride and epoxy functionalities for PLA-based blends. A ethylene-MA-GMA terpolymer was used as a compatibilizer in PC/PLA blends together with talc as a nucleation agent; the synergistic effects of the compatibilizer and talc on the properties of the resulting composites were comprehensively discussed [69,70]. Weng et al. [71] studied the compatibilization of starch/PLA blends by the use of poly-1,4-butylene glycol adipate diol-based polyurethane prepolymer (PBAPU); the isocyanate ( $-NCO$ ) groups in the PBAPU would react with the  $-OH$  groups in starch, and the soft segments in the prepolymer was very compatible with PLA since both of them belong to aliphatic polyesters. Tetrasilanol phenyl polyhedral oligomeric silsesquioxane and glycidyl isooctyl-polyhedral oligomeric silsesquioxane were used as compatibilizers for PC/PLA blends, and their compatibilizing effects were compared to those of commercial epoxy- and MA-functionalized copolymers [61]. To overcome the inherent brittleness of PLA, a castor oil-based polyurethane prepolymer (COPUP) containing terminal  $-NCO$  groups was successfully synthesized and then mixed with PLA; the interfacial adhesion between the COPUP and PLA was strengthened by the reaction between the  $-NCO$  groups from the COPUP and the  $-OH$  groups from PLA [72,73]. Subsequently, the obtained COPUP/PLA blends were incorporated with reactive organoclay to improve the tensile strength and modulus of the resulting composites [74].

## **1.2.2 Incorporation of monomers**

The commonly used monomers as compatibilizers in PLA-based blends and composites normally contain reactive functional groups that can react with both PLA and the incorporated components. This is able to establish a chemical connection

between PLA and the incorporated components and form a transition layer at the interface through the generated copolymers.

#### *1.2.2.1 Anhydrides*

With respect to MA-grafted polymers, the direct incorporation of MA into the blends actually involves the combination of the grafting process of MA onto PLA and the reaction between the anhydride groups from MA and the –OH groups from the components in the course of melt-compounding; therefore, an initiator was meanwhile added to induce the free-radical polymerization of MA with PLA or other polymers. In the work of Lv et al. [75], WFs/PLA biocomposites were prepared by using MA as a modifier and dicumyl peroxide (DCP) as an initiator; the compatibilized biocomposites had much higher tensile and flexural strengths than the unmodified biocomposites. WFs/PLA biocomposites were compatibilized with MA and 2,5-bis(tert-butylperoxy)-2,5-dimethylhexane (Luperox 101, L101) as an initiator; the properties of the biocomposites were compared to those of the WFs biocomposites from other biodegradable biopolymers [76]. For PPC/PLLA blends, the anhydride groups of MA was expected to react with the –OH groups of PLLA, while the C=C bonds of MA performed a grafting process with PPC with the initiation of L101; hence, considerable improvement in the interfacial adhesion of the blends was achieved [77]. Two different mixing order of MA with TPS/PLA blends, i.e., mixing of MA with PLA first and then TPS, and mixing of MA with TPS/PLA blends, were conducted to investigate the compatibilizing effects of MA on the blends; it was found that the pre-mixing of MA resulted in greatly higher interfacial adhesion of the blends in terms of mechanical and thermo-mechanical properties [78]. TPS/PLA blends were compatibilized with MA by using L101 and DCP as initiators, respectively; the DCP showed higher efficiency on reducing TPS domains and improving the interfacial adhesion of the blends than L101 [79]. However, based on the literature, there were few works on the direct use of MA in PLA-based products, which is probably because the reaction among MA, PLA and the incorporated components was too complicated and not easy to completely finish as expected.

Some multi-functional anhydrides such as maleinized linseed oil (MLO) were used to compatibilize TPS/PLA blends because the anhydride groups of MLA could react with the terminal –OH groups of both TPS and PLA; the simultaneous addition of MLO and TPS generated a good combined plasticizing-compatibilizing effect for the PLA-based blends [80]. Similar work was reported by Quiles-Carrillo et al. [81] for the compatibilization of almond shell flour (ASF)/PLA biocomposites with MLO because the multiple MA functionalities in MLO would react with the –OH groups of both ASF and PLA as evidenced by the new generated carboxylic ester bonds. In the work of Carbonell-Verdu et al. [82], maleinized and epoxidized cottonseed oils (MCO and ECO) were respectively incorporated into PBAT/PLA blends, and their toughening capacities on the blends were compared to that of a conventional styrene-acrylic oligomer; the optimum elongation at break was achieved for the blends with 7.5 wt% MCO.

#### 1.2.2.2 Epoxy monomers

Vegetable oils (VOs), consisting of triglycerides, are important biobased materials because of their advantages such as abundance and renewability [83]. Epoxidized VOs (EVOs) are derived from VOs through epoxidation of the unsaturated sites in the fatty acid chains [84]. Taking soybean oil for an example, the synthesis route of epoxidized soybean oil (ESO) was given in Figure 1-6 [85]. The epoxy value of EVOs is closely related to the unsaturated degree of VOs and the conversion rate of C=C bond to epoxy groups during epoxidation. As multi-functional

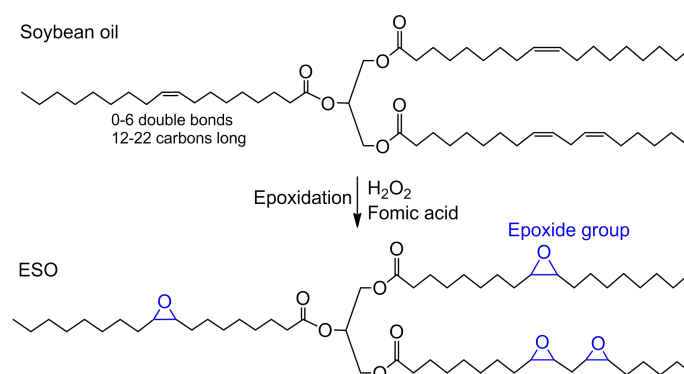


**Figure 1-6** Synthesis of ESO from soybean oil via a epoxidation route [85]

epoxides, EVOs have widely been used as biobased compatibilizers for PLA-based products because the epoxy groups of EVOs would react with terminal –COOH and –OH groups of PLA and other incorporated components. The commonly used EVOs include ESO [86-90], epoxidized linseed oil (ELO) [89,90], epoxidized palm oil [91], and ECO [82]. The TPS/PLA composites with 25 wt% TPS were produced by melt extrusion with ESO as a reactive modifier, and the addition of 0.5–2 wt% ESO significantly increased the impact strength, elongation at break and water resistance of the composites [86]. As reported by Xiong et al. [87], the starch granules were grafted with MA to improve its reactivity towards ESO, and the reactions among ESO, MA-grafted starch, and PLA generated a compatible ESO/starch/PLA ternary blends with greatly improved elongation at break. Meng et al. [88] prepared PLA ternary nanocomposites from CNFs and ESO, and found that ESO improved the ductility of the nanocomposites 5- to 10-fold with only slight reduce in strength and modulus when the nanocomposites containing 10 wt% CNFs. Garcia-Campo et al. [89] developed a series of fully biodegradable PLA-based formulations by blending PLA with poly(3-hydroxybutyrate) (PHB) and two succinic acid derived polyester, i.e., PBS and poly(butylene succinate-co-adipate) (PBSA); the obtained ternary blends were further reactively compatibilized with ESO and ELO to further increase their ductile properties.

Regarding other biobased epoxides, epoxidized citric acid (ECA) was synthesized from citric acid via a two-step process (Figure 1-7) and then used to increase the interfacial adhesion of MCC/PLA biocomposites; the flexural strength, flexural modulus and impact strength of the composites significantly increased after the addition of ECA [92]. A biobased di-functional glycidyl ether epoxy cardanol (ECard) was used as a plasticizer for PLA; the in-situ reactive grafting of ECard with

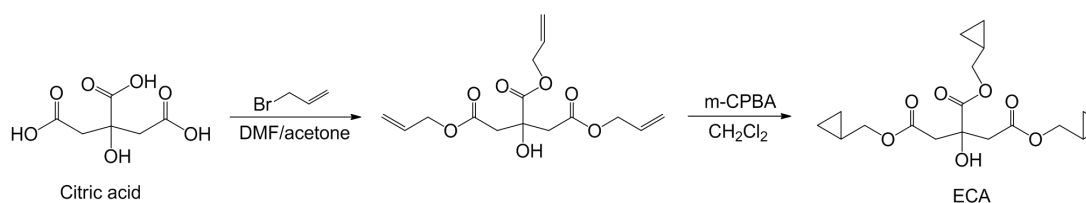


**Figure 1-7** Synthesis of ECA from citric acid via a two-step process [92]

PLA was initiated by ethyltriphenyl phosphonium bromide (ETPB) in a twin-screw extruder; the ETPB catalyst considerably facilitated the reaction of epoxy groups from ECard with the –COOH and –OH groups of PLA, and hence significantly enhanced the plasticizing effect of ECard on the blends [93].

### 1.2.2.3 Isocyanates

Isocyanates can readily react with the –OH groups of PLA and hence is suitable for compatibilizing PLA-based products, especially for the blends containing the incorporated components with reactive groups such as –OH and amino groups. The possible reaction between the –OH groups of PLA and the –NCO groups of isocyanates is proposed in [Figure 1-8](#). To establish effective chemical connections between PLA and the incorporated components, isocyanate monomers containing more than one –NCO group are necessary. The commonly used isocyanates for the compatibilization of PLA-based products are summarized in [Figure 1-9](#).

Isocyanates are very suitable compatibilizers for thermoplastic polyurethane (TPU)/PLA blends due to the presence of terminal –OH and –NCO groups in the TPU.

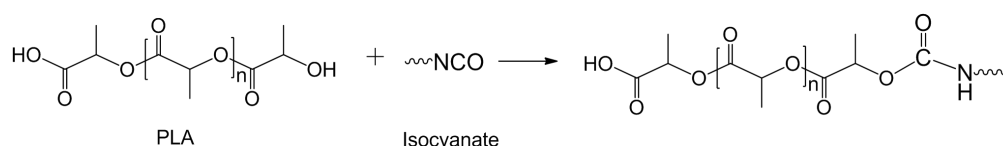


**Figure 1-8** Proposed reaction between PLA and isocyanate

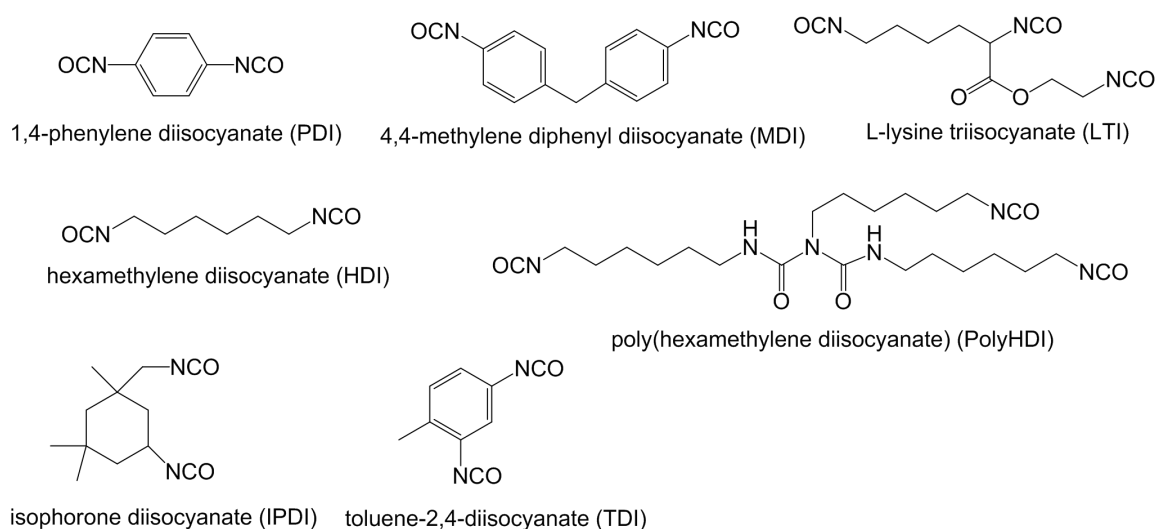


**Figure 1-9** Commonly used isocyanates in PLA-based products

TPU/PLA blends were added with different contents of 1,4-phenylene diisocyanate (PDI) to compatibilize the components; the results indicated that the shape recovery ratio was greatly increased by PDI addition, and the highest value was achieved for the blends with 3 wt% PDI [94]. Polycaprolactone-based polyurethane (PCLU)/PLA blends were compatibilized with isophorone diisocyanate (IPDI), which contributed to the blends with significantly increased elongation at break (20 times) and impact strength (5 times) when compared to neat PLA [95]. The toughness of PLA was increased by incorporating three thermoplastic elastomers, i.e., poly(ether-b-ester) (PEEs), poly(ether-b-amide) (PEBA) and poly(ether-b-urethane) (PEU); the toughening efficiency of the elastomers were further improved with the addition of 4,4-methylene diphenyl diisocyanate (MDI) as a compatibilizer to improve the interfacial compatibility of the blends [96].

González-Ausejo et al. [97,98] compared three diisocyanates, i.e., hexamethylene diisocyanate (HDI), poly(hexamethylene diisocyanate) (PolyHDI), and PDI, for their compatibilizing capacities on poly(3-hydroxybutyrate-co-3-hydroxyvalerate) (PHBV) /PLA composites; it was found that all the three diisocyanates could enhance the polymer compatibility and mechanical properties, but no significant difference in compatibilizing effects was concluded. With the purpose of increasing the interaction between poly( $\epsilon$ -caprolactone) (PCL) and PLA, the physical-mechanical properties of the PCL/PLA blends were investigated with the incorporation of ethyl ester L-lysine triisocyanate (LTI) as a compatibilizer [99]. It was found that LTI addition induced an increase in the ductility of the blends and lowered the formation of crystalline phase for both polymer, confirming an improved interaction of the components.

Ramie fibers (RFs)/PLA biocomposites by using three diisocyanates, i.e., HDI, IPDI and MDI, as coupling agents were prepared via extrusion and injection techniques [100]. As schemed in [Figure 1-10](#), one  $-NCO$  group of the introduced diisocyanates was expected to react with the  $-OH$  of RFs and the other  $-NCO$  group was covalently bonded with the  $-OH$  of PLA, hence forming a chemical bridge between RFs and PLA matrix. The results indicated that significant improvements in the mechanical and thermal properties were obtained for all the compatibilized

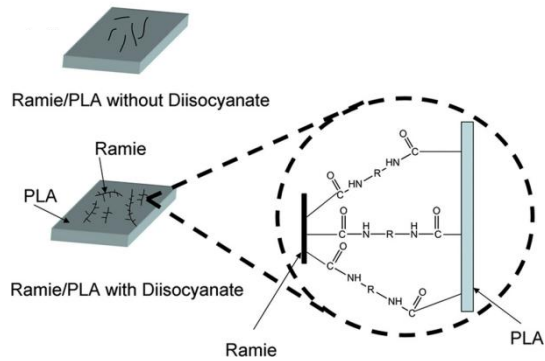


**Figure 1-10** Reaction mechanism of diisocyanates in RFs/PLA biocomposites [100]

composites because of the improved fiber-matrix interfacial adhesion induced by the diisocyanates.

#### 1.2.2.4 Free-radical initiators

Free-radical initiators are thermally decomposable and can be used in PLA-based blends to induce polymerization during melt compounding. As given in [Figure 1-11](#) [4], the free-radicals are generated from initiators at evaluated temperature and then react with PLA or the blended components to form macromolecular free-radicals, which could further react with PLA or the blended components. Hence, the grafted copolymers are formed at the interface of the blends, resulting in improved miscibility between each component. Fully biodegradable PPC/PLA blends were prepared and in-situ compatibilized by using DCP as an initiator due to the similar chemical structures of PPC and PLA [101]. In-situ crosslinking reaction between PPC and PLA was successfully initiated, and thereby

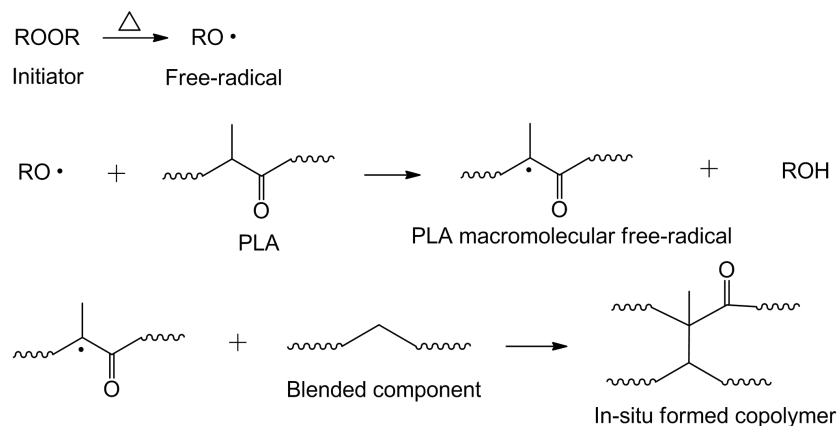


**Figure 1-11** In-situ formation of copolymer between PLA and the incorporated components initiated by free-radical initiator [4]

the compatibility of the blends was increased, which significantly changed the phase structures as well as increased the mechanical and shape memory properties of the blends. Ji et al. [102] compatibilized PBS/PLA blends with DCP in the melt state and found that some crosslinked/branched structures were generated between PBS and PLA at the interface, which functioned as a compatible interface layer between PLA and PBS phases. Similar work was reported by Srimalanon et al. [103] on PBS/PLA blends with the presence of 2-hydroxypropyl-3-piperazinylquinoline carboxylic acid methacrylate as an antibacterial agent, and results indicated that great increases in the elongation at break and tensile toughness of blends were obtained at a DCP concentration of 0.2 wt%. Ma et al. [104] reported the compatibilization of PBAT/PLA blends initiated with DCP. Significant increases in the elongation at break from 4 to 300% and impact toughness from 28 to 110 J/m of the blends were observed due to the improved interfacial bonding between PBAT and PLA. A thermally stable, PLA-grafted CNCs nanocomposite film was prepared using DCP as an initiator via a single reactive extrusion method [105]. The results indicated that the amorphous PLA chains were grafted on CNCs surface through the formation of C–C bonds, which resulted in efficient stress transfer of CNCs to PLA matrix, hence greatly increasing the tensile strength and modulus of the films when compared to neat PLA. The obtained films are circularly processable without changing their molecular weight, thermal and mechanical properties.

#### *1.2.2.5 Other monomers*

A biobased phenolic compound, i.e., cardanol, was used as an interfacial compatibilizer in ABS/PLA blends by Rigoussen et al. [106] for the first time. It was proposed that the main compatibilizing mechanism for the blends was the grafting of cardanol onto ABS, where the ABS free-radicals was generated due to thermal-mechanical degradation and then trapped by the phenol of cardanol via a typical anti-oxidant mechanism. This led to an increased compatibility of the blends as confirmed by the decrease of ABS nodules size within PLA and the convergence of glass transition temperatures of ABS and PLA.

Vachon et al. [107] prepared PEBA/PLA blends with a variety of reactive compatibilizers, i.e., poly(ethyleneco-methyl acrylate-co-glycidyl methacrylate) (PEAGM), poly(maleic anhydride-alt-1-octadecene) (PMAOD), 1,10-carbonyl biscaprolactam (CBC) and MDI, to compare the compatibilizing effects of these compatibilizers. PMAOD, PEAGM and CBC were able to increase the compatibility of the immiscible polymers and thus resulted in a moderate increase in the impact strength of the blends. An excellent toughening effect was obtained for the blends with MDI, where their notched Izod and Garner impact strengths achieved 7 and 63 times increases than those of the uncompatibilized blends, respectively.

### **1.2.3 Dynamic vulcanization**

Dynamic vulcanization is a process that involves the melt blending of the blended polymers and simultaneous formation of a crosslinked rubbery phase with PLA matrix and chemical reactions between PLA and the rubbery phase. Therefore, dynamic vulcanization in PLA-based blends refers to two process, i.e., crosslinking of the incorporated component and in-situ compatibilization of the blends. This strategy is very attractive to compatibilize PLA-based blends with crosslinkable polymers because the phase morphology and properties of the blends can be tailored by adjusting the degrees of vulcanization and compatibilization. The commonly utilized crosslinkable polymers include unsaturated elastomers, natural rubbers, vegetable oil derivatives, and polyurethane prepolymer.

#### *1.2.3.1 Unsaturated elastomers*

Free-radical initiators are usually used to induce the crosslinking of unsaturated elastomers during its blending with PLA. The selection of initiators normally depends on the decomposition temperature, which should match the thermal processing conditions of PLA blends.

Zhang et al. [108] investigated the free-radical competitions in the reactive blends from free-radical initiator (L101), biobased unsaturated polyurethane (Bio-TPU) and PLLA. It was demonstrated that the C=C bonds in Bio-TPU were

more prone to react with free-radicals, and excellent ductility and high tensile strength were achieved after the reactive compatibilization due to the greatly enhanced compatibility and much higher crystallinity degree. Biobased thermoplastic vulcanizates (TPV) from PLA and ethylene-co-vinyl acetate rubber (EVA) was prepared with different concentrations of DCP as an initiator to reveal the competing reaction mechanism of EVA crosslinking and interfacial compatibilization [109]. It was indicated that the EVA crosslinking was dominated at low DCP concentration and then leveled off when DCP concentration was higher than 1 wt%, which regulated the toughening effect of EVA on the blends. Ma et al. [110] investigated the dynamic crosslinking of PLA and EVA with the presence of 2,5-dimethyl-2,5-di(tertbutyl peroxy)hexane (AD) as an initiator. As shown in [Figure 1-12](#), it is proposed that there were three crosslinking reactions occurring during the dynamic vulcanization, i.e., EVA-EVA, EVA-PLA and PLA-PLA, which promoted the vulcanization and compatibilization of the blends together. However, EVA had a higher reactivity towards free-radicals and obtained a higher gel content of EVA phase than PLA, where the crosslinking of EVA reached a saturation point when AD content was higher than 1 wt%.

The dynamic vulcanization of PLA with poly(ethylene glycol) methyl ether acrylate (AcrylPEG) under the initiation of L101 was performed to prepare poly(AcrylPEG)/PLA blends with high toughness; the obtained blends had much

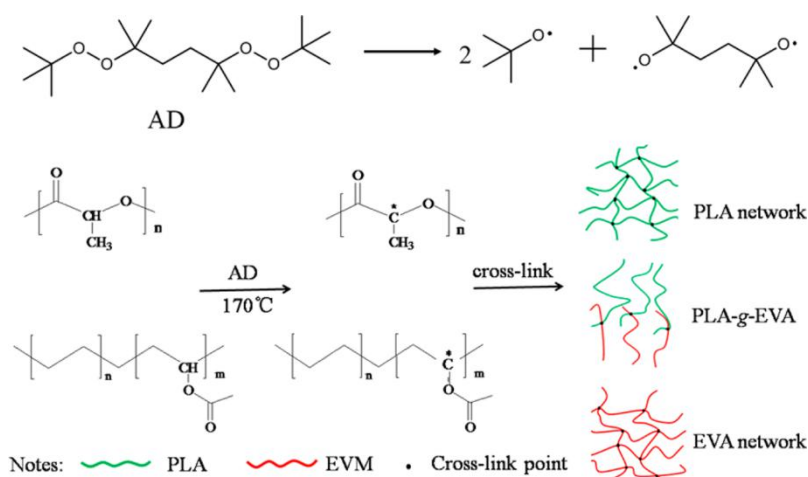


**Figure 1-12** Reaction mechanism of PLA/EVA blends in the presence of AD [110]

higher impact resistance and elongation at break than the blends prepared from physical blending of PLA and poly(AcrylPEG) [111]. Similar work was done by Kfoury et al. [112] on the dynamic vulcanization of PLA with poly(ethylene glycol) methyl ether methacrylate (MAPEG) and AcrylPEG; the results found that AcrylPEG presented a better plasticizing effect on PLA-based blends than MAPEG.

A fully biobased and supertough PLA-based blend was fabricated from PLA and a biobased vulcanized unsaturated polyester elastomer (UPE) through peroxide-induced (DCP) dynamic vulcanization by Liu et al. [113]. The dynamic vulcanization facilitated the change of the blend morphology from a typical phase-separate structure to a quasi cocontinuous phase with vulcanized UPE compactly dispersed within PLA matrix, which explained the supertough characteristics of the blends. Simultaneous crosslinking and compatibilization of poly(glycerol succinate-co-maleate) (PGSMA) within PLA matrix was initiated by L101 as an initiator to formulate PGSMA/PLA blends, as reported by Valerio et al [114]. The degree of dynamic vulcanization was tailored by the unsaturated level of the PGSMA via changing composition ratios, which resulted in different increments in the tensile toughness and impact resistance of the blends. A biobased elastomer, i.e., poly(lactate-butanediol-sebacate-itaconate) (PLBSI) was synthesized and blended with PLA via in-situ dynamic vulcanization in the presence of DCP to prepare PLBSI/PLA blends for 3D-printing application [115]. The vulcanization process led to the PLBSI elastomer dispersed as microparticles within PLA matrix, achieving a good toughening effect on the PLA blends. In the work of Si et al. [116], a biobased UPE was used for the dynamic vulcanization with a mixture of PLLA and poly(D-lactide) (PDLA). During the dynamic vulcanization, PDLA cocrystallized with PLLA to form stereocomplex (SC) crystallites, which resulted in achieving a fully sustainable PLLA/UPE/PDLA ternary blend with highly crystalline matrix as well as excellent heat resistance and impact toughness.

#### *1.2.3.2 Natural rubbers*

Natural rubber (NR), known as a green and renewable material from rubber tree, has been applied as suitable alternatives for petroleum-based impact modifiers for PLA-based products. However, the poor interfacial compatibility between NR and PLA was the main challenge that limits the toughening efficiency of NR on PLA-based products.

The dynamic vulcanization of PLA with NR by free-radical initiator (DCP) was firstly investigated by Chen et al. [117], where the traditional concept of a sea-island morphology formed after dynamic vulcanization was broken, and a continuous network-like dispersion of the crosslinked NR with PLA matrix was proofed. The cocontinuous structure endowed the NR/PLA blends with super-toughness. This situation was also confirmed by the epoxidized NR/PLA blends using DCP as an initiator, where a novel “sea-sea” cocontinuous phase in the blends was obtained as given in Figure 1-13 [118]. Subsequently, the formation mechanism of the cocontinuous structure and its effects on the properties of NR/PLA blends were discussed in details [118-120]. To reveal the effect of DCP on the dynamical vulcanization of NR/PLA blends, the distribution of DCP in PLA and NR phases was tailored by changing feeding procedures [120]. The results indicated that the blends produced by premixing DCP with PLA and NR separately, exhibited higher

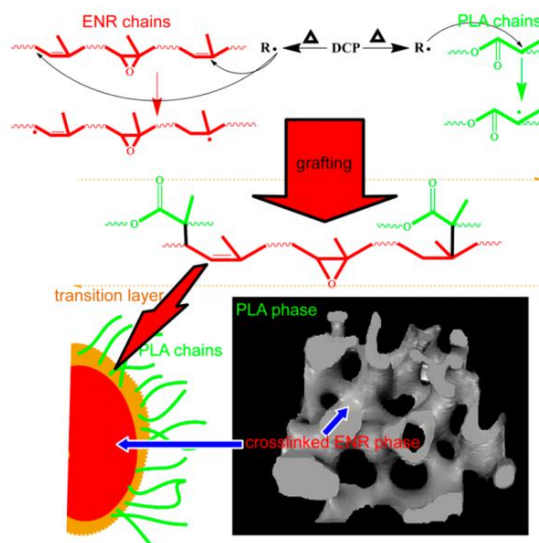


**Figure 1-13** Possible reaction during in-situ compatibilization and the formed transition layer at the interface between PLA and epoxidized NR phases [118]

toughness and comparable tensile properties to that from direct blending of PLA, NR and DCP. This was explained by the synergistic effect of the improved PLA molecular chain entanglement due to DCP initiated branch reaction and enhanced interfacial compatibility of the blends. The novel "netlike" continuous phase in PLA matrix also induced the NR/PLA blends with superior shape memory properties [121,122]. For instance, in the work of Yuan et al. [122], a surprising shape memory property, i.e., shape fixity ~100%, shape recovery > 95%, and fast recovery speed < 15 s at the switching temperature (~60°C), was achieved in the NR/PLA blends; the crosslinked NR continuous phase was considered to offer strong resilience and the PLA matrix served as the heat-control switch.

To develop NR/PLA blends with balanced stiffness and toughness, ternary blends composed of PLA, PMMA-grafted NR and NR were fabricated via peroxide-induced dynamic vulcanization by Chen et al. [123]. Significantly enhanced tensile strength (41.7 MPa) and impact strength (91.30 kJ/m<sup>2</sup>) were obtained for the blends with 10 wt% of NR and PMMA-grafted NR, which were 38% lower and 32 times higher than those of neat PLA, respectively. This was attributed by the flexibility of the "soft" NR core and outer "hard" PMMA-grafted NR shell with excellent interfacial adhesion of the blends.

Excluding free-radical initiators, sulphur and phenolic resin were also used as crosslinking agents for the dynamical vulcanization of NR/PLA blends to generate a cocontinuous structure [124,125]. An improved compatibility between PLA and NR was obtained from phenolic resin-induced dynamic vulcanization, but the increase in impact strength of the blends was limited, which was probably due to the degradation of PLA caused by the alkali impurities in phenolic resin system [125].

#### *1.2.3.3 Vegetable oil derivatives*

Vegetable oils (VOs) are triglycerides that contain three long flexible aliphatic chains in each molecule. Therefore, VOs derivatives such as ESO have been extensively utilized as plasticizers in PLA and polyvinyl chloride. There are many

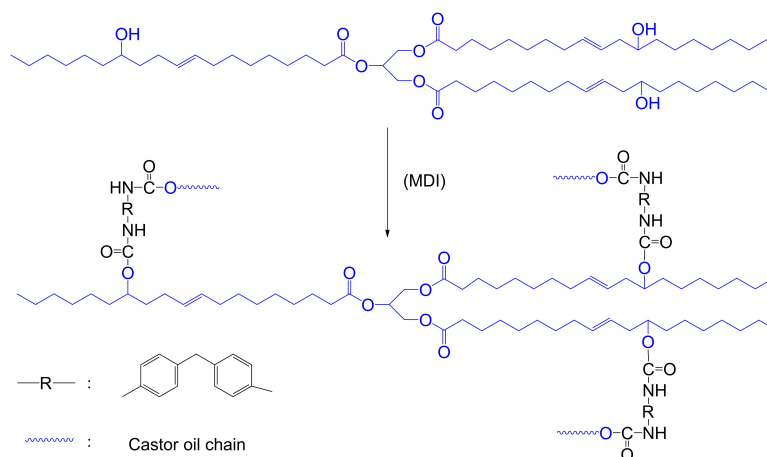


**Figure 1-14** Reaction mechanism of CO with MDI during dynamic vulcanization of PLA with CO [126]

functional groups including epoxy and  $\text{-OH}$  groups presented in the VOs derivatives, which gives the derivatives with reactive sites for dynamic vulcanization.

Castor oil (CO) has several  $\text{-OH}$  groups that are able to react with  $\text{-NCO}$  groups to generate polyurethane. Zhao et al. [126] reported the dynamic vulcanization of CO using MDI as a crosslinker in PLA matrix. The crosslinking of CO with MDI during dynamic vulcanization was proposed in Figure 1-14. The interfacial adhesion between PLA and the CO derived polyurethane (CO-d-PU) also occurred due to the reaction between the  $\text{-NCO}$  groups of MDI and the  $\text{-OH}$  groups of PLA. This resulted in the formation of a phase-separated morphology with a CO-d-PU dispersed phase and a PLA continuous phase. The CO-d-PU content in the blends significantly affected the size of dispersed CO-d-PU particles as well as the mechanical properties, rheological and crystallization behaviors of the resulting blends. The CO-d-PU/PLA blends with 5 wt% CA-d-PU had 45 times higher elongation at break than neat PLA while maintaining largely mechanical strength and modulus. Moreover, three diisocyanates, i.e., MDI, HDI and IPDI, were used as crosslinking agents, respectively, for the dynamic vulcanization of CO/PLA system [127]. The reactivity of the diisocyanates followed  $\text{MDI} > \text{HDI} > \text{IPDI}$  when reacting with CO. However, the CO-IPDI/PLA blends exhibited the finest morphology and the best toughening efficiency. Compared to neat PLA, the elongation at break and impact strength of the

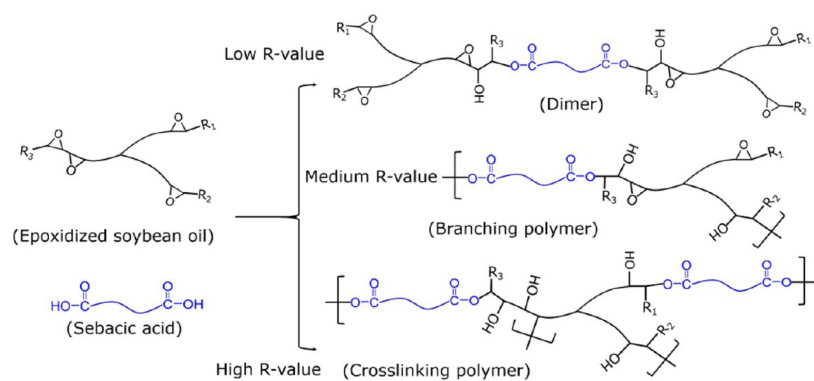


**Figure 1-15** Reaction mechanism between SA and ESO with different R values during dynamic vulcanization of PLA with ESO [128]

blends increased by 47.3 and 6.6 times, respectively, after the addition of 20 wt% CO-IPDI.

Regarding the use of ESO in PLA-based blends, a biobased dicarboxylic acid, i.e., sebacic acid (SA), was used to cure ESO during its blending with PLA [128]. Therefore, a series of SA-cured ESO precursors with different carboxyl/epoxy equivalent ratio (R) were incorporated with PLA to investigate the effect of chemical structure of the SA-cured ESO phase on the properties of the resulting SA-cured ESO/PLA blends. The reaction mechanism between SA and ESO with different R values was shown in [Figure 1-15](#). It was revealed that at the optimized R value of SA-cured ESO, supertough PLA-based blend was obtained with significant improved tensile toughness ( $150.6 \text{ MJ/m}^3$ ) and impact strength ( $542.3 \text{ J/m}^2$ ). Furthermore, the content of SA-cured ESO was increased up to 80 wt% to develop thermoset ESO/PLA blends with high performance and thermoplasticity via dynamic vulcanization [129]. A phase-separated morphology with SA-cured ESO dispersed with PLA matrix was observed for the blends even with the content of SA-cured ESO as high as 80 wt%. The obtained blends possessed high toughness with large tensile strains even though both SA-cured ESO and PLA are brittle materials.

#### 1.2.3.4 Polyurethane

The dynamic vulcanization of polyurethane elastomer prepolymer (PUEP)/PLA blends was initiated by using dibutyl tin dilaurate as a catalyst [130]. It was demonstrated that the PUEP carrying  $\text{-NCO}$  groups was successfully vulcanized and

the in-situ compatibilization was achieved via the reaction between the –NCO groups of PUEP and the –OH groups of PLA, which led to a relatively uniform phase morphology and generated supertough PUEP/PLA blends. Polyurethane (PU)/PLA blends were fabricated by reactive extrusion with in-situ formation of PU phase with PLA matrix via the reaction between PEG and toluene-2,4-diisocyanate (TDI) [131]. The interfacial compatibility of the blends was considerably increased by the formation of grafted copolymer from the reaction between the –OH groups of PLA and the –NCO groups of TDI. Super-toughness of PCL/PLA blends was achieved by reactive incorporation of glycerol and MDI. The formation of crosslinked PU and its connection with PLA matrix significantly affected the morphology and increased the toughness of the blends [132].

#### 1.2.4 Interchange reactions

Transesterification usually can occur when two polyesters are blended at melting state (Figure 1-16). In the work of Spinella et al. [133], reactive extrusion was used to fabricate fully biobased poly( $\omega$ -hydroxytetradecanoic acid) (PC14)/PLA blends in the presence of titanium tetrabutoxide (Ti(BuO)<sub>4</sub>) as the catalyst of transesterification. The in-situ formation of PLA-b-PC14 copolymers at the interface of the blends was evidenced by NMR analysis, which was responsible for the enhanced elongation at break of the blends from 3 to 140 % relative to neat PLA. During the melt-blending of PLA and PPC, the transesterification between PLA and PPC was initiated by tetrabutyl titanate, which contributed to forming a PLA-b-PPC block copolymer at the interface of the blends [134]. The feeding composition of the blends was tuned to change the level of esterification between PLA and PPC. The PPC/PLA blend with a weight ratio of 40:60 and a catalyst amount of 0.5 wt% had the most conspicuous transesterification and inconspicuous chain scission reaction. The elongation at break of the optimum blends was nearly as twice as that of the

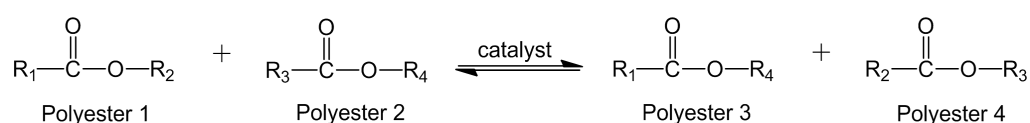


**Figure 1-16** Transesterification between two polyester

uncompatibilized blends due to the improved miscibility. Chelghoum et al. [135] reported that samarium acetylacetonate (Sm-Acac) could act as two roles in PC/PLA blends. Firstly, Sm-Acac worked as a plasticizer and led to significantly decreasing the glass transition temperature of PLA phase. Moreover, Sm-Acac was effective in catalyzing the transesterification between PC and PLA as confirmed by the decrease in crystallinity rate of PLA because of the hindering effect of the introduced PC units on the PLA chains. It was concluded that the PC/PLA blends with 0.25 wt% Sm-Acac exhibited a significant strengthening effect, i.e., increased glass transition temperature and storage modulus. A new transesterification agents, i.e., sulfonic acidic ionic liquids (ILs), was synthesized and used to compatibilize EVA/PLA blends [136]. The catalyst efficiency of the ILs was investigated and compared with that of  $Ti(BuO)_4$ . Results indicated that the degradation of PLA was minimized when the ILs was used, whereas  $Ti(BuO)_4$  facilitated a reduction in the molar mass of the PLA chains. The highest compatibilization efficiency of the ILs was reached by using only 1 wt% ILs, where the blends had the optimum mechanical and dynamical mechanical properties.

Ester-amide exchange reaction between PLA and polyamide 11 (PA11) was induced by using suitable catalysts during the melt-compounding process to improve the interfacial compatibility of PA11/PLA blends, as given in Figure 1-17 [137,138]. The reactive extrusion of PA11/PLA blends with using p-toluenesulfonic acid (TsOH) as a catalyst would result in forming PA11-PLA copolymers at the interface and hence reducing the interfacial tension of the blends [137]. A 50% increase in elongation at break was seen in the PA11/PLA blends with 0.5 wt% TsOH. However, significant degradation of PLA can not be avoided during the processing, hence

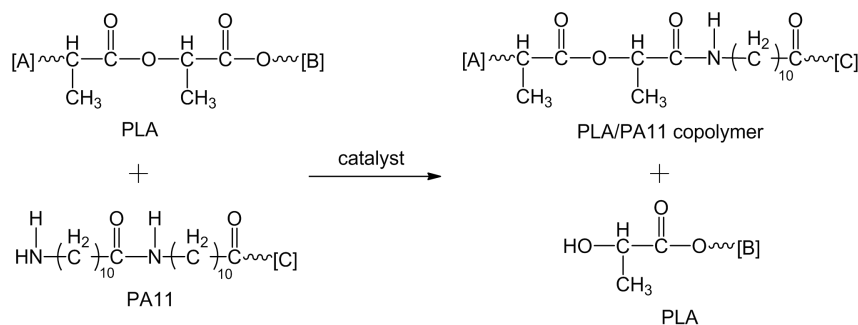


**Figure 1-17** Ester-amide exchange reaction between PLA and PA11 [137,138]

leading to a decreased mechanical strength of the blends. To address this issue, a thermal stabilizer, i.e., tris(nonylphenyl) phosphite was further added into the blends, which endowed the blends with both improved tensile strength and elongation at break [138].

### **1.3 Current issues and future trend**

Concerning the reactive compatibilization of PLA-based blends and composites, many strategies including incorporation of reactive monomers and polymers have been successfully developed and outlined in this review. However, the addition of reactive polymers as compatibilizers requires the functionalization of polymers with anhydride and epoxy functionalities, which might complicate the preparation procedure and increase the production cost of PLA-based products. The direct blending of monomers into PLA system could provide a convenient method to compatibilize the PLA-based products, while the main drawbacks are the poor dispersion of the monomers on the blends and the potential volatilization of some toxic monomers such as isocyanates. Dynamic vulcanization is highly effective in toughening and compatibilizing the PLA-based blends. Concerning the dynamic vulcanization of PLA-based blends, the incorporated components must contain crosslinkable functionalities; the suitable polymers include natural rubber, unsaturated polyester, functionalized vegetable oils, and polyurethane. The key issue of dynamic vulcanization is to control the crosslinking degree of the generated rubbery phase and the formation of chemical connections between the crosslinked phase and PLA matrix, which is significantly related to the toughening efficiency of the rubbery phase on the PLA matrix.

Although much achievements in reactive compatibilization of PLA-based products have been obtained, future discoveries regarding novel compatibilization strategies and new applications of PLA-based products are still desired. Firstly, green and sustainable methods for toughening PLA are extremely attractive. The PLA-based products are developed to replace traditional and petroleum-based polymers; hence, the toughening of PLA should not sacrifice the sustainability of the PLA-based

products. Therefore, it is needed to utilize the incorporated components and compatibilizers from renewable materials during the reactive compatibilization. For example, vegetable oil derivatives are suitable materials for blending with PLA, while the exploitation of effective biobased crosslinker for the derivatives is the main challenge. What's more, obtaining high toughness for PLA-based composites remains a challenge. The incorporation of reinforcing fibers/fillers into PLA not only improves the mechanical strength and modulus of the PLA-based composites, but reduces the production cost of the products. However, the toughening principles and methods of PLA-based blends are not completely adequate for PLA-based composites. The toughening of PLA-based composites should consider the presence of reinforcing fibers/fillers and the formed interfacial adhesion between the fibers/fillers and PLA matrix, which makes the toughening more complicated. Thirdly, it is required to correlate the fabrication, toughening and properties of PLA-based products with their practical application. Especially, the emerging 3D printing technology provides a good direction for the preparation and modification of PLA-based products.

## **1.4 Contribution from this dissertation**

PLA is highly brittle in nature. Conventional polymerized ESO resins cannot be thermally remolded because of its three-dimensional network structure. Concerning these two challenges, the main objective of this project aims at manufacturing fully biobased, thermally remoldable, and highly tough blends from ESO and PLA in a large-scale production via twin-screw extrusion and injection molding. To perform the dynamic vulcanization process of PLA with ESO, two strategies were proposed to induce the crosslinking of ESO, which resulted in the formation of a stable crosslinked-ESO phase dispersed within continuous PLA matrix and an improved interfacial compatibility between ESO and PLA. In [Chapter 3](#), dynamic vulcanization of PLA with ESO was activated by using a cationic initiator to induce the self-polymerization of ESO. In [Chapter 4](#), a biobased monomer, i.e., tannic acid (TA), was used as a green vulcanizing agent for ESO to prepare tough TA-ESO/PLA blends.

To broaden the application area of PLA products, the TA-ESO/PLA blends were further utilized for the production of conductive nanocomposites and fiber-reinforced biocomposites. To repair the sacrificial strength of the TA-ESO/PLA blends and impart the composites with electrical conductivity, different concentrations of carbon nanotubes (CNTs) were incorporated into the TA-ESO/PLA blends to prepare CNT/TA-ESO/PLA nanocomposites (Chapter 5). In Chapter 6, bamboo fibers (BFs) were introduced into the TA-ESO/PLA blends to produce ternary BF-reinforced TA-ESO/PLA biocomposites with tailorable performance. At a low content of TA-ESO (0.5 wt%), the TA-ESO could form strong interaction with BFs via natural polyphenol-inspired chemistry, hence generating a flexible interface layer at the interface between BFs and PLA matrix. When the TA-ESO content was further increased, the TA-ESO would diffuse into PLA matrix and thereby give a toughening effect on PLA matrix.

**The features of this project are as follows.**

(1) Fully biobased, thermally reprocessable, and highly tough blends were formulated from PLA and ESO with the presence of biobased TA or cationic initiator as vulcanizing agents via dynamic vulcanization technique, which simultaneously improves the toughness of PLA products and endows the ESO-based thermosets with thermal processability.

(2) The highly tough ESO/PLA blends were successfully utilized for the development of CNT conductive nanocomposites and BF-reinforced biocomposites, which provides new route for the application of PLA products.

(3) The successful completion of this study not only provide cost-competitive, commercially viable, and biodegradable PLA products, but also enable us to gain a good understanding of the mechanisms for toughening and reinforcing PLA and its composites.

## Abbreviations

ABS, acrylonitrile-butadiene-styrene; AcrylPEG, poly(ethylene glycol) methyl ether acrylate; AD, 2,5-dimethyl-2,5-di(tertbutylperoxy)hexane; ASF, almond shell flour; bioPE, biopolyethylene; Bio-TPU, biobased unsaturated polyurethane; CBC, 1,10-carbonyl biscaprolactam; CFs, carbon fibers; CNCs, cellulose nanocrystals; CNFs, cellulose nanofibers; CNTs, carbon nanotubes; CNTs-COOH, carboxylated carbon nanotubes; CO, castor oil; CO-d-PU, castor oil derived polyurethane; COPUP, castor oil-based polyurethane prepolymer; DCP, dicumyl peroxide; EBA, ethylene butyl acrylate; ECA, epoxidized citric acid; ECard, biobased di-functional glycidyl ether epoxy cardanol; ECO, epoxidized cottonseed oil; EFG, epoxy-functionalized graphene; ELO, epoxidized linseed oil; EMA, ethylene methyle acrylate; ESBS, epoxidized poly(styrene-b-butadiene-b-styrene); ESO, epoxidized soybean oil; ETPB, ethyltriphenyl phosphonium bromide; EVA, ethylene-co-vinyl acetate; EVOs, epoxidized vegetable oils; GMA, glycidyl methacrylate; GNPs, graphite nanoplatelets; HDI, hexamethylene diisocyanate; HDT, heat deflection temperature; IA, itaconic anhydride; ILs, sulfonic acidic ionic liquids; IPDI, isophorone diisocyanate; L101, 2,5-bis(tert-butylperoxy)-2,5-dimethylhexane; LLDPE, linear low density polyethylene; LTI, ethyl ester L-lysine triisocyanate; MA, maleic anhydride; MAPEG, poly(ethylene glycol) methyl ether methacrylate; MCC, microcrystalline cellulose; MCO, maleinized cottonseed oils; MDI, 4,4-methylene diphenyl diisocyanate; MLO, maleinized linseed oil; NFs, natural fibers; NR, natural rubber; PA11, polyamide 11; PBAPU, poly-1,4-butylene glycol adipate diol-based polyurethane prepolymer; PBAT, poly(butylene adipate-co-terephthalate); PBS, poly(butylene succinate); PBSA, poly(butylene succinate-co-adipate); PBT, poly(butylene terephthalate); PC, polycarbonate; PC14, poly( $\omega$ -hydroxytetradecanoic acid); PCL, poly( $\epsilon$ -caprolactone); PCLU, polycaprolactone-based polyurethane; PDI, 1,4-phenylene diisocyanate; PDLA, poly(D-lactide); PEAGM, poly(ethyleneco-methyl acrylate-co-glycidyl methacrylate); PEBA, poly(ether-b-amide); PEEs, poly(ether-b-ester); PEG, polyethylene glycol; PEU, poly(ether-b-urethane); PGSMA, poly(glycerol

succinate-co-maleate); PHB, poly(3-hydroxybutyrate); PHBV, poly(3-hydroxybutyrate-co-3-hydroxyvalerate); PLA, poly(lactic acid); PLBSI, poly(lactate-butanediol-sebacate-itaconate); PMAOD, poly(maleic anhydride-alt-1-octadecene); PMMA, poly(methyl methacrylate); PolyHDI, poly(hexamethylene diisocyanate); PP, polypropylene; PPC, poly(propylene carbonate); PTT, poly(trimethylene terephthalate); PU, polyurethane; PUEP, polyurethane elastomer prepolymer; RFs, ramie fibers; SA, sebacic acid; Sm-Acac, samarium acetylacetonate; TA, tannic acid; TDI, toluene-2,4-diisocyanate; Ti(BuO)<sub>4</sub>, titanium tetrabutoxide; TPS, thermoplastic starch; TPU, thermoplastic polyurethane; TPV, thermoplastic vulcanizates; TsOH, p-toluenesulfonic acid; UPE, unsaturated polyester; VOs, vegetable oils; WFs, wood fibers.

## References

- [1] Castro-Aguirre, E.; Iñiguez-Franco, F.; Samsudin, H.; Fang, X.; Auras, R. Poly(lactic acid)—mass production, processing, industrial applications, and end of life. *Adv. Drug Deliv. Rev.* 2016, 107, 333-366.
- [2] Liu, H.; Zhang, J. Research progress in toughening modification of poly(lactic acid). *J. Polym. Sci. Pol. Phys.* 2011, 49, 1051-1083.
- [3] Krishnan, S.; Pandey, P.; Mohanty, S.; Nayak, S.K. Toughening of polylactic acid: An overview of research progress. *Polym. Plast. Technol. Eng.* 2016, 55, 1623-1652.
- [4] Zeng, J.-B.; Li, K.-A.; Du, A.-K. Compatibilization strategies in poly(lactic acid)-based blends. *RSC Adv.* 2015, 5, 32546-32565.
- [5] Ding, Y.; Lu, B.; Wang, P.; Wang, G.; Ji, J. PLA-PBAT-PLA tri-block copolymers: Effective compatibilizers for promotion of the mechanical and rheological properties of PLA/PBAT blends. *Polym. Degrad. Stabil.* 2018, 147, 41-48.
- [6] Ding, Y.; Feng, W.; Lu, B.; Wang, P.; Wang, G.; Ji, J. PLA-PBAT-PLA tri-block copolymers: Effective compatibilizers for promotion of the interfacial structure and mechanical properties of PLA/PBAT blends. *Polymer* 2018, 146, 179-187.
- [7] Brown, S.B. Reactive compatibilization of polymer blends. In *Polymer Blends Handbook*, Springer: 2003; pp 339-415.
- [8] Murariu, M.; Dubois, P. PLA composites: From production to properties. *Adv. Drug Deliv. Rev.* 2016, 107, 17-46.
- [9] Siakeng, R.; Jawaid, M.; Ariffin, H.; Sapuan, S.; Asim, M.; Saba, N. Natural fiber reinforced polylactic acid composites: A review. *Polym. Compos.* 2018/01/26, doi: 10.1002/pc.24747.

- [10] Gonçalves, C.; Gonçalves, I.C.; Magalhães, F.D.; Pinto, A.M. Poly(lactic acid) composites containing carbon-based nanomaterials: A review. *Polymers* 2017, 9, 269.
- [11] Karger-Kocsis, J.; Mahmood, H.; Pegoretti, A. Recent advances in fiber/matrix interphase engineering for polymer composites. *Prog. Mater. Sci.* 2015, 73, 1-43.
- [12] Hamad, K.; Kaseem, M.; Ayyoob, M.; Joo, J.; Deri, F. Polylactic acid blends: The future of green, light and tough. *Prog. Polym. Sci.* 2018, 85, 83-127.
- [13] Nagarajan, V.; Mohanty, A.K.; Misra, M. Perspective on polylactic acid (PLA) based sustainable materials for durable applications: Focus on toughness and heat resistance. *ACS Sustain. Chem. Eng.* 2016, 4, 2899-2916.
- [14] Yang, Y.; Zhang, L.; Xiong, Z.; Tang, Z.; Zhang, R.; Zhu, J. Research progress in the heat resistance, toughening and filling modification of PLA. *Sci. China Chem.* 2016, 59, 1355-1368.
- [15] Wang, M.; Wu, Y.; Li, Y.-D.; Zeng, J.-B. Progress in toughening poly(lactic acid) with renewable polymers. *Polym. Rev.* 2017, 57, 557-593.
- [16] Nagarajan, V.; Mohanty, A.K.; Misra, M. Blends of polylactic acid with thermoplastic copolyester elastomer: Effect of functionalized terpolymer type on reactive toughening. *Polym. Eng. Sci.* 2017, 58, 280-290.
- [17] Carrasco, F.; Santana, O.; Cailloux, J.; Sánchez-Soto, M.; Maspoch, M.L. Poly(lactic acid) and acrylonitrile-butadiene-styrene blends: Influence of adding ABS-g-MAH compatibilizer on the kinetics of the thermal degradation. *Polym. Test.* 2018, 67, 468-476.
- [18] Ghozali, M.; Sinaga, P.D.B.; Maranata, S.; Rohmah, E.N. Study and development of linear low density polyethylene (LLDPE) and poly(lactic acid) (PLA) biodegradable compounds using compatibilizer LLDPE-g-MA. *World Chem. Eng. J.* 2016, 1, 11-16.
- [19] Pivsa-Art, S.; Kord-Sa-Ard, J.; Pivsa-Art, W.; Wongpajan, R.; Narongchai, O.; Pavasupree, S.; Hamada, H. Effect of compatibilizer on PLA/PP blend for injection molding. *Energy Proc.* 2016, 89, 353-360.
- [20] Bai, Z.; Dou, Q. Rheology, morphology, crystallization behaviors, mechanical and thermal properties of poly(lactic acid)/polypropylene/maleic anhydride-grafted polypropylene blends. *J. Polym. Environ.* 2018, 26, 959-969.
- [21] Rajan, K.P.; Thomas, S.P.; Gopanna, A.; Al-Ghamdi, A.; Chavali, M. Rheology, mechanical properties and thermal degradation kinetics of polypropylene (PP) and polylactic acid (PLA) blends. *Mater. Res. Express* 2018, 5, 085304.
- [22] Anstey, A.; Codou, A.; Misra, M.; Mohanty, A.K. Novel compatibilized nylon-based ternary blends with polypropylene and poly(lactic acid): Fractionated crystallization phenomena and mechanical performance. *ACS Omega* 2018, 3, 2845-2854.
- [23] Codou, A.; Anstey, A.; Misra, M.; Mohanty, A.K. Novel compatibilized nylon-based ternary blends with polypropylene and poly(lactic acid): Morphology evolution and rheological behaviour. *RSC Adv.* 2018, 8, 15709-15724.

- [24] Pongsathit, S.; Pattamaprom, C. Irradiation grafting of natural rubber latex with maleic anhydride and its compatibilization of poly(lactic acid)/natural rubber blends. *Radia. Phys. Chem.* 2018, 144, 13-20.
- [25] Mohammad, N.; Arsad, A.; Rahmat, A.; Sani, N.A.; Mohsin, M.A. Influence of compatibilizer on the structure properties of polylactic acid/natural rubber blends. *Polym. Sci. Ser. A* 2016, 58, 177-185.
- [26] Teamsinsungvon, A.; Jarapanyacheep, R.; Ruksakulpiwat, Y.; Jarukumjorn, K. Melt processing of maleic anhydride grafted poly(lactic acid) and its compatibilizing effect on poly(lactic acid)/poly(butylene adipate-co-terephthalate) blend and their composite. *Polym. Sci. Ser. A* 2017, 59, 384-396.
- [27] Zhang, L.; Lv, S.; Sun, C.; Wan, L.; Tan, H.; Zhang, Y. Effect of MAH-g-PLA on the properties of wood fiber/polylactic acid composites. *Polymers* 2017, 9, 591.
- [28] Pan, Y.-J.; Lin, Z.-I.; Lou, C.-W.; Huang, C.-L.; Lee, M.-C.; Liao, J.-M.; Lin, J.-H. Polylactic acid/carbon fiber composites: Effects of polylactic acid-g-maleic anhydride on mechanical properties, thermal behavior, surface compatibility, and electrical characteristics. *J. Compos. Mater.* 2018, 52, 405-416.
- [29] Phetwarotai, W.; Maneechot, H.; Kalkornsurapranee, E.; Phusunti, N. Thermal behaviors and characteristics of polylactide/poly(butylene succinate) blend films via reactive compatibilization and plasticization. *Polym. Adv. Technol.* 2018, 29, 2121-2133.
- [30] Phetwarotai, W.; Tanrattanakul, V.; Phusunti, N. Synergistic effect of nucleation and compatibilization on the polylactide and poly(butylene adipate-co-terephthalate) blend films. *Chin. J. Polym. Sci.* 2016, 34, 1129-1140.
- [31] Moghaddam, M.R.A.; Razavi, S.M.A.; Jahani, Y. Effects of compatibilizer and thermoplastic starch (TPS) concentration on morphological, rheological, tensile, thermal and moisture sorption properties of plasticized polylactic acid/TPS blends. *J. Polym. Environ.* 2018, 26, 3202-3215.
- [32] Du, J.; Wang, Y.; Xie, X.; Xu, M.; Song, Y. Styrene-assisted maleic anhydride grafted poly(lactic acid) as an effective compatibilizer for wood flour/poly(lactic acid) bio-composites. *Polymers* 2017, 9, 623.
- [33] Dogu, B.; Kaynak, C. Behavior of polylactide/microcrystalline cellulose biocomposites: Effects of filler content and interfacial compatibilization. *Cellulose* 2016, 23, 611-622.
- [34] Ghasemi, S.; Behrooz, R.; Ghasemi, I.; Yassar, R.S.; Long, F. Development of nanocellulose-reinforced PLA nanocomposite by using maleated PLA (PLA-g-MA). *J. Thermoplast. Compos. Mater.* 2018, 31, 1090-1101.
- [35] Ghasemi, S.; Behrooz, R.; Ghasemi, I. Investigating the properties of maleated poly(lactic acid) and its effect on poly(lactic acid)/cellulose nanofiber composites. *J. Polym. Eng.* 2018, 38, 391-398.

- [36] Chen, J.; He, H.; Yu, P.; Jia, Y.; Meng, S.; Wang, J. Preparation and properties of poly(lactic acid)/cellulose nanocrystals nanocomposites compatibilized with maleated poly(lactic acid). *Polym. Compos.* 2017, 39, 3092-3101.
- [37] Issaadi, K.; Pillin, I.; Habi, A.; Grohens, Y. Synergetic association of grafted PLA and functionalized graphene on the properties of the designed nanocomposites. *Polym. Bull.* 2017, 74, 997-1010.
- [38] Cai, C.; Liu, L.; Fu, Y. Processable conductive and mechanically reinforced polylactide/graphene bionanocomposites through interfacial compatibilizer. *Polym. Compos.* 2017/11/22, doi: 10.1002/pc.24663.
- [39] Walallavita, A.; Verbeek, C.; Lay, M. Morphology and mechanical properties of itaconic anhydride grafted poly(lactic acid) and thermoplastic protein blends. *Int. Polym. Proc.* 2018, 33, 153-163.
- [40] Santos, L.G.; Costa, L.C.; Pessan, L.A. Development of biodegradable PLA/PBT nanoblends. *J. Appl. Polym. Sci.* 2018, 135, 45951.
- [41] Zhou, Y.; Wang, J.; Cai, S.-Y.; Wang, Z.-G.; Zhang, N.-W.; Ren, J. Effect of POE-g-GMA on mechanical, rheological and thermal properties of poly(lactic acid)/poly(propylene carbonate) blends. *Polym. Bull.* 2018/04/21, doi: 10.1007/s00289-018-2339-5.
- [42] Forghani, E.; Azizi, H.; Karabi, M.; Ghasemi, I. Compatibility, morphology and mechanical properties of polylactic acid/polyolefin elastomer foams. *J. Cell. Plast.* 2018, 54, 235-255.
- [43] Thurber, C.; Gu, L.; Myers, J.C.; Lodge, T.P.; Macosko, C.W. Toughening polylactide with a catalyzed epoxy-acid interfacial reaction. *Polym. Eng. Sci.* 2018, 58, 28-36.
- [44] Wu, N.; Zhang, H. Mechanical properties and phase morphology of super-tough PLA/PBAT/EMA-GMA multicomponent blends. *Mater. Lett.* 2017, 192, 17-20.
- [45] Hao, M.; Wu, H.; Zhu, Z. In situ reactive interfacial compatibilization of polylactide/sisal fiber biocomposites via meltblending with an epoxy-functionalized terpolymer elastomer. *RSC Adv.* 2018, 7, 32399.
- [46] Zhou, Y.; Lei, L.; Yang, B.; Li, J.; Ren, J. Preparation and characterization of polylactic acid (PLA) carbon nanotube nanocomposites. *Polym. Test.* 2018, 68, 34-38.
- [47] Nagarajan, V.; Mohanty, A.K.; Misra, M. Reactive compatibilization of polytrimethylene terephthalate (PTT) and polylactic acid (PLA) using terpolymer: Factorial design optimization of mechanical properties. *Mater. Des.* 2016, 110, 581-591.
- [48] Brito, G.F.; Agrawal, P.; Mélo, T.J. Mechanical and morphological properties of PLA/bioPE blend compatibilized with E-GMA and EMA-GMA copolymers. *Macromol. Symp.* 2016, 367, 176-182.
- [49] Agrawal, P.; Alves, A.M.; Brito, G.F.; Cavalcanti, S.N.; Araújo, A.P.; Mélo, T.J. Effect of ethylene-methyl acrylate compatibilizer on the thermo-mechanical, rheological, and morphological properties of poly(lactic acid)/biopolyethylene/clay biocomposites. *Polym. Compos.* 2018, 39, E164-E173.

- [50] Acik, E.; Orbey, N.; Yilmazer, U. Rheological properties of poly(lactic acid) based nanocomposites: Effects of different organoclay modifiers and compatibilizers. *J. Appl. Polym. Sci.* 2016, 133, 42915.
- [51] Sajna, V.; Mohanty, S.; Nayak, S.K. Influence of nanoclay and graft copolymer on the thermal and flammability properties of poly(lactic acid)/banana fiber biocomposites. *J. Vinyl Addit. Technol.* 2017, 23, E81-E91.
- [52] Mohanty, S.; Nayak, S.K. Effect of poly(lactic acid)-graft-glycidyl methacrylate as a compatibilizer on properties of poly(lactic acid)/banana fiber biocomposites. *Polym. Adv. Technol.* 2016, 27, 515-524.
- [53] Khan, B.A.; Na, H.; Chevali, V.; Warner, P.; Zhu, J.; Wang, H. Glycidyl methacrylate-compatible poly(lactic acid)/hemp hurd biocomposites: Processing, crystallization, and thermo-mechanical response. *J. Materi. Sci. Technol.* 2018, 34, 387-397.
- [54] Thanh, C.N.; Chaiwat, R.; Yupaporn, R. In Biocomposites of poly(lactic acid) and cellulose nanofibers from cassava pulp, *Key Engineering Materials*, 2017; Trans Tech Publ: pp 13-17.
- [55] Zhang, B.; Sun, B.; Bian, X.; Li, G.; Chen, X. High melt strength and high toughness PLLA/PBS blends by copolymerization and in situ reactive compatibilization. *Ind. Eng. Chem. Res.* 2016, 56, 52-62.
- [56] Li, S.; Deng, L.; Xu, C.; Wu, Q.; Wang, Z. Making a supertough flame-retardant polylactide composite through reactive blending with ethylene-acrylic ester-glycidyl methacrylate terpolymer and addition of aluminum hypophosphite. *ACS Omega* 2017, 2, 1886-1895.
- [57] Wang, Y.; Wei, Z.; Li, Y. Highly toughened polylactide/epoxidized poly(styrene-*b*-butadiene-*b*-styrene) blends with excellent tensile performance. *Eur. Polym. J.* 2016, 85, 92-104.
- [58] Chang, B.P.; Mohanty, A.K.; Misra, M. Tuning the compatibility to achieve toughened biobased poly(lactic acid)/poly(butylene terephthalate) blends. *RSC Adv.* 2018, 8, 27709-27724.
- [59] Li, X.; Ai, X.; Pan, H.; Yang, J.; Gao, G.; Zhang, H.; Yang, H.; Dong, L. The morphological, mechanical, rheological, and thermal properties of PLA/PBAT blown films with chain extender. *Polym. Adv. Technol.* 2018, 29, 1706-1717.
- [60] Wang, S.; Pang, S.; Pan, L.; Xu, N.; Li, T. Isothermal cold crystallization, heat resistance, and tensile performance of polylactide/thermoplastic polyester elastomer (PLA/TPEE) blends: Effects of annealing and reactive compatibilizer. *Polymers* 2016, 8, 417.
- [61] Yemisci, F.; Aytac, A. Compatibilization of poly(lactic acid)/polycarbonate blends by different coupling agents. *Fiber. Polym.* 2017, 18, 1445-1451.
- [62] Walha, F.; Lamnawar, K.; Maazouz, A.; Jaziri, M. Rheological, morphological and mechanical studies of sustainably sourced polymer blends based on poly(lactic acid) and polyamide 11. *Polymers* 2016, 8, 61.

- [63] Vadori, R.; Misra, M.; Mohanty A.K. Sustainable biobased blends from the reactive extrusion of polylactide and acrylonitrile butadiene styrene. *J. Appl. Polym. Sci.* 2016, 133, 43771.
- [64] Nanthananon, P.; Seadan, M.; Pivsa-Art, S.; Hamada, H.; Suttiruengwong, S. Facile preparation and characterization of short-fiber and talc reinforced poly(lactic acid) hybrid composite with in situ reactive compatibilizers. *Materials* 2018, 11, 1183.
- [65] Battegazzore, D.; Frache, A.; Abt, T.; Maspoch, M.L. Epoxy coupling agent for PLA and PHB copolymer-based cotton fabric bio-composites. *Compos. Part B Eng.* 2018, 148, 188-197.
- [66] Hao, M.; Wu, H.; Qiu, F.; Wang, X. Interface bond improvement of sisal fibre reinforced polylactide composites with added epoxy oligomer. *Materials* 2018, 11, 398.
- [67] Schneider, J.; Manjure, S.; Narayan, R. Reactive modification and compatibilization of poly(lactide) and poly(butylene adipate-co-terephthalate) blends with epoxy functionalized-poly(lactide) for blown film applications. *J. Appl. Polym. Sci.* 2016, 133, 43310.
- [68] Dong, W.; He, M.; Wang, H.; Ren, F.; Zhang, J.; Zhao, X.; Li, Y. PLLA/ABS blends compatibilized by reactive comb polymers: Double  $T_g$  depression and significantly improved toughness. *ACS Sustain. Chem. Eng.* 2015, 3, 2542-2550.
- [69] Qu, Z.; Bu, J.; Pan, X.; Hu, X. Probing the nanomechanical properties of PLA/PC blends compatibilized with compatibilizer and nucleation agent by AFM. *J. Polym. Res.* 2018, 25, 138.
- [70] Qu, Z.; Hu, X.; Pan, X.; Bu, J. Effect of compatibilizer and nucleation agent on the properties of poly(lactic acid)/polycarbonate (PLA/PC) blends. *Polym. Sci. Ser. A* 2018, 60, 499-506.
- [71] Weng, F.; Wang, M.; Koranteng, E.; Ma, N.; Wu, Z.; Wu, Q. Effects of PBA-based polyurethane prepolymer as compatibilizer on the properties of polylactic acid-starch composites. *Starch*, 2018/08/21, doi: 10.1002/star.201800205.
- [72] Gurunathan, T.; Mohanty, S.; Nayak, S.K. Preparation and performance evaluation of castor oil-based polyurethane prepolymer/polylactide blends. *J. Mater. Sci.* 2014, 49, 8016-8030.
- [73] Gurunathan, T.; Chung, J.S.; Nayak, S.K. Reactive compatibilization of biobased polyurethane prepolymer toughening polylactide prepared by melt blending. *J. Polym. Environ.* 2016, 24, 287-297.
- [74] Gurunathan, T.; Nayak, S.K. The influence of reactive organoclay on a biorenewable castor oil-based polyurethane prepolymers toughened polylactide nanocomposites. *Polym. Adv. Technol.* 2016, 27, 1484-1493.
- [75] Lv, S.; Gu, J.; Tan, H.; Zhang, Y. Modification of wood flour/PLA composites by reactive extrusion with maleic anhydride. *J. Appl. Polym. Sci.* 2016, 133, 43295.

- [76] Yatigala, N.S.; Bajwa, D.S.; Bajwa, S.G. Compatibilization improves physico-mechanical properties of biodegradable biobased polymer composites. *Compos. Part A Appl. Sci. Manuf.* 2018, 107, 315-325.
- [77] Hwang, S.W.; Park, D.H.; Kang, D.H.; Lee, S.B.; Shim, J.K. Reactive compatibilization of poly(L-lactic acid)/poly(propylene carbonate) blends: Thermal, thermomechanical, and morphological properties. *J. Appl. Polym. Sci.* 2016, 133, 43388.
- [78] Ali Nezamzadeh, S.; Ahmadi, Z.; Afshari Taromi, F. From microstructure to mechanical properties of compatibilized polylactide/thermoplastic starch blends. *J. Appl. Polym. Sci.* 2017, 134, 44734.
- [79] Bher, A.; Auras, R.; Schvezov, C.E. Improving the toughening in poly(lactic acid)-thermoplastic cassava starch reactive blends. *J. Appl. Polym. Sci.* 2018, 135, 46140.
- [80] Ferri, J.; Garcia-Garcia, D.; Sánchez-Nacher, L.; Fenollar, O.; Balart, R. The effect of maleinized linseed oil (mlo) on mechanical performance of poly(lactic acid)-thermoplastic starch (PLA-TPS) blends. *Carbohydr. Polym.* 2016, 147, 60-68.
- [81] Quiles-Carrillo, L.; Montanes, N.; Sammon, C.; Balart, R.; Torres-Giner, S. Compatibilization of highly sustainable polylactide/almond shell flour composites by reactive extrusion with maleinized linseed oil. *Ind. Crop. Prod.* 2018, 111, 878-888.
- [82] Carbonell-Verdu, A.; Ferri, J.; Dominici, F.; Boronat, T.; Sanchez-Nacher, L.; Balart, R.; Torre, L. Manufacturing and compatibilization of PLA/PBAT binary blends by cottonseed oil-based derivatives. *Express Polym. Lett.* 2018, 12, 808-823.
- [83] Montero de Espinosa, L.; Meier, M.A. Plant oils: The perfect renewable resource for polymer science? *Eur. Polym. J.* 2011, 47, 837-852.
- [84] Gandini, A. Polymers from renewable resources: A challenge for the future of macromolecular materials. *Macromolecules* 2008, 41, 9491-9504.
- [85] Gangireddy, C.S.R.; Hu, Y. Efficient chemical transformations of epoxidized soybean oil to cross-linked polymers by phosphorus-containing nucleophiles and study their thermal properties. *Polym. Degrad. Stabil.* 2017, 140, 156-165.
- [86] Przybytek, A.; Sienkiewicz, M.; Kucińska-Lipka, J.; Janik, H. Preparation and characterization of biodegradable and compostable PLA/TPS/ESO compositions. *Ind. Crop. Prod.* 2018, 122, 375-383.
- [87] Xiong, Z.; Yang, Y.; Feng, J.; Zhang, X.; Zhang, C.; Tang, Z.; Zhu, J. Preparation and characterization of poly(lactic acid)/starch composites toughened with epoxidized soybean oil. *Carbohydr. Polym.* 2013, 92, 810-816.
- [88] Meng, X.; Bocharova, V.; Tekinalp, H.; Cheng, S.; Kisliuk, A.; Sokolov, A.P.; Kunc, V.; Peter, W.H.; Ozcan, S. Toughening of nanocellulose/PLA composites via bio-epoxy interaction: Mechanistic study. *Mater. Des.* 2018, 139, 188-197.
- [89] Garcia-Campo, M.; Quiles-Carrillo, L.; Sanchez-Nacher, L.; Balart, R.; Montanes, N. High toughness poly(lactic acid)(PLA) formulations obtained by ternary blends with

- poly(3-hydroxybutyrate)(PHB) and flexible polyesters from succinic acid. *Polym. Bull.* 2018/08/03, doi: 10.1007/s00289-018-2475-y.
- [90] Orue, A.; Eceiza, A.; Arbelaiz, A. Preparation and characterization of poly(lactic acid) plasticized with vegetable oils and reinforced with sisal fibers. *Ind. Crop. Prod.* 2018, 112, 170-180.
- [91] Awale, R.; Ali, F.; Azmi, A.; Puad, N.; Anuar, H.; Hassan, A. Enhanced flexibility of biodegradable polylactic acid/starch blends using epoxidized palm oil as plasticizer. *Polymers* 2018, 10, 977.
- [92] Dai, X.; Xiong, Z.; Ma, S.; Li, C.; Wang, J.; Na, H.; Zhu, J. Fabricating highly reactive bio-based compatibilizers of epoxidized citric acid to improve the flexural properties of polylactide/microcrystalline cellulose blends. *Ind. Eng. Chem. Res.* 2015, 54, 3806-3812.
- [93] Mihai, I.; Hassouna, F.; Fouquet, T.; Laachachi, A.; Raquez, J.M.; Ibn El Ahrach, H.; Dubois, P. Reactive plasticization of poly(lactide) with epoxy functionalized cardanol. *Polym. Eng. Sci.* 2018, 58, E64-E72.
- [94] Dogan, S.; Boyacioglu, S.; Kodal, M.; Gokce, O.; Ozkoc, G. Thermally induced shape memory behavior, enzymatic degradation and biocompatibility of PLA/TPU blends: Effects of compatibilization. *J. Mech. Behav. Biomed. Mater.* 2017, 71, 349-361.
- [95] Chen, H.; Yu, X.; Zhou, W.; Peng, S.; Zhao, X. Highly toughened polylactide (PLA) by reactive blending with novel polycaprolactone-based polyurethane (PCLU) blends. *Polym. Test.* 2018, 70, 275-280.
- [96] Vuillaume, P.Y.; Vachon, A.; Grey, W.; Pépin, K.; Zhang, C.J. Compatibilisation of various PLA/thermoplastic elastomer blends with diisocyanate coupling agent. *Plast. Rubber Compos.* 2018, 47, 95-105.
- [97] González-Ausejo, J.; Sánchez-Safont, E.; Lagarón, J.M.; Balart, R.; Cabedo, L.; Gámez-Pérez, J. Compatibilization of poly(3-hydroxybutyrate-co-3-hydroxyvalerate)-poly(lactic acid) blends with diisocyanates. *J. Appl. Polym. Sci.* 2017, 134, 44806.
- [98] González-Ausejo, J.; Sanchez-Safont, E.; Lagaron, J.M.; Olsson, R.T.; Gamez-Perez, J.; Cabedo, L. Assessing the thermoformability of poly(3-hydroxybutyrate-co-3-hydroxyvalerate)/poly(lactic acid) blends compatibilized with diisocyanates. *Polym. Test.* 2017, 62, 235-245.
- [99] Visco, A.; Nocita, D.; Giamporcaro, A.; Ronca, S.; Forte, G.; Pistone, A.; Espro, C. Effect of ethyl ester L-lysine triisocyanate addition to produce reactive PLA/PCL bio-polyester blends for biomedical applications. *J. Mech. Behav. Biomed. Mater.* 2017, 68, 308-317.
- [100] Yu, T.; Hu, C.; Chen, X.; Li, Y. Effect of diisocyanates as compatibilizer on the properties of ramie/poly(lactic acid)(PLA) composites. *Compos. Part A Appl. Sci. Manuf.* 2015, 76, 20-27.

- [101] Qin, S.-X.; Yu, C.-X.; Chen, X.-Y.; Zhou, H.-P.; Zhao, L.-F. Fully biodegradable poly(lactic acid)/poly(propylene carbonate) shape memory materials with low recovery temperature based on in situ compatibilization by dicumyl peroxide. *Chin. J. Polym. Sci.* 2018, 36, 783-790.
- [102] Ji, D.; Liu, Z.; Lan, X.; Wu, F.; Xie, B.; Yang, M. Morphology, rheology, crystallization behavior, and mechanical properties of poly(lactic acid)/poly(butylene succinate)/dicumyl peroxide reactive blends. *J. Appl. Polym. Sci.* 2014, 131, 39580.
- [103] Srimalanon, P.; Prapagdee, B.; Markpin, T.; Sombatsompop, N. Effects of DCP as a free radical producer and HPQM as a biocide on the mechanical properties and antibacterial performance of in situ compatibilized PBS/PLA blends. *Polym. Test.* 2018, 67, 331-341.
- [104] Ma, P.; Cai, X.; Zhang, Y.; Wang, S.; Dong, W.; Chen, M.; Lemstra, P. In-situ compatibilization of poly(lactic acid) and poly(butylene adipate-co-terephthalate) blends by using dicumyl peroxide as a free-radical initiator. *Polym. Degrad. Stabil.* 2014, 102, 145-151.
- [105] Dhar, P.; Tarafder, D.; Kumar, A.; Katiyar, V. Thermally recyclable polylactic acid/cellulose nanocrystal films through reactive extrusion process. *Polymer* 2016, 87, 268-282.
- [106] Rigoussen, A.; Verge, P.; Raquez, J.-M.; Habibi, Y.; Dubois, P. In-depth investigation on the effect and role of cardanol in the compatibilization of PLA/ABS immiscible blends by reactive extrusion. *Eur. Polym. J.* 2017, 93, 272-283.
- [107] Vachon, A.; Pépin, K.; Balampanis, E.; Veilleux, J.; Vuillaume, P.Y. Compatibilization of PLA/PEBA blends via reactive extrusion: A comparison of different coupling agents. *J. Polym. Environ.* 2017, 25, 812-827.
- [108] Zhang, L.; Xiong, Z.; Shams, S.S.; Yu, R.; Huang, J.; Zhang, R.; Zhu, J. Free radical competitions in polylactide/bio-based thermoplastic polyurethane/free radical initiator ternary blends and their final properties. *Polymer* 2015, 64, 69-75.
- [109] Ma, P.; Xu, P.; Liu, W.; Zhai, Y.; Dong, W.; Zhang, Y.; Chen, M. Bio-based poly(lactide)/ethylene-co-vinyl acetate thermoplastic vulcanizates by dynamic crosslinking: Structure vs. property. *RSC Adv.* 2015, 5, 15962-15968.
- [110] Ma, P.; Xu, P.; Zhai, Y.; Dong, W.; Zhang, Y.; Chen, M. Biobased poly(lactide)/ethylene-co-vinyl acetate thermoplastic vulcanizates: Morphology evolution, superior properties, and partial degradability. *ACS Sustain. Chem. Eng.* 2015, 3, 2211-2219.
- [111] Kfoury, G.; Raquez, J.M.; Hassouna, F.; Leclère, P.; Toniazzo, V.; Ruch, D.; Dubois, P. Toughening of poly(lactide) using polyethylene glycol methyl ether acrylate: Reactive versus physical blending. *Polym. Eng. Sci.* 2015, 55, 1408-1419.
- [112] Kfoury, G.; Hassouna, F.; Raquez, J.M.; Toniazzo, V.; Ruch, D.; Dubois, P. Tunable and durable toughening of polylactide materials via reactive extrusion. *Macromol. Mater. Eng.* 2014, 299, 583-595.

- [113] Liu, G.-C.; He, Y.-S.; Zeng, J.-B.; Li, Q.-T.; Wang, Y.-Z. Fully biobased and supertough polylactide-based thermoplastic vulcanizates fabricated by peroxide-induced dynamic vulcanization and interfacial compatibilization. *Biomacromolecules* 2014, 15, 4260-4271.
- [114] Valerio, O.; Misra, M.; Mohanty, A.K. Sustainable biobased blends of poly(lactic acid)(PLA) and poly(glycerol succinate-co-maleate)(PGSMA) with balanced performance prepared by dynamic vulcanization. *RSC Adv.* 2017, 7, 38594-38603.
- [115] Hu, X.; Kang, H.; Li, Y.; Geng, Y.; Wang, R.; Zhang, L. Preparation, morphology and superior performances of biobased thermoplastic elastomer by in situ dynamical vulcanization for 3D-printed materials. *Polymer* 2017, 108, 11-20.
- [116] Si, W.-J.; An, X.-P.; Zeng, J.-B.; Chen, Y.-K.; Wang, Y.-Z. Fully bio-based, highly toughened and heat-resistant poly(L-lactide) ternary blends via dynamic vulcanization with poly(D-lactide) and unsaturated bioelastomer. *Sci. China Mater.* 2017, 60, 1008-1022.
- [117] Chen, Y.; Yuan, D.; Xu, C. Dynamically vulcanized biobased polylactide/natural rubber blend material with continuous cross-linked rubber phase. *ACS Appl. Mater. Inter.* 2014, 6, 3811-3816.
- [118] Wang, Y.; Chen, K.; Xu, C.; Chen, Y. Supertoughened biobased poly(lactic acid)-epoxidized natural rubber thermoplastic vulcanizates: Fabrication, co-continuous phase structure, interfacial in situ compatibilization, and toughening mechanism. *J. Phys. Chem. B* 2015, 119, 12138-12146.
- [119] Yuan, D.; Xu, C.; Chen, Z.; Chen, Y. Crosslinked bicontinuous biobased polylactide/natural rubber materials: Super toughness, "net-like"-structure of NR phase and excellent interfacial adhesion. *Polym. Test.* 2014, 38, 73-80.
- [120] Liu, L.; Hou, J.; Wang, L.; Zhang, J.; Duan, Y. Role of dicumyl peroxide on toughening PLLA via dynamic vulcanization. *Ind. Eng. Chem. Res.* 2016, 55, 9907-9914.
- [121] Chen, Y.; Chen, K.; Wang, Y.; Xu, C. Biobased heat-triggered shape-memory polymers based on polylactide/epoxidized natural rubber blend system fabricated via peroxide-induced dynamic vulcanization: Co-continuous phase structure, shape memory behavior, and interfacial compatibilization. *Ind. Eng. Chem. Res.* 2015, 54, 8723-8731.
- [122] Yuan, D.; Chen, Z.; Xu, C.; Chen, K.; Chen, Y. Fully biobased shape memory material based on novel cocontinuous structure in poly(lactic acid)/natural rubber TPVS fabricated via peroxide-induced dynamic vulcanization and in situ interfacial compatibilization. *ACS Sustain. Chem. Eng.* 2015, 3, 2856-2865.
- [123] Chen, Y.; Wang, W.; Yuan, D.; Xu, C.; Cao, L.; Liang, X. Bio-based PLA/NR-PMMA/NR ternary thermoplastic vulcanizates with balanced stiffness and toughness: "Soft-hard" core-shell continuous rubber phase, in situ compatibilization, and properties. *ACS Sustain. Chem. Eng.* 2018, 6, 6488-6496.

- [124] Yuan, D.; Chen, K.; Xu, C.; Chen, Z.; Chen, Y. Crosslinked bicontinuous biobased PLA/NR blends via dynamic vulcanization using different curing systems. *Carbohydr. Polym.* 2014, 113, 438-445.
- [125] Yuan, D.; Chen, Z.; Chen, K.; Mou, W.; Chen, Y. Phenolic resin-induced dynamically vulcanized polylactide/natural rubber blends. *Polym. Plast. Technol. Eng.* 2016, 55, 1115-1123.
- [126] Zhao, T.-H.; He, Y.; Li, Y.-D.; Wang, M.; Zeng, J.-B. Dynamic vulcanization of castor oil in a polylactide matrix for toughening. *RSC Adv.* 2016, 6, 79542-79553.
- [127] He, Y.; Zhao, T.-H.; Li, Y.-D.; Wang, M.; Zeng, J.-B. Toughening polylactide by dynamic vulcanization with castor oil and different types of diisocyanates. *Polym. Test.* 2017, 59, 470-477.
- [128] Zhao, T.-H.; Yuan, W.-Q.; Li, Y.-D.; Weng, Y.-X.; Zeng, J.-B. Relating chemical structure to toughness via morphology control in fully sustainable sebacic acid cured epoxidized soybean oil toughened polylactide blends. *Macromolecules* 2018, 51, 2027-2037.
- [129] Zhao, T.-H.; Wu, Y.; Li, Y.-D.; Wang, M.; Zeng, J.-B. High performance and thermal processable dicarboxylic acid cured epoxidized plant oil resins through dynamic vulcanization with poly(lactic acid). *ACS Sustain. Chem. Eng.* 2017, 5, 1938-1947.
- [130] Lu, X.; Wei, X.; Huang, J.; Yang, L.; Zhang, G.; He, G.; Wang, M.; Qu, J. Supertoughened poly(lactic acid)/polyurethane blend material by in situ reactive interfacial compatibilization via dynamic vulcanization. *Ind. Eng. Chem. Res.* 2014, 53, 17386-17393.
- [131] Zhao, X.; Ding, Z.; Lin, Q.; Peng, S.; Fang, P. Toughening of polylactide via in situ formation of polyurethane crosslinked elastomer during reactive blending. *J. Appl. Polym. Sci.* 2017, 134, 44383.
- [132] Ma, M.; Zheng, H.; Chen, S.; Wu, B.; He, H.; Chen, L.; Wang, X. Super-toughened poly(L-lactic acid) fabricated via reactive blending and interfacial compatibilization. *Polym. Int.* 2016, 65, 1187-1194.
- [133] Spinella, S.; Cai, J.; Samuel, C.; Zhu, J.; McCallum, S.A.; Habibi, Y.; Raquez, J.-M.; Dubois, P.; Gross, R.A. Polylactide/poly( $\omega$ -hydroxytetradecanoic acid) reactive blending: A green renewable approach to improving polylactide properties. *Biomacromolecules* 2015, 16, 1818-1826.
- [134] Wang, Z.; Zhang, M.; Liu, Z.; Zhang, S.; Cao, Z.; Yang, W.; Yang, M. Compatibilization of the poly(lactic acid)/poly(propylene carbonate) blends through in situ formation of poly(lactic acid)-b-poly(propylene carbonate) copolymer. *J. Appl. Polym. Sci.* 2018, 135, 46009.
- [135] Chelghoum, N.; Guessoum, M.; Fois, M.; Haddaoui, N. Contribution of catalytic transesterification reactions to the compatibilization of poly(lactic acid)/polycarbonate blends: Thermal, morphological and viscoelastic characterization. *J. Polym. Environ.* 2018, 26, 342-354.

- [136] Pereira, E.C.L.; da Silva, J.M.F.; Jesus, R.B.; Soares, B.G.; Livi, S. Bronsted acidic ionic liquids: New transesterification agents for the compatibilization of polylactide/ethylene-co-vinyl acetate blends. *Eur. Polym. J.* 2017, 97, 104-111.
- [137] Gug, J.; Sobkowicz, M.J. Improvement of the mechanical behavior of bioplastic poly(lactic acid)/polyamide blends by reactive compatibilization. *J. Appl. Polym. Sci.* 2016, 133, 43350.
- [138] Gug, J.; Soule, J.; Tan, B.; Sobkowicz, M.J. Effects of chain-extending stabilizer on bioplastic poly(lactic acid)/polyamide blends compatibilized by reactive extrusion. *Polym. Degrad. Stabil.* 2018, 153, 118-129.

## **Chapter 2 Materials, Experiment and Characterization**

### **2.1 Materials**

Poly(lactic acid) (PLA, Ingeo 3001D) was obtained from NatureWorks Japan (Tokyo, Japan). Epoxidized soybean oil (ESO) with an average molar ratio of epoxy group/ESO of 4 mol was purchased from Aladdin Industrial Corporation (Shanghai, China). Bamboo fibers (BFs) with an average particle size of 126  $\mu\text{m}$  were given by Fujian HBS Chemical Technology (Fujian, China). Multi-walled carbon nanotubes (CNTs) (NANOCYL® NC7000™) with an average diameter of 9.5 nm and an average length of 1.5  $\mu\text{m}$  were obtained from Nanocyl Japan (Chiba, Japan). Boron trifluoride ethylamine complex ( $\text{BF}_3\text{NH}_2\text{Et}$ , > 99.9%) was purchased Sigma-Aldrich (Tokyo, Japan). Tannic acid (TA) with a molar ratio of  $-\text{OH}$  group/TA of 25 mol, Chloroform (> 99.9%), and acetone were obtained from Nacalai Tesque, INC (Tokyo, Japan). All the chemicals were used without further purification.

### **2.2 Preparation of PLA-based blends and composites**

The dynamic vulcanization process of PLA-based products was carried out on a twin-screw extruder (Technovel Corporation Japan, KZW25TW-60MG-NH (-1200)-AKT). The temperatures in six zones were set at 150, 160, 170, 170, 180, and 180 °C from feeding zone to die section, respectively; the screw speed was constantly maintained at 50 r/min. The extruded PLA-based blends were quenched in a water bath, chopped into pellets, and then oven-dried at 80 °C for 12 h for injection molding. Dumbbell and rectangular samples were prepared on an injection molding machine (Nissei Plastic Industrial, Japan, NP7-1F). The nozzle temperature, injection speed, mold temperature, and cooling time were 170 °C, 17.6 mm/s, 40 °C, and 40 s, respectively.

## 2.3 Characterization

### 2.3.1 Measurement of gel fraction

The PLA-based blend with a weight ( $m_1$ ) of about 2 g was immersed in chloroform (40 mL) for 24 h to dissolve PLA and uncrosslinked ESO molecules. The insoluble part was isolated via centrifugation, and further purified with chloroform for 2 times and acetone for 3 times. After being vacuum-dried at 50 °C for 12 h, the gel was weighted as  $m_2$ . The gel fraction ( $G_f$ ) of the crosslinked ESO was calculated as the [Equation 2-1](#),

$$G_f = \frac{m_2}{w_{\text{ESO phase}} \times m_1} \times 100\% \quad (2-1)$$

where  $w_{\text{ESO phase}}$  is the weight fraction of ESO phase in the blends.

### 2.3.2 Fourier transform infrared spectroscopy (FTIR)

FTIR experiments were carried out on a Nicolet iN10 FTIR spectrometer (Thermo Fisher Scientific, MA, USA) over a scanning range from 4000 to 400  $\text{cm}^{-1}$  at a spectral resolution of 4  $\text{cm}^{-1}$ . The solid sample was powdered and mixed with KBr, and then the obtained mixture was pressed at 15 MPa to generate pellets for analysis. The liquid sample was coated on the surface of a neat KBr pellet for analysis.

### 2.3.3 X-ray photoelectron spectroscopy (XPS)

XPS experiments were performed on a PHI 5000 Series XPS instrument (ULVAC-PHI, Kanagawa, Japan) equipped with Al  $K\alpha$  radiation source. Atomic high-resolution spectra were run with a pass energy of 70.0 eV and an increment of 0.2 eV. The obtained C1s spectra were resolved with the software of XPS Peak 4.0 (The Chinese University of Hong Kong, Hong Kong, China).

### 2.3.4 Nuclear magnetic resonance (NMR)

The soluble PLA part in chloroform from gel fraction measurements was precipitated by using excess acetone. After washing with acetone for 3 times, the

obtained precipitates were used for  $^1\text{H}$  NMR analysis on an Avance III 500 NMR spectrometer (Bruker, MA, USA) with  $\text{CDCl}_3$  as a solvent and tetramethylsilane (TMS) as an internal chemical shift standard.

### 2.3.5 Gel permeation chromatography (GPC)

Molecular weight distributions of the PLA blends were determined using a Tosoh EcoSEC HLC-8320GPC instrument (Tokyo, Japan) equipped with RI and UV detectors. The specimen concentration was 2 mg/mL in chloroform, and an injection volume of 20 mL was used with a flow rate of 1.0 mL/min. The GPC system was calibrated with polystyrene standards ranging from 495 to 1,090,000 g/mol.

### 2.3.6 Differential scanning calorimetry (DSC)

DSC analyses were performed on a STA 449 F3 Jupiter Simultaneous Thermal Analyzer (NETZSCH, Selb, Germany). Samples with a weight of 5–10 mg was placed in a standard porcelain crucible with a lid. The tests were conducted from 25 to 210 °C with a heating rate of 10 °C/min under  $\text{N}_2$  (flow rate: 30 mL/min). The glass transition temperature ( $T_g$ ), cold crystallization peak ( $T_{cc}$ ), and melt peak temperature ( $T_m$ ) of the PLA products were obtained from the DSC curves. The degree of crystallinity ( $X_c$ ) for PLA was calculated as the [Equation 2-2](#) [36]:

$$X_c = \frac{\Delta H_m - H_{cc}}{\Delta H_{100} \times x_{\text{PLA}}} \times 100 \quad (2-2)$$

where  $\Delta H_m$  and  $\Delta H_{cc}$  are the melting and cold crystallization enthalpies, respectively;  $\Delta H_{100}$  is the theoretical melting enthalpy of a completely crystalline PLA (93.6 J/g), and  $x_{\text{PLA}}$  is the weight fraction of PLA in the products.

### 2.3.7 Dynamic mechanical analysis (DMA)

Rectangular samples ( $55 \times 10 \text{ mm}^2$ ) of the blends were prepared for DMA tests on a RSA-G2 solids analyzer (TA Instrument, DE, USA) under three point bending mode with a strain of 0.1%. The tests were conducted from 30 to 100 °C at a heating rate of 2 °C/min and a frequency of 1 Hz.

### **2.3.8 Thermogravimetric (TG) analysis**

TG analysis was conducted on a DTG-60 TG instrument (Shimadzu, Japan). Samples with a weight of 4–6 mg were placed in aluminum crucibles. The tests were performed from room temperature to 600 °C at a scan rate of 10 °C/min under N<sub>2</sub> atmosphere at a flow rate of 50 mL/min.

### **2.3.9 Tensile testing**

A Series 3360 universal testing machine (Instron, MA, USA) was used to evaluate the tensile properties of the PLA blends in accordance with ASTM D 638-10. Dumbbell specimens with 25 mm gauge length, 2 mm thickness, and 5 mm narrow section width were used for the test at a crosshead speed of 10 mm/s. Five replicates were conducted for each sample.

### **2.3.10 Impact testing**

Notched Izod impact strength was measured using rectangular samples (80 × 10 × 4 mm<sup>3</sup>) on a Toyoseiki IT impact tester (Tokyo, Japan) at room temperature according to ASTM D 256-10. Five measurements were conducted for each sample.

### **2.3.11 Electrical properties**

The volume electrical conductivity of rectangular specimens was measured on a double loop resistance meter (UPMCP-HT450, Mitsubishi Chemical Cooperation, Tokyo, Japan). Five replicates were conducted for each nanocomposite.

### **2.3.12 Scanning electron microscope (SEM)**

The SEM images of the samples were obtained from a JEOL JSM-7500F SEM (JEOL, Tokyo, Japan) at an accelerating voltage of 4.0 kV. Before testing, specimens were coated with an elemental gold film (8–10 nm). The particle size distributions on the surfaces were measured using Nano Measurer 1.2.5 Software (Fudan University, Shanghai, China). At least 200 particles were measured for each blend.

### **2.3.13 Transmission electron microscopy (TEM)**

The TEM images of the samples were obtained from a Tecnai G2 F30 TEM (FEI, Oregon, USA). For TEM analysis, ultrathin samples (~100 nm) were cryogenically cut at a temperature of  $-80^{\circ}\text{C}$  using a Leica EM UC7 ultramicrotome (Leica Microsystems K.K., Tokyo, Japan).

## **Chapter 3 Cationic Polymerization of Epoxidized Soybean Oil for Toughening PLA via Dynamic Vulcanization**

### **3.1 Introduction**

Sustainable polymers derived from renewable resources have been widely developed to replace their petroleum-based counterparts due to the ever-increasing environmental issues and depletion of oil resources. Triglyceride-based vegetable oils (VOs) are considered to be ideal feedstocks for producing sustainable polymers. VOs are composed of glycerol esters with saturated and unsaturated fatty acids, where the carried functional groups, such as esters and C=C bonds, enable formulation of various VO-based polymers through different chemical modification routes [1-3]. Epoxidized soybean oil (ESO) is derived from soybean oil via epoxidation of the C=C bonds, and it has been commercialized in the preparation of biobased polymers [4-7]. The replacement of ESO to nonrenewable diglycidyl ether of bisphenol A in forming epoxy resins were generally performed by using amines, acids, and anhydrides as curing agents; however, the use of petroleum-based hardeners sacrifices the sustainability of the resulting ESO-based resins [8-12]. Fully sustainable ESO thermosets can be formulated by directly cationic polymerization or curing with renewable hardeners including tannic acid and citric acid, while the obtained ESO resins exhibited poor mechanical strength, toughness and thermal resistance [13-16]. For instance, the tensile strength of citric acid-cured ESO resins was only around 0.6 MPa, and its glass transition temperature ranged from 0 to 30°C [13]. In addition, this kind of materials is three-dimensional crosslinking structure and hence cannot be recycled after curing, which is the main drawback of thermosets.

Due to its attractive advantages such as high strength, easy processability, and biodegradability, PLA has been applied in many areas including packaging materials [17-21]. The brittle nature of PLA is the key barrier for its broader application. Incorporation of VO derivatives, including ESO [22,23], acrylated ESO [24], epoxidized palm oil [25], maleinized hempseed oil [26], maleinized linseed oil [27],

maleinized and epoxidized cottonseed oils [28,29], and modified fatty acids [30], as plasticizers into PLA could greatly increase the toughness of the resulting PLA blends. However, the VO derivatives are immiscible with PLA and might leach or migrate to the surface of PLA products when in use; thus, sufficient toughening efficiency is not achievable for the products. The introduction of a PLA star polymer with acrylated ESO core into soybean oil/PLA blends significantly increased the compatibility between soybean oil and PLA and hence tensile properties of the blends [31]. The tensile toughness of the blends from polymerized soybean oil and PLA was greatly improved by using poly(isoprene-*b*-L-lactide) block copolymer as a compatibilizer [32]. Dynamic vulcanization technique is an efficient and easy way in improving compatibility of two-phase blends [33]. The dynamic vulcanization of PLA with castor oil by using diisocyanates as crosslinkers generated a tough blend with superior toughness and mechanical strength [34,35]; however, the toxic isocyanates is highly undesired for being used as vulcanizing agents.

To simultaneously endow the ESO-based thermosets with thermal processability and improve the toughness of PLA products, sebacic acid-cured ESO resins with high performance and thermoplasticity were formulated via dynamic vulcanization with PLA [36]. It was concluded that the incorporation of crystalline thermoplastics, such as PLA [37], poly(butylene succinate) [38], and castor oil-based polyamide [39], into ESO resins significantly enhanced the mechanical strength and toughness, and thermal stability of the resins. Inspired by these studies, the present chapter aimed at developing fully biobased and thermally remoldable ESO/PLA products in a large-scale production via twin-screw extrusion. Cationic polymerization of ESO was selectively utilized during melt-compounding with PLA, which would generate a stable phase-separated structure while maintaining the sustainability of the resulting ESO/PLA products. The reaction mechanism, tensile properties, dynamic mechanical properties, rheological properties, crystallization behavior, thermal stability, and morphologies of the sustainable blends were discussed in details.

## 3.2 Experimental section

### 3.2.1 Materials

PLA (Ingeo 3001D) was purchased from NatureWorks Japan (Tokyo, Japan). ESO ( $\geq 99.5\%$ ) containing averagely 4 epoxy groups per molecule was obtained from Aladdin Industrial Corporation (Shanghai, China). Boron trifluoride ethylamine complex ( $\text{BF}_3\text{NH}_2\text{Et}$ ,  $> 99.9\%$ ) was purchased Sigma-Aldrich (Tokyo, Japan). Chloroform ( $> 99.9\%$ ) was obtained from Nacalai Tesque, INC (Tokyo, Japan). All the chemicals were used without further purification.

### 3.2.2 Preparation of PESO/PLA blends

ESO was blended with 1 wt%  $\text{BF}_3\text{NH}_2\text{Et}$  (based on the weigh of ESO) with a vigorous stirring for 5 min. PLA pellets were oven-dried at  $80^\circ\text{C}$  for 12 h and then mixed with the obtained ESO mixture at weigh ratios of 90:10, 80:20, 70:30, and 60:40 (PLA:ESO), respectively. The melt-compounding of PLA with ESO was performed on a twin-screw extruder (KZW25TW-60MG-NH(-1200)-AKT, Technovel Corporation, Osaka, Japan). The temperatures in six zones were 150, 160, 170, 170, 180, and  $180^\circ\text{C}$  from feeding zone to die section, respectively; the screw speed was constantly kept at 50 r/min. The extruded polymerized ESO/PLA (PESO/PLA) blends were quenched in a water bath, chopped into pellets, and then oven-dried at  $80^\circ\text{C}$  for 12 h for injection molding. Standard samples were prepared on an injection molding machine (NP7-1F, Nissei Plastic Industrial, Nagano, Japan). The nozzle temperature, injection speed, mold temperature, and cooling time were  $170^\circ\text{C}$ , 17.6 mm/s,  $40^\circ\text{C}$ , and 40 s, respectively. For comparison, neat PLA was also melt-extruded and injected into samples for evaluation under same conditions. The obtained PESO/PLA blends containing 10, 20, 30, and 40 wt% PESO were abbreviated to 10PESO, 20PESO, 30PESO, and 40PESO, respectively.

### 3.2.3 Characterization

The PESO/PLA blends with a weight ( $m_1$ ) of about 1 g was immersed in

chloroform (40 mL) for 24 h to dissolve PLA and uncrosslinked ESO molecules. The insoluble part was isolated via centrifugation and purified with chloroform for 3 times. After being vacuum-dried at 50°C for 12 h, the gel was weighted as  $m_2$ . The gel fraction ( $G_f$ ) of the blend was calculated as the Equation 3-1,

$$G_f = \frac{m_2}{x_{\text{ESO}} \times m_1} \times 100\% \quad (3-1)$$

where  $x_{\text{ESO}}$  is the weight fraction of ESO in the blends.

Differential scanning calorimetry (DSC) analyses were conducted on a STA 449 F3 Jupiter Simultaneous Thermal Analyzer (NETZSCH, Selb, Germany). Samples with a weight of 5–10 mg was placed in a standard porcelain crucible with a lid and was tested under  $\text{N}_2$  (flow rate: 30 mL/min). The temperatures were ranged from 25 to 210°C with a heating rate of 10 °C/min. The glass transition temperature ( $T_g$ ), cold crystallization peak ( $T_{cc}$ ), and melt peak temperature ( $T_m$ ) were obtained from the DSC curves. The degree of crystallinity ( $X_c$ ) for PLA was calculated from the following equation [40]:

$$X_c = \frac{\Delta H_m - H_{cc}}{\Delta H_{100} \times x_{\text{PLA}}} \times 100 \quad (3-2)$$

where  $\Delta H_m$  and  $\Delta H_{cc}$  are the melting and cold crystallization enthalpies of the blends, respectively;  $\Delta H_{100}$  is the theoretical melting enthalpy of a completely crystalline PLA (93.6 J/g), and  $x_{\text{PLA}}$  is the weight fraction of PLA in the blends.

Rheological behavior was measured on a HAAKE MARS III rotational rheometer (Thermo Electron, MA, USA) equipped with a PP35Ti parallel plate (gap: 0.105 mm); the tests were performed in dynamic frequency sweep mode in the frequency range of 0.1–100 Hz with an oscillation strain of 1.0% at 190°C.

Dynamic mechanical analysis (DMA) tests were conducted on a RSA-G2 solids analyzer (TA Instrument, DE, USA) under three point bending mode with a strain of 0.1%. Rectangular samples ( $55 \times 10 \text{ mm}^2$ ) were used for the tests from 30 to 100°C at a heating rate of 2 °C/min and a frequency of 1Hz.

Thermogravimetric (TG) analyses were carried out using a DTG-60 TG instrument (Shimazu, Japan). Samples (4–6 mg) were placed in aluminum crucibles

with an empty aluminum crucible as reference. The tests were conducted from room temperature to 600°C at a heating rate of 10 °C/min in N<sub>2</sub> atmosphere with a flow rate of 50 mL/min.

Tensile properties of the blends were evaluated on a universal testing machine (Instron, Series 3360, MA, USA) with a crosshead speed of 10 mm/s at room temperature. Dumbbell specimens with 25 mm gauge length, 2 mm thickness, and 5 mm narrow section width were used for the test based on ASTM D 638-10. Five replicate tests were taken for each blend.

Scanning electron microscope (SEM) images of the tensile-fractured and cryo-fractured surfaces of the blends were obtained from a JEOL JSM-7500F SEM (JEOL, Tokyo, Japan) at an accelerating voltage of 4.0 kV. Specimens were coated with a gold film (8 to 10 nm) before testing.

### 3.3 Results and discussion

#### 3.3.1 Dynamic crosslinking of ESO in PLA matrix

During the melt-compounding of PLA with ESO, the cationic polymerization of ESO would occur with the initiation of BF<sub>3</sub>NH<sub>2</sub>Et and hence generate a stable PESO phase inside PLA blends. As presented in Figure 3-1, the protons provided by BF<sub>3</sub>NH<sub>2</sub>Et would attach on the epoxy rings of ESO, leading the rings to open to perform the cationic polymerization of ESO; the polymerization could occur in the intra-molecular and inter-molecular epoxy rings [41]. Theoretically, two secondary

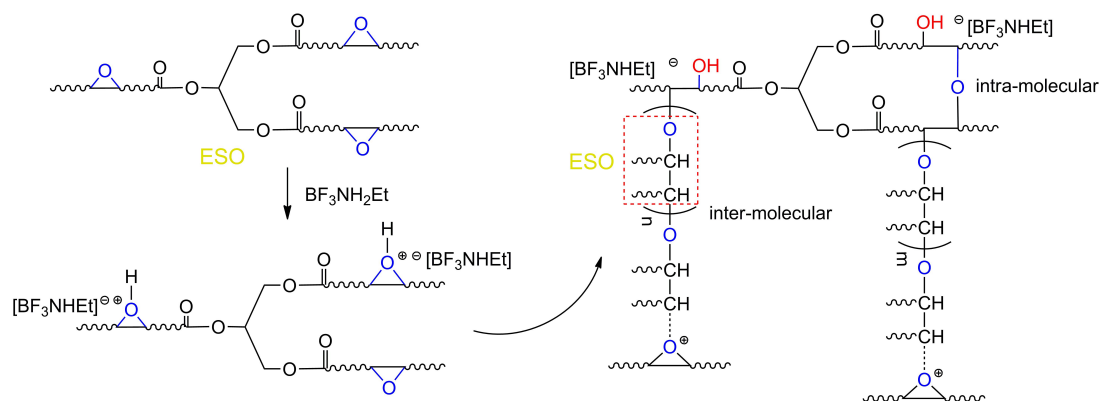


**Figure 3-1** Proposed cationic polymerization of ESO initiated by BF<sub>3</sub>NH<sub>2</sub>Et

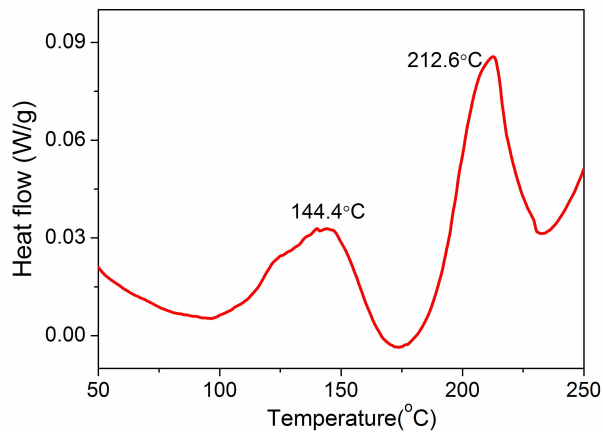


**Figure 3-2** DSC curve of polymerization process of ESO initiated by  $\text{BF}_3\text{NH}_2\text{Et}$

reactions might occur: 1) the newly generated  $-\text{OH}$  groups function as a ring-opening agent for epoxy groups of ESO, further facilitating the self-polymerization of ESO molecules; 2) the epoxy rings of ESO might react with the terminal  $-\text{OH}$  or  $-\text{COOH}$  groups of PLA at high temperature [42], which would contribute to an improved interfacial adhesion between the PESO phase and PLA matrix. The cationic polymerization of ESO initiated with  $\text{BF}_3\text{NH}_2\text{Et}$  was monitored by DSC analysis (Figure 3-2). There were two main exothermic peaks at 144.4 and 212.6°C in the DSC curve, which correspond to the catalyzed homopolymerization of ESO and the uncatalyzed reaction, respectively [43]. Therefore, the curing of ESO could occur to generate the PESO with an incompletely network during the melt-compounding process because the processing temperature (180°C) was much higher than the first curing temperature but lower than the high curing temperature. This was confirmed by the gel fractions of the blends, which are 63%, 59%, 54%, and 44%, respectively, for 10PESO, 20PESO, 30PESO, and 40PESO.

### 3.3.2 Crystallization behavior of PESO/PLA blends

Three thermal transitions were observed in the DSC thermograms of PESO/PLA blends (Figure 3-3 and Table 3-1). For neat PLA, the glass transition temperature ( $T_g$ ) was 61.2°C; the cold crystallization temperature ( $T_{cc}$ ) located at 101.1°C was ascribed to cold crystallization process; finally, the melting process of crystalline PLA phase showed a single melting peak at 170.2°C (melting temperature,  $T_m$ ). After the

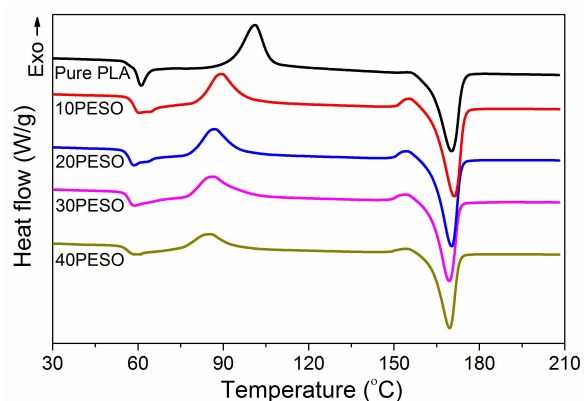


**Figure 3-3** DSC curves of PESO/PLA blends

**Table 3-1** DSC results of PESO/PLA blends

References	$T_g$ (°C)	$T_{cc}$ (°C)	$T_m$ (°C)	$\Delta H_{cc}$ (J/g)	$\Delta H_m$ (J/g)	$X_c$ (%)
Pure PLA	61.2	101.1	170.2	23.7	37.8	15.0
10PESO	60.8	90.2	168.9	20.0	43.3	27.8
20PESO	58.7	87.8	168.1	17.7	39.1	28.8
30PESO	58.9	87.8	167.5	15.8	35.9	30.9
40PESO	58.8	85.9	167.6	12.2	31.9	35.5

incorporation of PESO, the  $T_{cc}$ s of the blends shifted to much lower temperatures (85.9–90.2°C) when compared to pure PLA, indicating a significantly improved crystallization rate; the  $T_{cc}$ s of the blends decreased as the increasing PESO content. This is attributed to the nucleation effect of the added PESO, i.e., the PESO particles give additional heterogeneous nucleation sites for the crystallization of PLA. The cold crystallization enthalpy ( $\Delta H_{cc}$ ) of the blends continuously decreased from 23.7 to 12.2 J/g with the increase of PESO usage, which is due to the reduced PLA component in the blends that is able to recrystallize with increased temperature. This also resulted in significantly reduced  $T_m$ s of the blends after the addition of PESO.

In addition, the 10PESO exhibited a much higher melting enthalpy ( $\Delta H_m$ ) than neat PLA, which was in agreement with the significantly increased crystallinity ( $X_c$ ) from 15.0% for pure PLA to 27.8% for 10PESO due to the nucleation effect of separated PESO phase. The  $X_c$ s of the blends slightly increased from 27.8 to 35.5% with the increase of PESO usage from 10 to 40 wt%. However, further increase in PESO content led to slight reductions in the  $\Delta H_m$  due to the reduced crystalline PLA phase in the blends, and the  $\Delta H_m$ s of the blends were lower than that of neat PLA

when the PESO usage increased up to 30 wt%. Furthermore, the  $T_g$ s of the blends showed a decreasing trend with the incorporation of PESO because the PESO has a much lower  $T_g$  (17°C) than that of PLA [37]. Also, the ESO monomers with a much low molecular weight might diffuse inside the PLA matrix and exist between the PLA molecular chains in the form of PESO, which would increase the distance between polymer chains and thus increase the free volume that makes the molecular chains move at lower temperatures [29].

### 3.3.3 Rheological behavior of PESO/PLA blends

The rheological properties of PESO/PLA blends at 190°C as functions of frequency are given in Figure 3-4. The effect of PESO content on the viscosity and shear-shinning behavior of the blends were revealed from the dependence of complex viscosity ( $|\eta^*|$ ) versus frequency (Figure 3-4a). The  $|\eta^*|$ s of the blends at low frequency increased with the increase of PESO content. Regarding the  $|\eta^*|$ s of pure

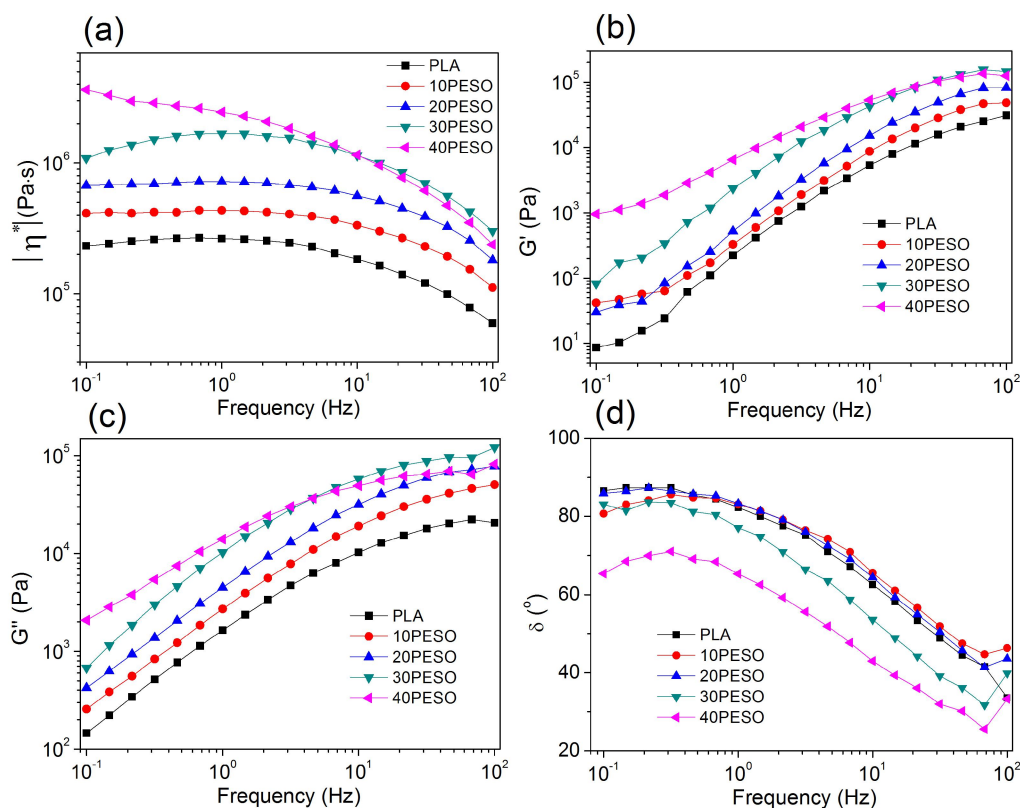


**Figure 3-4** Dependence of (a) complex viscosity, (b) storage modulus, (c) loss modulus, and (d) phase angle ( $\delta$ ) of PESO/PLA blends at 190°C as functions of frequency

PLA and the blends with 10–30 wt% PESO, an obvious Newtonian plateau was seen at middle frequency range and a significant decrease was observed at high frequency region; the  $|\eta^*|$  of 40PESO reduced with the increasing frequency, i.e., a frequency-dependent viscosity, indicating a non-Newtonian flow behavior at low frequency area. Similar results were reported for the PLA blends with a castor oil-derived polyurethane [34].

Both storage modulus ( $G'$ ) and loss modulus ( $G''$ ) of the blends showed an increased tendency as the increase of PESO usage in the full frequency range, excluding the  $G'$  and  $G''$  of 40PESO at high frequency region (Figure 3-4bc). The  $G'$  represents the elasticity of microstructure, and the  $G''$  shows the molecular mobility in molten state. The increase in  $G'$  indicates enhanced elastic strength of the melt, while the increased  $G''$  demonstrates decreased molecular chain mobility, which shows a solid-like behavior of the blends. This is consistent with the increased  $|\eta^*|$ s of the blends after the incorporation of PESO. The incorporated PESO in PLA matrix is a crosslinked polymer with a three-dimensional network; and the formed network with frozen molecular chains would entangle with PLA molecules, hence restricting the mobility of PLA molecular chains and increasing the melting strength.

More information on the formation of crosslinked PESO phase in PLA matrix can be obtained from the change in phase angle ( $\delta$ ) of the blends with frequency (Figure 3-4d). Overall, the  $\delta$  values of the blends decreased as the increasing frequency, indicating a terminal behavior of a liquid-like material. The  $\delta$  values of 10PESO and 20PESO were comparable with that of neat PLA; further increase in PESO usage to 30 and 40 wt% resulted in continuously reduced  $\delta$  values of the blends at full frequency range. With the increase of PESO content, the  $\delta$  values of the blends were less frequency-dependent, which indicates a transition of the blends from liquid-like to gel-like behavior.

### 3.3.4 Dynamic mechanical properties of PESO/PLA blends

The storage modulus ( $E'$ ), loss modulus ( $E''$ ) and damping parameter ( $\tan \delta$ ) of PESO/PLA blends were obtained by DMA analysis (Figure 3-5 and Table 3-2). The

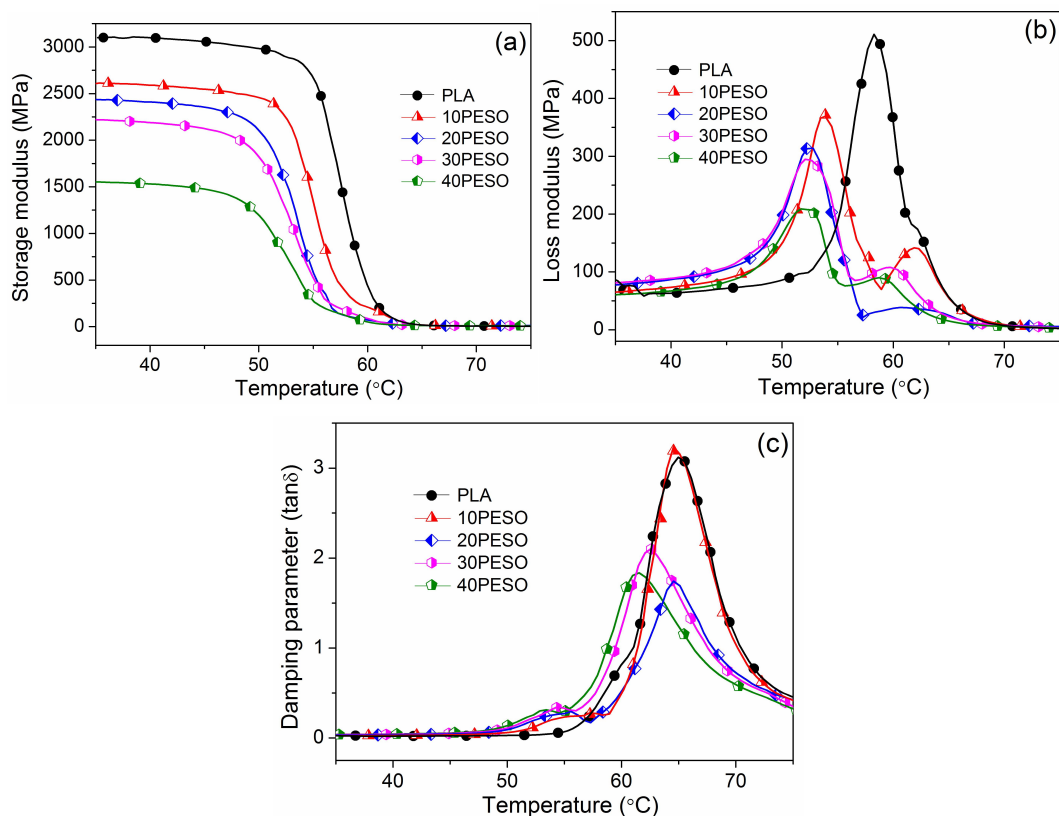


**Figure 3-5** DMA curves of PESO/PLA blends. (a) Storage modulus; (b) loss modulus; (c) damping parameter

**Table 3-2** DMA results of PESO/PLA blends

Reference	Storage modulus at 35°C (GPa)	Peak temperature from loss modulus (°C)		$T_g$ from $\tan \delta$ (°C)
		Peak 1	Peak 2	
Pure PLA	3.19	58.2	-	65.0
10PESO	2.96	53.7	62.1	64.7
20PESO	2.60	52.6	61.0	64.6
30PESO	2.31	52.2	59.7	62.5
40PESO	1.57	52.1	58.9	61.4

$E'$  curves of all the blends were identical in shape, showing a flat plot from room temperature to 50°C and then a dramatic decrease at temperatures of 50–65°C due to glass transition behavior. The  $E'$  of neat PLA in the initial stage was 3.19 GPa, which decreased to 1.57–2.96 GPa for PESO/PLA blends due to the incorporation of PESO with a much lower modulus; the  $E'$ s of the blends reduced with the increase of PESO usage. The incorporated PESO phase with a superior compatibility with PLA matrix might destroy the dense arrangement of PLA molecules in the amorphous region,

hence leading to reduced  $E'$ 's of the blends [42].

The  $E''$  of neat PLA, showing the ability of the material to dissipate energy, showed a peak at 58.2°C because of the mobility of polymer molecules, which shows the glass transition behavior of the polymers from another perspective. The transition temperatures of the blends decreased to lower temperatures after the addition of PESO phase due to their plasticizing effects, which is in accordance with the change in the  $T_g$  from DSC tests. A small shoulder in the  $E''$  curve at high temperature was seen for pure PLA, which corresponds to the chain rearrangement of oriented amorphous regions into crystalline phase [44]. The introduction of PESO phase into PLA blends resulted in obvious  $E''$  peaks after glass transition; the peak temperatures showed a decreasing trend with the increased PESO concentration. This is because the PESO could promote the segmental movements of mobile and amorphous regions.

The  $\tan \delta$ , calculated from the ratio of  $E''$  to  $E'$ , indicates the ratio of energy lost to energy retained in the loading cycle. The  $\tan \delta$  peak of neat PLA was sharp and intensive, while the PESO/PLA blends have lower height and higher width of the  $\tan \delta$  peak excluding 10PESO. The temperature at the  $\tan \delta$  peak was usually defined as the  $T_g$  of a material. The  $T_g$  of neat PLA was 65.0°C, which was slightly higher than the value determined by DSC scan due to the different basal theories of these two technologies. The  $T_g$ s of the blends decreased to 61.4–64.7°C as the increase of PESO usage from 10 to 40 wt%, which are associated with the molecular composition and structure of the blends as discussed in crystallization behavior of PESO/PLA blends.

### 3.3.5 Thermal stability of PESO/PLA blends

The thermal degradation behaviors of neat PLA, PESO and their blends were shown in [Figure 3-6](#). For briefly, the 10PESO and 30PESO were omitted. It is observed that pure PESO exhibited a  $T_{max}$  of 401.5°C, which was much higher than that of neat PLA (363.4°C). The thermal decomposition of polymers involves the cleavage of functional groups including C–C, C–O, and C=O bonds. The PESO phase with aliphatic chains presents higher thermal stability than the PLA chains featured by ester groups, which results in the increased thermal stability of PESO with regard to

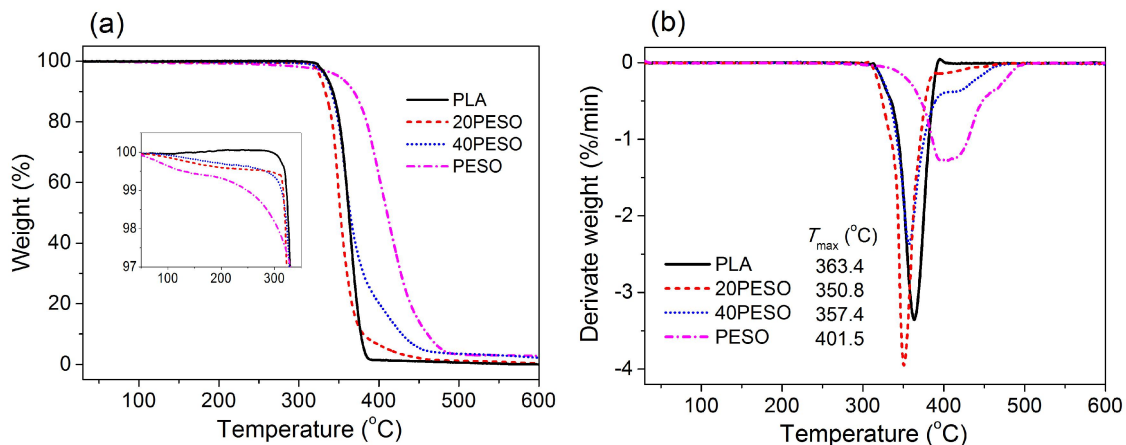


**Figure 3-6** TG and DTG curves of PESO/PLA blends

PLA. However, the incorporation of 20 wt% PESO into PLA blends significantly reduced the  $T_{max}$  of the blends. This is opposite to the fact that epoxidized vegetable oils have been normally used as thermal stabilizers in PLA products because their oxirane rings can scavenge acid groups from PLA by thermal decomposition [25, 27, 45]. As presented in Figure 3-1, the ring opening reaction of ESO generate the PESO with ether linkages and –OH groups that are sensitive to thermal decomposition. This is evidenced by the higher initial degradation rate of PESO than PLA when the temperature was lower than 330°C, as shown in the magnified TG curves in Figure 3-6a. However, a significant increment in the  $T_{max}$  was observed for 40PESO when compared to 20PESO. In this case, the decomposition of the main compositions of PESO, i.e., aliphatic chains play a more important role than the ether bonds and –OH groups that affect the thermal degradation of the 40PESO.

### 3.3.6 Tensile properties of PESO/PLA blends

The stress-strain curves of PESO/PLA blends are given in Figure 3-7. A typical brittle fracture behavior was observed for pure PLA, while all the PESO/PLA blends presented an obviously ductile character, i.e., more stable neck growth with the increased PESO contents. The tensile strength, tensile modulus, elongation at break, and tensile toughness (the area of stress-strain curve) of the blends are shown in Figure 3-8. Rigid PLA has high tensile strength and tensile modulus of 63.2 MPa and 1.5 GPa, respectively, with very low elongation at break and tensile toughness of 10%

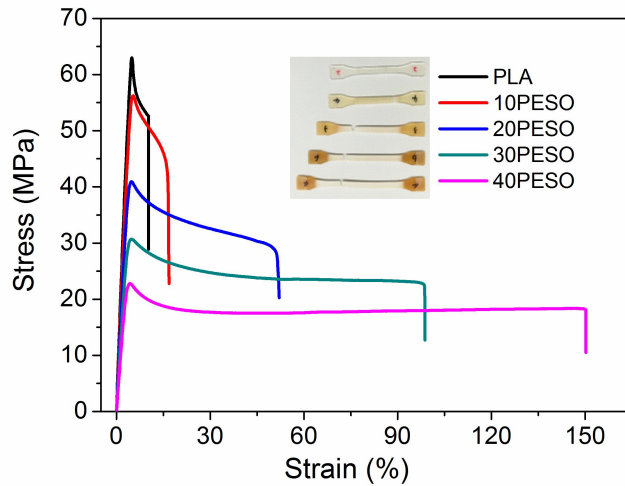


**Figure 3-7** Stress-strain curves of PESO/PLA blends

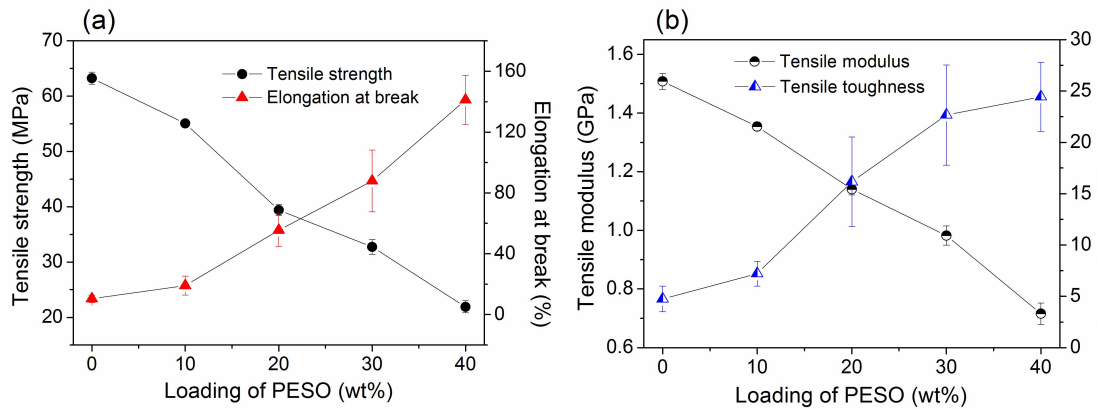


**Figure 3-8** Tensile properties of PESO/PLA blends

and 4.8 MJ/m<sup>3</sup>. It is reported that the tensile strength and elongation at break of PESO polymerized with a thermally latent cationic catalyst as initiator were only 1.2 MPa and 13%, respectively, which is resulted from the short crosslink structure between two molecules [37]. However, the combination of both brittle PESO and PLA resulted in the PESO/PLA blends with significantly enhanced flexibility. The elongation at break and tensile toughness of 10PESO blend were increased by 84% and 52% to 19% and 7.2 MJ/m<sup>3</sup>, respectively, compared to neat PLA. Further increase PESO usage from 20 to 40 wt% resulted in considerable and continuous improvements in elongation at break and tensile toughness to 56–141% and 16.2–24.4 MJ/m<sup>3</sup>, respectively. The 40PESO blend achieved 12.5 and 4.1 times higher elongation at break and tensile toughness than those of pure PLA, respectively. The toughness of the PESO/PLA blends is closely correlated with the ratio of compositions and their

interfacial compatibility. The polymerization of ESO would accelerate the formation of a stable PESO rubbery phase in the PLA blends, and improve the interfacial adhesion between the PESO phase with PLA matrix through the possible reaction between PESO and PLA. However, a decreased situation was observed in both tensile strength and modulus after the incorporation of PESO into the PLA blends due to the relatively lower rigidity of PESO. The tensile strength and modulus of the blends dramatically decreased to 21.9–55.1 MPa and 0.71–1.35 GPa, respectively, depending on the usage of PESO. Also, the added PESO might diffuse into PLA amorphous area and interact with PLA molecular segments via possible covalent bonding, hydrogen bonding, and Van der Waals force [46], which would destroy the interactions between PLA molecular chains, reduce the molecular density of PLA, and thus result in decreased tensile strength and modulus.

### 3.3.7 Toughening mechanism

The cryo-fractured surfaces of PESO/PLA blends were observed by SEM scans

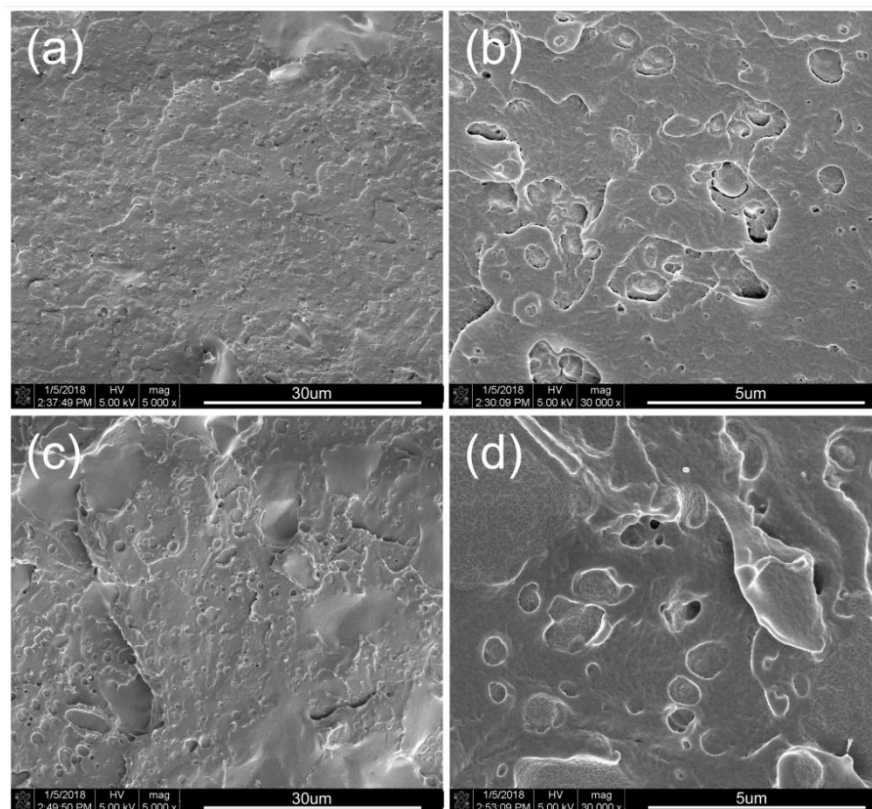


**Figure 3-9** SEM images of cryo-fractured surfaces of 20PESO (a and b) and 40 PESO (c and d) blends with magnifications of 5,000 (a and c) and 30,000 (b and d)

(Figure 3-9). Both 20PESO and 40PESO blends showed rough surfaces with obvious phase separation; raised particles and voids were seen for the blends, indicating the pulling out of dispersed PESO phase when the blends were cryo-fractured. The PESO phase were uniformly dispersed with PLA matrix for 20PESO, indicating an effective mixing for PESO and PLA via a twin-screw extruding process. The size of the dispersed PESO phase significantly increased with the increase of PESO usage from 20 to 40 wt%; obvious PESO blocks were generated and aggregated on the surface of 40PESO due to the coalescence of PESO resulted from its high concentration. As shown in the SEM images with higher magnifications (Figure 3-9bd), an ambiguous PESO-PLA interface was obtained on the surface, which confirms a superior interfacial adhesion between the dispersed PESO phase and PLA matrix because of their possible crosslinking during the mixing process.

For revealing the toughening mechanism of PESO phase on the PLA blends, the morphology for the tensile-fractured surfaces of the blends are shown in Figure 3-10. Brittle PLA shows a flat and smooth surface on the fractured surfaces, suggesting no evidence of plastic deformation (SEM image was not given for briefly). Both 20PESO and 40PESO showed large amount of elongated cells with significantly plastic

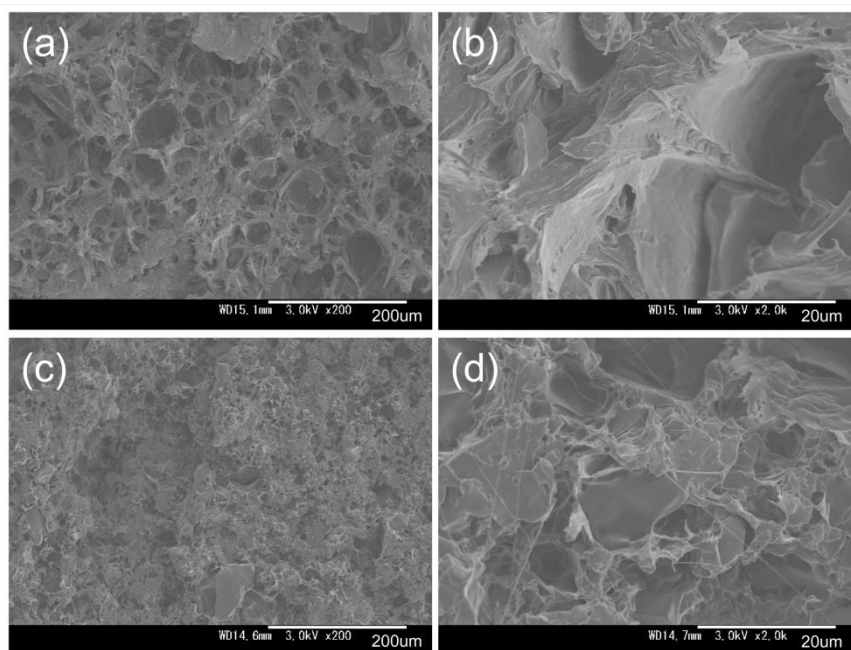


**Figure 3-10** SEM images of tensile-fractured surfaces of 20PESO (a and b) and 40 PESO (c and d) blends with magnifications of 200 (a and c) and 2,000 (b and d)

deformation occurred, which is responsible for their high elongation at break and tensile toughness. When the blend was loaded under tension and the stress was higher than the interfacial adhesion between the two phases, the dispersed PESO particles would be debonded from PLA matrix, hence generating cavities and causing large matrix plastic deformation due to the shear yielding caused by rubber particle debonding [34]. The average size of the elongated cells decreased when the PESO usage increased from 20 to 40 wt%, i.e., 20PESO showed larger cavities than 40PESO, while some filamentous materials appeared on the surface of 40PESO due to the plastic deformation. This seems to conflict with the results from [Figure 3-9](#), where the size for the undeformed PESO particles was larger for 40PESO than 20PESO. Compared to those of 40PESO, the PESO particles in 20PESO were smaller and less in distribution; therefore, when a same deformation occurred for the bulk blends, each PESO particle in 20PESO might withstand a higher average loading, which would result in the PESO particles deformed to a greater extent. However, the blend with larger PESO particles and higher concentration of PESO phase contributes to an improved plastic deformation ability, which is in line with the fact that the elongation at break and tensile toughness of the blends increased with the increasing PESO usage.

### **3.4 Conclusion**

Fully biobased, thermally remoldable, and highly tough PESO/PLA blends were successfully manufactured by melt-compounding of PLA with ESO using  $\text{BF}_3\text{NH}_2\text{Et}$  as a cationic initiator for the polymerization ESO. Results indicated the incorporated ESO could form a PESO phase dispersed on the PLA matrix and a superior interfacial compatibility with PLA matrix, which contributed to an improved toughening efficiency of PESO phase on the PLA blends. The tensile properties of the blends were tailored by changing the added PESO content; increase in PESO usage significantly increased in the elongation at break and tensile toughness; the highest elongation at break (141%) and tensile toughness ( $24.4 \text{ MJ/m}^3$ ) were achieved for the blend with 40 wt% PESO. This was correlated with the large-sized cavities formed

during tension on the SEM images of the blend. The blends presented slightly lower glass transition temperature and thermal stabilities than the pure PLA, while the crystallinity of PLA significantly increased after the addition of PESO due to the heterogeneous nucleation effect of PESO phase. In summary, in situ crosslinking of ESO with PLA matrix through melt-compounding was successfully conducted to greatly improve the toughness of PLA products and impart the PESO thermosets with thermoplasticity.

## References

- [1] Zhang, C.; Garrison, T.F.; Madbouly, S.A.; Kessler, M.R. Recent advances in vegetable oil-based polymers and their composites. *Prog. Polym. Sci.* 2017, 71, 91-143.
- [2] Llevot, A. Sustainable synthetic approaches for the preparation of plant oil-based thermosets. *J. Am. Oil Chem. Soc.* 2017, 94, 169-186.
- [3] Celikbag, Y.; Meadows, S.; Barde, M.; Adhikari, S.; Buschle-Diller, G.; Auad, M.L.; Via, B.K. Synthesis and characterization of bio-oil-based self-curing epoxy resin. *Ind. Eng. Chem. Res.* 2017, 56, 9389-9400.
- [4] Di Serio, M.; Russo, V.; Santacesaria, E.; Tesser, R.; Turco, R.; Vitiello, R. Liquid-liquid-solid model for the epoxidation of soybean oil catalyzed by Amberlyst-16. *Ind. Eng. Chem. Res.* 2017, 56, 12963-12971.
- [5] Wang, X.L.; Chen, L.; Wu, J.N.; Fu, T.; Wang, Y.Z. Flame-retardant pressure-sensitive adhesives derived from epoxidized soybean oil and phosphorus-containing dicarboxylic acids. *ACS Sustain. Chem. Eng.* 2017, 5, 3353-3361.
- [6] Gangireddy, C.S.R.; Hu, Y. Efficient chemical transformations of epoxidized soybean oil to cross-linked polymers by phosphorus-containing nucleophiles and study their thermal properties. *Polym. Degrad. Stabil.* 2017, 140, 156-165.
- [7] Liu, W.; Xie, T.; Qiu, R. Biobased thermosets prepared from rigid isosorbide and flexible soybean oil derivatives. *ACS Sustain. Chem. Eng.* 2017, 5, 774-783.
- [8] Ding, C.; Matharu, A.S. Recent developments on biobased curing agents: a review of their preparation and use. *ACS Sustain. Chem. Eng.* 2014, 2, 2217-2236.
- [9] Li, Y.; Yang, L.; Zhang, H.; Tang, Z. Synthesis and curing performance of a novel bio-based epoxy monomer from soybean oil. *Eur. J. Lipid Sci. Technol.* 2017, 119, 1600429.
- [10] Kumar, S.; Samal, S.K.; Mohanty, S.; Nayak, S.K. Epoxidized soybean oil-based epoxy blend cured with anhydride-based cross-linker: Thermal and mechanical characterization. *Ind. Eng. Chem. Res.* 2017, 56, 687-698.
- [11] Li, A.; Li, K. Pressure-sensitive adhesives based on epoxidized soybean oil and dicarboxylic acids. *ACS Sustain. Chem. Eng.* 2014, 2, 2090-2096.

- [12] Karger-Kocsis, J.; Grishchuk, S.; Soroachynska, L.; Rong, M.Z. Curing, gelling, thermomechanical, and thermal decomposition behaviors of anhydride-cured epoxy (DGEBA)/epoxidized soybean oil compositions. *Polym. Eng. Sci.* 2014, 54, 747-755.
- [13] Altuna, F.I.; Pettarin, V.; Williams, R.J. Self-healable polymer networks based on the cross-linking of epoxidised soybean oil by an aqueous citric acid solution. *Green Chem.* 2013, 15, 3360-3366.
- [14] Shibata, M.; Teramoto, N.; Makino, K. Preparation and properties of biocomposites composed of epoxidized soybean oil, tannic acid, and microfibrillated cellulose. *J. Appl. Polym. Sci.* 2011, 120, 273-278.
- [15] Li, Y.; Wang, D.; Sun, X.S. Copolymers from epoxidized soybean oil and lactic acid oligomers for pressure-sensitive adhesives. *RSC Adv.* 2015, 5, 27256-27265.
- [16] Biswas, A.; Liu, Z.; Cheng, H. Polymerization of epoxidized triglycerides with fluorosulfonic acid. *Int. J. Polym. Ana. Char.* 2016, 21, 85-93.
- [17] Maroufkhani, M.; Katbab, A.; Liu, W.; Zhang, J. Polylactide (PLA) and acrylonitrile butadiene rubber (NBR) blends: The effect of ACN content on morphology, compatibility and mechanical properties. *Polymer* 2017, 115, 37-44.
- [18] Dhar, P.; Gaur, S.S.; Soundararajan, N.; Gupta, A.; Bhasney, S.M.; Milli, M.; Kumar, A.; Katiyar, V. Reactive extrusion of polylactic acid/cellulose nanocrystal films for food packaging applications: Influence of filler type on thermomechanical, rheological, and barrier properties. *Ind. Eng. Chem. Res.* 2017, 56, 4718-4735.
- [19] Oguz, O.; Bilge, K.; Simsek, E.; Citak, M.K.; Wis, A.A.; Ozkoc, G.; Menciloglu, Y.Z. High-performance green composites of poly(lactic acid) and waste cellulose fibers prepared by high-shear thermokinetic mixing. *Ind. Eng. Chem. Res.* 2017, 56, 8568-8579.
- [20] Liu, W.; Liu, T.; Liu, T.; Liu, T.; Xin, J.; Hiscox, W.C.; Liu, H.; Liu, L.; Zhang, J. Improving grafting efficiency of dicarboxylic anhydride monomer on polylactic acid by manipulating monomer structure and using comonomer and reducing agent. *Ind. Eng. Chem. Res.* 2017, 56, 3920-3927.
- [21] Vasile, C.; Rapa, M.; Stefan, M.; Stan, M.; Macavei, S.; Darie-Nita, R.N.; Barbu-Tudoran, L.; Vodnar D.C.; Popa E.E.; Ștefan R.; Borodi G.; Brebu M. New PLA/ZnO: Cu/Ag bionanocomposites for food packaging. *Express Polym. Lett.* 2017, 11, 531-544.
- [22] Vijayarajan, S.; Selke, S.E.; Matuana, L.M. Continuous blending approach in the manufacture of epoxidized soybean-plasticized poly(lactic acid) sheets and films. *Macro. Mater. Eng.* 2014, 299, 622-630.
- [23] Xiong, Z.; Yang, Y.; Feng, J.; Zhang, X.; Zhang, C.; Tang, Z.; Zhu, J. Preparation and characterization of poly(lactic acid)/starch composites toughened with epoxidized soybean oil. *Carbohydr. Polym.* 2013, 92, 810-816.
- [24] Quiles-Carrillo, L.; Duart, S.; Montanes, N.; Torres-Giner, S.; Balart, R. Enhancement of the mechanical and thermal properties of injection-molded polylactide parts by the addition of

- acrylated epoxidized soybean oil. *Mater. Des.* 2018, 140, 54-63.
- [25] Al-Mulla, E.A.J.; Yunus, W.M.Z.W.; Ibrahim, N.A.B.; Rahman, M.Z.A. Properties of epoxidized palm oil plasticized polylactic acid. *J. Mater. Sci.* 2010, 45, 1942-1946.
- [26] Quiles-Carrillo, L.; Blanes-Martínez, M.; Montanes, N.; Fenollar, O.; Torres-Giner, S.; Balart, R. Reactive toughening of injection-molded polylactide pieces using maleinized hemp seed oil. *Eur. Polym. J.* 2018, 98, 402-410.
- [27] Ferri, J.; Garcia-Garcia, D.; Sánchez-Nacher, L.; Fenollar, O.; Balart, R. The effect of maleinized linseed oil (MLO) on mechanical performance of poly(lactic acid)-thermoplastic starch (PLA-TPS) blends. *Carbohydr. Polym.* 2016, 147, 60-68.
- [28] Carbonell-Verdu, A.; Garcia-Garcia, D.; Dominici, F.; Torre, L.; Sanchez-Nacher, L.; Balart, R. PLA films with improved flexibility properties by using maleinized cottonseed oil. *Eur. Polym. J.* 2017, 91, 248-259.
- [29] Carbonell-Verdu, A.; Samper, M.D.; Garcia-Garcia, D.; Sanchez-Nacher, L.; Balart, R. Plasticization effect of epoxidized cottonseed oil (ECSO) on poly(lactic acid). *Ind. Crop. Prod.* 2017, 104, 278-286.
- [30] Ferri, J.; Samper, M.; García-Sanoguera, D.; Reig, M.; Fenollar, O.; Balart, R. Plasticizing effect of biobased epoxidized fatty acid esters on mechanical and thermal properties of poly(lactic acid). *J. Mater. Sci.* 2016, 51, 5356-5366.
- [31] Mauck, S.C.; Wang, S.; Ding, W.; Rohde, B.J.; Fortune, C.K.; Yang, G.; Ahn, S.-K.; Robertson, M.L. Biorenewable tough blends of polylactide and acrylated epoxidized soybean oil compatibilized by a polylactide star polymer. *Macromolecules* 2016, 49, 1605-1615.
- [32] Robertson, M.L.; Chang, K.; Gramlich, W.M.; Hillmyer, M.A. Toughening of polylactide with polymerized soybean oil, *Macromolecules* 2010, 43, 1807-1814.
- [33] Chen, Y.; Yuan, D.; Xu, C. Dynamically vulcanized biobased polylactide/natural rubber blend material with continuous cross-linked rubber phase. *ACS Appl. Mater. Inter.* 2014, 6, 3811-3816.
- [34] Zhao, T.-H.; He, Y.; Li, Y.-D.; Wang, M.; Zeng, J.-B. Dynamic vulcanization of castor oil in a polylactide matrix for toughening. *RSC Adv.* 2016, 6, 79542-79553.
- [35] He, Y.; Zhao, T.-H.; Li, Y.-D.; Wang, M.; Zeng, J.-B. Toughening polylactide by dynamic vulcanization with castor oil and different types of diisocyanates. *Polym. Test.* 2017, 59, 470-477.
- [36] Zhao, T.-H.; Wu, Y.; Li, Y.-D.; Wang, M.; Zeng, J.-B. High performance and thermal processable dicarboxylic acid cured epoxidized plant oil resins through dynamic vulcanization with poly(lactic acid). *ACS Sustain. Chem. Eng.* 2017, 5, 1938-1947.
- [37] Tsujimoto, T.; Uyama, H. Full biobased polymeric material from plant oil and poly(lactic acid) with a shape memory property. *ACS Sustain. Chem. Eng.* 2014, 2, 2057-2062.
- [38] Jian, X.Y.; He, Y.; Li, Y.D.; Wang, M.; Zeng, J.B. Curing of epoxidized soybean oil with crystalline oligomeric poly(butylene succinate) towards high performance and sustainable

- epoxy resins. *Chem. Eng. J.* 2017, 326, 875-885.
- [39] Jian, X.Y.; An, X.P.; Li, Y.D.; Chen, J.H.; Wang, M.; Zeng, J.B. All plant oil derived epoxy thermosets with excellent comprehensive properties. *Macromolecules* 2017, 50, 5729-5738.
- [40] Wang, L.; Lee, R.E.; Wang, G.; Chu, R.K.; Zhao, J.; Park, C.B. Use of stereocomplex crystallites for fully-biobased microcellular low-density poly(lactic acid) foams for green packaging. *Chem. Eng. J.* 2017, 327, 1151-1162.
- [41] Yang, Z.; Narayanan, J.; Ravalli, M.; Rupp, B.T.; Ryu, C.Y. Structure–property relationships of epoxy thermoset networks from photoinitiated cationic polymerization of epoxidized vegetable oils, in: C. Tang, C.Y. Ryu (Eds.), *Sustainable Polymers from Biomass*, Wiley-VCH Verlag GmbH & Co. KGaA, Weinheim, 2017, pp 209-226.
- [42] Meng, X.; Bocharova, V.; Tekinalp, H.; Cheng, S.; Kisluk, A.; Sokolov, A.P.; Kunc, V.; Peter, W.H.; Ozcan, S. Toughening of nanocellulose/PLA composites via bio-epoxy interaction: mechanistic study. *Mater. Des.* 2018, 139, 188-197.
- [43] Pin, J.M.; Guigo, N.; Vincent, L.; Sbirrazzuoli, N.; Mija, A. Copolymerization as a strategy to combine epoxidized linseed oil and furfuryl alcohol: the design of a fully bio-based thermoset. *ChemSusChem* 2015, 8, 4149-4161.
- [44] Radjabian, M.; Kish, M.; Mohammadi, N. Structure–property relationship for poly(lactic acid) (PLA) filaments: Physical, thermomechanical and shape memory characterization. *J. Polym. Res.* 2012, 19, 9870.
- [45] Chieng, B.W.; Ibrahim, N.A.; Then, Y.Y.; Loo, Y.Y. Epoxidized vegetable oils plasticized poly(lactic acid) biocomposites: Mechanical, thermal and morphology properties, *Molecules* 2014, 19, 16024-16038.
- [46] Qian, S.; Zhang, H.; Yao, W.; Sheng, K. Effects of bamboo cellulose nanowhisker content on the morphology, crystallization, mechanical, and thermal properties of PLA matrix biocomposites. *Compos. Part B–Eng.* 2018, 133, 203-209.

# **Chapter 4 Tannic Acid-Induced Crosslinking of Epoxidized Soybean Oil for Toughening PLA via Dynamic Vulcanization**

## **4.1 Introduction**

Biodegradable polymers originated from renewable feedstocks have been utilized instead of their nondegradable and petroleum-based counterparts due to the growing environmental awareness and shortage of oil resources. PLA is one of the most promising biobased and biodegradable polymers. Because of its compelling advantages including high strength, easy processability, and non-toxicity to human beings and environmental friendliness, PLA has great potential for applications in many areas [1-5]. However, some significant shortcomings of PLA, including inherent brittleness, high prices, and low glass transition temperature, have greatly inhibited its wider application.

Many strategies, such as plasticization, copolymerization, and polymer blending, have been developed to toughen PLA [6]. Polymer blending is a convenient and efficient method via directly incorporating ductile polymers into PLA system. Vegetable oils, which consist of glycerol esters with three flexible long-chain fatty acids, are cost-effective products characterized by high availability and superb environmental credentials [7]. These characteristics make vegetable oil derivatives very attractive to be used as plasticizers for PLA. Extensive research has been addressed to improve the toughness of PLA by blending PLA with epoxidized soybean oil (ESO) [8-10], epoxidized palm oil [11], maleinized linseed oil [12], maleinized and epoxidized cottonseed oils [13,14], and modified fatty acids [15], etc. However, they are immiscible with PLA and might leach or migrate to the surface of PLA products when in use; hence, sufficient toughening efficiency is not accessible for the blends. In addition, the introduction of these flexible polymers into PLA is usually accompanied with a significant compromise in mechanical strength and

thermal stability. Therefore, a PLA star polymer with acrylated epoxidized soybean oil (AESO) core was synthesized and introduced into ESO/PLA blends to increase the compatibility between ESO and PLA, which resulted in a great enhancement in the tensile properties of the blends [16]. The tensile toughness of the blends from polymerized soybean oil and poly(L-lactide) was greatly improved after the use of poly(isoprene-*b*-L-lactide) block copolymer as a compatibilizer [17].

Dynamic vulcanization technique is effective in improving the interfacial compatibility of PLA-based blends and hence the toughening efficiency of the incorporated flexible components on the blends. Dynamic vulcanization for rubber phase and thermoplastic PLA is a melt-compounding process which results in a two-phase blend consisting of vulcanized rubber phase and thermoplastic PLA [18]. Much work has been done on toughening PLA blends by dynamic vulcanization with various elastomers such as thermoplastic polyurethane [19-21], biobased polyester [22,23], unsaturated low-molecular-weight poly(ethylene glycol)s [24], epoxy-containing elastomer [25], ethylene-*co*-vinyl acetate rubber [26,27], and natural rubber [18,28-30]. The most commonly used vulcanizing agents are free radical initiators such as Luperox 101 [19,23,24] and dicumyl peroxide [18,29-31]. As for using vegetable oils in toughening PLA, the dynamic vulcanization of PLA with castor oil by using diisocyanates as crosslinkers resulted in the formulation of a tough blend with superior toughness and mechanical strength [32,33]. However, the use of petroleum-based isocyanates as vulcanizing agents reduces the sustainability and biodegradability of the toughened PLA blends.

In order not to sacrifice the renewability of PLA products, fully biobased ESO/PLA blends with high toughness were fabricated via selecting a green monomer, i.e., tannic acid (TA), as a vulcanizing agent to crosslink ESO during dynamic vulcanization. TA is a specific form of tannin that is widely distributed in many species of plants. The chemical formula of commercial TA is often given as  $C_{76}H_{52}O_{46}$ , as shown in [Figure 4-1](#). The presence of abundant phenolic –OH groups makes it highly reactive towards some chemicals such as acids and epoxy. It is known that most traditional epoxy hardeners, such as amines, acids, and anhydrides, are

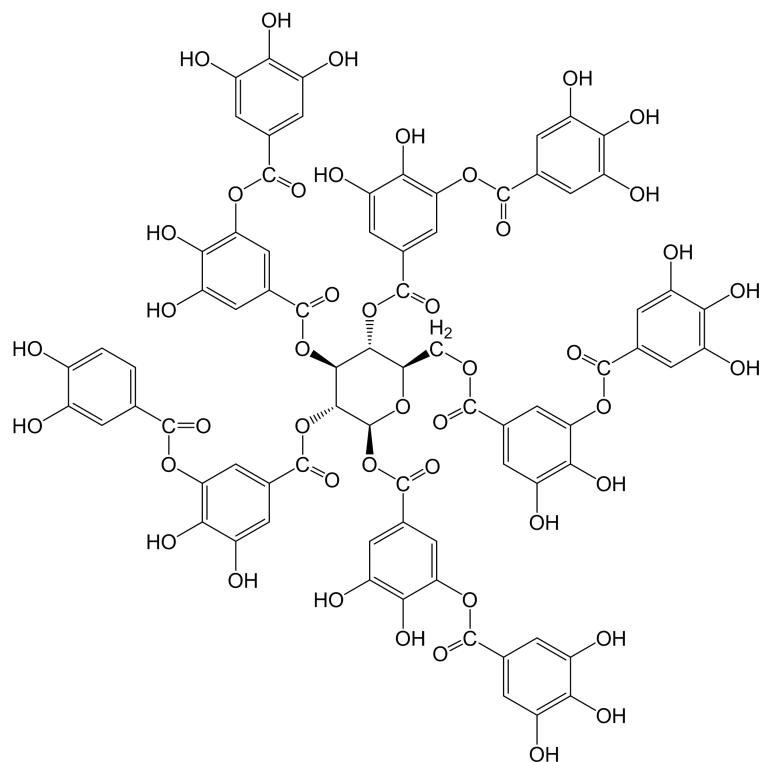


**Figure 4-1** Chemical structure of tannic acid

petroleum-based and toxic. Therefore, TA was employed as a green curing agent in the absence of catalysts to cure epoxy resins including ESO [34, 35]; however, the obtained TA-ESO thermoset showed inferior tensile strength, tensile modulus, and elongation at break. In this work, TA was selectively used to replace petroleum-based crosslinking agents to cure ESO during dynamic vulcanization with PLA, which would form a stable phase-separated structure while maintaining the mechanical strength, thermal resistance, and sustainability of the resulting PLA products. To the best of our knowledge, designing a completely biobased rubbery phase in the PLA system from rigid TA and flexible ESO via dynamic vulcanization technique has rarely been reported. The compositions and properties of the formed TA-ESO rubbery phase and its interfacial compatibility with PLA matrix were tailored via adjusting the stoichiometric ratio of TA to ESO. The toughening efficiency and mechanism of TA-ESO crosslinking on PLA were correlated with the tensile properties, dynamic mechanical properties, crystallization behavior, thermal stabilities and morphologies of the toughened PLA blends.

## 4.2 Experimental section

### 4.2.1 Materials

PLA (Ingeo 3001D) was obtained from NatureWorks Japan (Tokyo, Japan). ESO with an average molar ratio of epoxy group/ESO of 4 mol was purchased from Aladdin Industrial Corporation (Shanghai, China). TA with a molar ratio of –OH group/TA of 25 mol and acetone were obtained from Nacalai Tesque, INC (Tokyo, Japan). All the chemicals were used without further purification.

### 4.2.2 Preparation of TA-ESO/PLA blends

TA (2.06 g) was dissolved in acetone (20 g) to generate a TA solution. ESO (17.94 g) was then mixed with the solution with a vigorous stirring for 5 min. Then, the obtained TA-ESO mixture was dried in an oven at 80°C for 4 h to remove the acetone, and thus a ESO solution with dispersed TA (20 g) was generated. The molar ratio ( $n_{\text{-OH/epoxy}}$ ) of –OH groups from TA to epoxy groups from ESO in the TA-ESO solution was 0.4. As given in Table 4-1, TA-ESO solutions with different  $n_{\text{-OH/epoxy}}$  were designed for tailoring the properties of the formed TA-ESO systems.

PLA pellets (180 g) were dried in an oven at 80°C for 12 h and then mixed with the TA-ESO mixture. The weight of the TA-ESO mixture was kept at 10 wt% based on the total weight of the resulting TA-ESO/PLA blends. For briefly, the TA-ESO/PLA blends with different  $n_{\text{-OH/epoxy}}$  were abbreviated to 0.4TA-ESO, 0.6TA-ESO, 0.8TA-ESO, and 1.0TA-ESO, respectively (Table 4-1). The dynamic

**Table 4-1** Compositions and gel fractions of TA-ESO/PLA blends

References	Compositions (wt%)			$n_{\text{-OH/epoxy}}^a$	Gel fraction (wt%)
	PLA	TA	ESO		
Pure PLA	100	–	–	–	–
10ESO	90	–	10	–	–
0.4TA-ESO	90	1.03	8.97	0.4	15.5
0.6TA-ESO	90	1.46	8.54	0.6	29.0
0.8TA-ESO	90	1.86	8.14	0.8	32.2
1.0TA-ESO	90	2.22	7.78	1.0	31.0

<sup>a</sup> $n_{\text{-OH/epoxy}}$  represents the molar ratio of –OH groups from TA to epoxy groups from ESO.

vulcanization process of PLA with TA-ESO was carried out on a twin-screw extruder (Technovel Corporation Japan, KZW25TW-60MG-NH(-1200)-AKT). The temperatures in six zones were set at 150, 160, 170, 170, 180, and 180°C from feeding zone to die section, respectively; the screw speed was constantly maintained at 50 r/min. The extruded TA-ESO/PLA blends were quenched in a water bath, chopped into pellets, and then oven-dried at 80°C for 12 h for injection molding. Dumbbell and rectangular samples were prepared on an injection molding machine (Nissei Plastic Industrial, Japan, NP7-1F). The nozzle temperature, injection speed, mold temperature, and cooling time were 170°C, 17.6 mm/s, 40°C, and 40 s, respectively. For comparison, neat PLA and ESO/PLA blend with 10 wt% ESO (10ESO) were also melt-extruded and injected into samples for evaluation under same conditions.

#### 4.2.3. Characterization

The TA-ESO/PLA blend with a weight ( $m_1$ ) of about 2 g was immersed in chloroform (40 mL) for 24 h to dissolve PLA and uncrosslinked ESO molecules. The insoluble part was isolated via centrifugation, and further purified with chloroform for 2 times and acetone for 3 times to remove unreacted TA monomers. After being vacuum-dried at 50 °C for 12 h, the gel was weighted as  $m_2$ . The gel fraction ( $G_f$ ) of TA-crosslinked-ESO was calculated as the [Equation 4-1](#),

$$G_f = \frac{m_2}{w_{\text{TA-ESO}} \times m_1} \times 100\% \quad (4-1)$$

where  $w_{\text{TA-ESO}}$  is the weight fraction (10 wt%) of TA-ESO in the blends.

Fourier transform infrared spectroscopy (FTIR) experiments were carried out on a Nicolet iN10 FTIR spectrometer (Thermo Fisher Scientific, MA, USA) over a scanning range from 4000 to 400  $\text{cm}^{-1}$  at a spectral resolution of 4  $\text{cm}^{-1}$ . To reveal the chemical structure of the isolated TA-ESO, TA-ESO solution with a  $n_{\text{-OH/epoxy}}$  of 0.8 was cured in an oven at 180°C for 10 min for comparison. The samples were powdered and mixed with KBr, and then the obtained mixture was pressed at 15 MPa to generate pellets for analysis. For comparison, solid TA was directly mixed with

KBr, and liquid ESO was coated on the surface of a neat KBr pellet for analysis.

The soluble PLA part in chloroform from gel fraction measurements was precipitated by using excess acetone. After washing with acetone for 3 times, the obtained precipitates were used for  $^1\text{H}$  nuclear magnetic resonance (NMR) analysis on an Avance III 500 NMR spectrometer (Bruker, MA, USA) with  $\text{CDCl}_3$  as a solvent and tetramethylsilane (TMS) as an internal chemical shift standard.

Molecular weight distributions of the PLA blends were determined using a Tosoh EcoSEC HLC-8320 gel permeation chromatography (GPC) instrument (Tokyo, Japan) equipped with RI and UV detectors. The specimen concentration was 2 mg/mL in chloroform, and an injection volume of 20 mL was used with a flow rate of 1.0 mL/min. The GPC system was calibrated with polystyrene standards ranging from 495 to 1,090,000 g/mol.

Differential scanning calorimetry (DSC) analyses were performed on a STA 449 F3 Jupiter Simultaneous Thermal Analyzer (NETZSCH, Selb, Germany). Samples with a weight of 5–10 mg was placed in a standard porcelain crucible with a lid. The tests were conducted from 25 to 210°C with a heating rate of 10 °C/min under  $\text{N}_2$  (flow rate: 30 mL/min). The glass transition temperature ( $T_g$ ), cold crystallization peak ( $T_{cc}$ ), and melt peak temperature ( $T_m$ ) of the PLA blends were obtained from the DSC curves. The degree of crystallinity ( $X_c$ ) for PLA was calculated as the [Equation 4-2](#) [36]:

$$X_c = \frac{\Delta H_m - H_{cc}}{\Delta H_{100} \times x_{\text{PLA}}} \times 100 \quad (4-2)$$

where  $\Delta H_m$  and  $\Delta H_{cc}$  are the melting and cold crystallization enthalpies, respectively;  $\Delta H_{100}$  is the theoretical melting enthalpy of a completely crystalline PLA (93.6 J/g), and  $x_{\text{PLA}}$  is the weight fraction of PLA in the blends.

Rectangular samples ( $55 \times 10 \text{ mm}^2$ ) of the blends were prepared for dynamic mechanical analysis (DMA) tests on a RSA-G2 solids analyzer (TA Instrument, DE, USA) under three point bending mode with a strain of 0.1%. The tests were conducted from 30 to 100 °C at a heating rate of 2 °C/min and a frequency of 1 Hz.

Thermogravimetric (TG) analysis of the blends was conducted on a DTG-60 TG

instrument (Shimadzu, Japan). Samples with a weight of 4–6 mg were placed in aluminum crucibles. The tests were performed from room temperature to 600°C at a scan rate of 10 °C/min under N<sub>2</sub> atmosphere at a flow rate of 50 mL/min.

A Series 3360 universal testing machine (Instron, MA, USA) was used to evaluate the tensile properties of the PLA blends in accordance with ASTM D 638-10. Dumbbell specimens with 25 mm gauge length, 2 mm thickness, and 5 mm narrow section width were used for the test at a crosshead speed of 10 mm/s. Five replicates were conducted for each blend.

The scanning electron microscope (SEM) images of the cryo-fractured and tensile-fractured surfaces of the blends were obtained from a JEOL JSM-7500F SEM (JEOL, Tokyo, Japan) at an accelerating voltage of 4.0 kV. Before testing, specimens were coated with an elemental gold film (8–10 nm). The particle size distributions on the surfaces were measured using Nano Measurer 1.2.5 Software (Fudan University, Shanghai, China). At least 200 particles were measured for each blend.

## **4.3 Results and discussion**

### **4.3.1 Dynamic vulcanization mechanism of PLA with ESO and TA**

Dynamic vulcanization of PLA with ESO and TA would form a stable TA-crosslinked-ESO phase inside PLA blends, which is closely related to the reactions among TA, ESO and PLA (Figure 4-2). TA monomers contain a large number of phenolic –OH groups and thus are more reactive toward carboxyl and epoxy groups than alcohols in the absence of catalysts. The –OH groups of TA would react with the epoxy rings of ESO to generate ether linkages between TA and ESO and new –OH groups (Reaction I, Figure 4-2); the new generated –OH groups are capable of further reacting with other ESO epoxides, leading to the formation of ESO oligomers (Reaction II, Figure 4-2). Therefore, the crosslinking between TA and ESO refers to two types of reactions, i.e., polymerization between the phenolic –OH groups of TA and the epoxy groups of ESO, and self-polymerization of ESO monomers via the reaction between the newly generated aliphatic –OH groups and epoxy groups

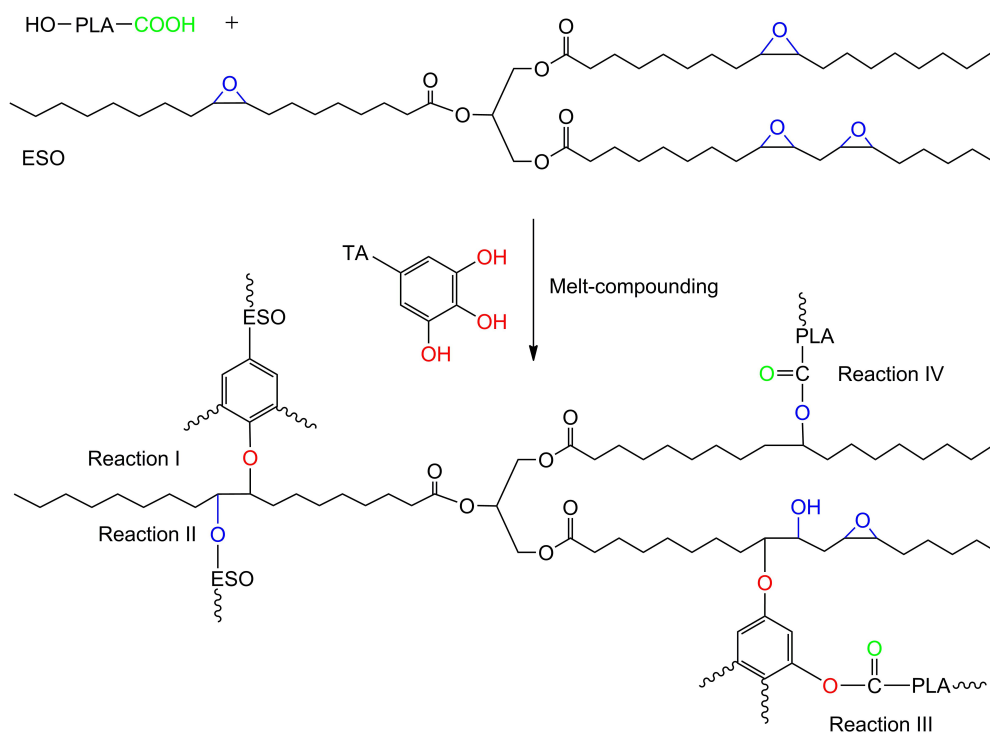


**Figure 4-2** Proposed reactions among TA, ESO and PLA during dynamic vulcanization

[37]. These two reactions can be verified by the two main curing peaks at 223.1 and 230.2°C in the DSC curve of TA-ESO blend with a  $n_{\text{-OH/epoxy}}$  of 0.8 (Figure 4-3A). An initial curing temperature of 169.6°C was observed for the crosslinking between TA and ESO, which was lower than the processing temperature (180°C) of the PLA blends during the process of mixing and injection. Therefore, the reaction between TA and ESO still could occur at a slow rate, although the maximum curing temperatures of the TA-ESO blend were higher than the processing temperature. This is in accordance with the gel fractions isolated from the blends (Table 1). The gel fraction increased from 15.5 to 29.0% with increasing  $n_{\text{-OH/epoxy}}$  from 0.4 to 0.8, while further increase in  $n_{\text{-OH/epoxy}}$  did not significantly affect the gel fraction. This indicates that the TA-crosslinked-ESO structure was formed but with a low crosslinking efficiency due to the insufficient curing temperature and short residence time in twin-screw extruder.

FTIR analysis was used to characterize the chemical structure of the isolated TA-ESO parts, and the results indicated that there were not obvious difference

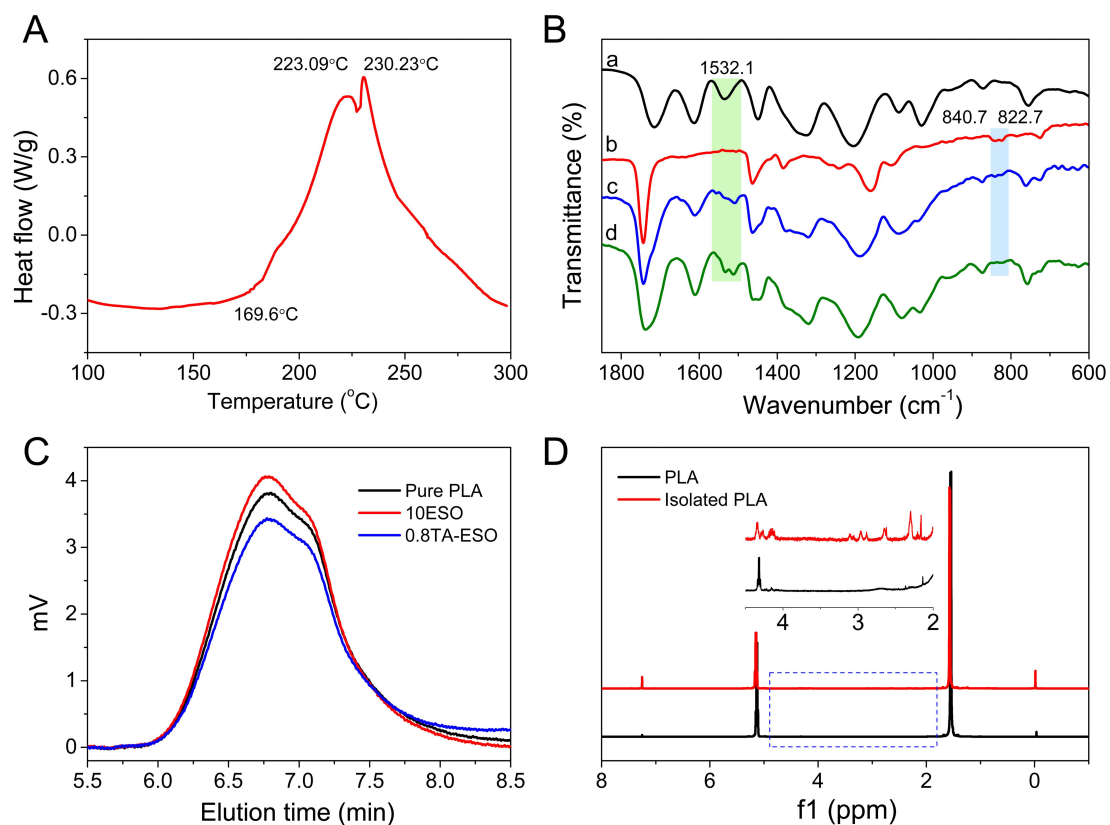


**Figure 4-3** Characterization of reactions among TA, ESO and PLA. (A) DSC curve of TA-ESO blend; (B) FTIR spectra of (a) TA, (b) ESO, (c) cured TA-ESO, and (d) isolated TA-ESO; (C) GPC profiles of pure PLA, and PLA from 10ESO and 0.8TA-ESO/PLA; (D)  $^1\text{H}$  NMR spectra of pure PLA and the isolated PLA from 0.8TA-ESO/PLA

between the samples with different  $n\text{-OH/epoxy}$  (Data not shown). To further reveal the reaction mechanism during dynamic vulcanization, the FTIR spectrum of the isolated sample was compared to that of the cured TA-ESO blend (Figure 4-3B). A decrease of the peaks at 822.7 and 840.7  $\text{cm}^{-1}$  corresponding to the stretching vibration of epoxy rings from ESO was observed in both TA-ESO blend compared to pure ESO, which confirms the ring opening polymerization of ESO initiated by TA. The main characteristic bands of the isolated TA-ESO were basically the same as that of the cured TA-ESO, showing the occurrence of crosslinking between TA and ESO during dynamic vulcanization. The band at 1532.1  $\text{cm}^{-1}$  ascribed to the stretching vibration of C=C bonds from aromatic ring of TA was shifted to a lower wavenumber of 1507.6  $\text{cm}^{-1}$  for the cured TA-ESO. This is due to the conversion of the phenolic -OH groups into ether connections after the crosslinking between TA and ESO. Furthermore, a

small peak corresponding to the C=C bonds from unreacted TA was retained in the spectrum of the isolated TA-ESO, indicating that the TA-ESO crosslinking was incomplete.

To further reveal the possible interaction of TA and ESO with PLA matrix, the molecular weight distribution of PLA in the blends was determined by GPC analysis (Figure 4-3C). The number average molar mass ( $M_n$ ) of neat PLA, and PLA from 10ESO and 0.8TA-ESO blends were 98,355, 104,066, and 110,822 g/mol, respectively. A slightly increase in the  $M_n$  of PLA was observed for 10ESO when compared to neat PLA, indicating that the reaction between the terminal –OH or –COOH groups of PLA with the epoxy rings of ESO might occur at high temperature (Reaction IV, Figure 4-2). Although the TA-crosslinked-ESO could not dissolve in chloroform, the dissolved PLA molecules carrying a small part of TA-ESO oligomers still could be analyzed. As shown in Figure 4-2 (Reaction III), the TA-ESO phase would form covalent linkages with PLA via esterification between the phenolic –OH groups of TA and the terminal –COOH groups of PLA, which leads to the increased  $M_n$  of PLA in the 0.8TA-ESO with respect to 10ESO. This also confirms an improvement in the interfacial adhesion between ESO phase and PLA matrix. The reaction between TA-ESO phase and PLA can be evidenced by the  $^1\text{H}$  NMR spectra of neat PLA and the separated PLA from the TA-ESO/PLA blend (Figure 4-3D). Both samples showed typical signals at 1.54 and 5.10 ppm for PLA molecules. As for the magnified spectra, some characteristic signals resulted from TA-ESO phase were observed in the separated PLA, which confirms the assumption that a small part of TA-ESO oligomers were covalently bonded onto PLA molecules. Similar situation was reported by using sebacic acid as vulcanizing agent for ESO/PLA blend [38].

#### 4.3.2 Crystallization behavior of TA-ESO/PLA blends

DSC analysis was conducted for the TA-ESO/PLA blends to reveal their thermal transition and crystallization behavior (Figure 4-4 and Table 4-2). The glass transition temperature ( $T_g$ ) of pure PLA was 61.15°C. A cold crystallization exothermic peak at 101.07°C (cold crystallization temperature,  $T_{cc}$ ) was clearly observed along with a

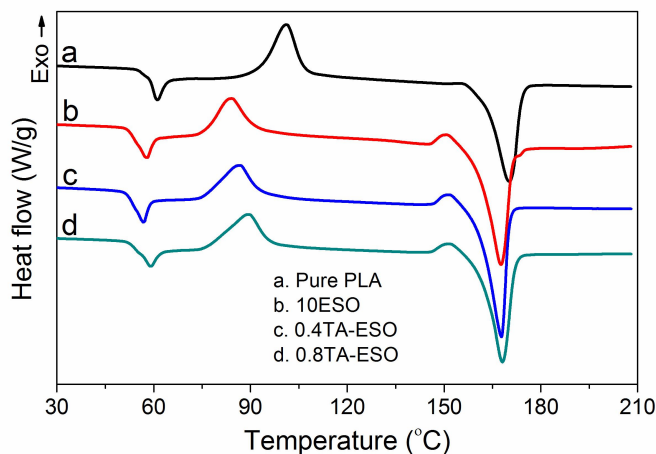


**Figure 4-4** DSC curves of TA-ESO/PLA blends

**Table 4-2** DSC results of TA-ESO/PLA blends

References	$T_g$ (°C)	$T_{cc}$ (°C)	$T_m$ (°C)	$\Delta H_{cc}$ (J/g)	$\Delta H_m$ (J/g)	$X$ (%)
Pure PLA	61.2	101.1	170.2	23.7	37.8	15.0
10ESO	57.7	80.0	167.6	22.9	47.8	29.5
0.4TA-ESO	56.9	86.7	167.9	20.5	44.0	27.9
0.8TA-ESO	59.1	89.3	168.0	20.8	42.2	25.4

cold crystallization enthalpy ( $\Delta H_{cc}$ ) of 23.73 J/g. The melting process of the crystalline phase in PLA showed a single melting peak at 170.18°C (melting temperature,  $T_m$ ) with a melting enthalpy ( $\Delta H_m$ ) of 37.81 J/g. Compared to those of neat PLA, the  $T_g$ ,  $T_{cc}$ , and  $T_m$  of the 10ESO decreased to 57.65, 80.01, and 167.60°C, respectively, which is intimately related to the plasticizing effect of ESO. Similar results were reported for the PLA blends plasticized with vegetable oil derivatives [13-15,39]. These plasticizers with a much low molecular weight would diffuse inside the PLA matrix and exist between the PLA molecular chains, which might increase the distance between polymer chains and hence increase the free volume that makes the molecular chains move at lower temperatures [14]. The dilution effect of ESO also resulted in a significant increased crystallinity ( $X_c$ ) from 15.03% for pure PLA to 29.49% for 10ESO because the PLA molecular chains with an improved mobility could easily move to a packed structure for the formation of crystalline phase, which is in agreement with some previous findings [13,14,32]. This seems to be contradicted when considering the relationship between  $T_g$  and crystallinity for a pure

semi-crystalline polymer. It was reported that the crystal domain in semi-crystalline polymers has a constraining effect on the relaxation of the amorphous phase, resulting in a higher  $T_g$  for the sample with higher crystallinity [40,41]. However, for the ESO/PLA blend, the ESO was dispersed in the PLA as a secondary phase, where the secondary ESO phase has a more profound effect on decreasing the  $T_g$  of the PLA blend than the constraining effect. The incorporation of TA monomer into ESO phase, the  $X_c$  of the blends slightly reduced to 27.87% and 25.38%, respectively, for the 0.4TA-ESO and 0.8TA-ESO. This can be interpreted by the following two reasons: (1) The crosslinking between TA and ESO increases the molecular weight of the TA-ESO phase and hence reduce its dilution effect on PLA phase due to the improved viscosity. (2) The reaction between TA-ESO phase and PLA matrix not only would constrain the chain motions of PLA due to the hindrance of the connected TA-ESO phase, but also might destroy the structural integrity of PLA crystalline phase. These effects also explain the significantly increased  $T_{ccs}$ s of the TA-ESO/PLA blends with regard to that of 10ESO. However, the addition of TA monomer has not significant influence on the  $T_m$ s of the blends. Furthermore, the  $T_g$  of 0.4TA-ESO was comparable with that of 10ESO; while further increase in TA concentrations, i.e.,  $n\text{-OH/epoxy}$ , in the TA-ESO phase from 0.4 to 0.8 resulted in a slightly increased  $T_g$  from 56.92 to 59.11°C thanks to the increased crosslinking density of the TA-ESO phase.

### 4.3.3 Dynamic mechanical properties of TA-ESO/PLA blends

DMA curves and their characteristic results of the PLA blends were given in [Figure 4-5](#) and [Table 4-3](#). Regarding PLA blends with ESO or different TA-ESO phases, the curves of storage modulus ( $E'$ ) were identical in shape, indicating a platform from room temperature to 50°C and then undergoing a dramatic drop at temperatures of 50–65°C due to glass transition behavior. The  $E'$  of pure PLA in the initial stage was 3.19 GPa, which decreased to 3.03 GPa for 10ESO, indicative of a clear plasticization effect of ESO. The addition of TA monomer into ESO phase further resulted in slightly reduction in the  $E'$ s of the blends; the  $E'$ s of the TA-ESO/PLA blends at room temperature decreased from 2.86 to 2.77 GPa as the

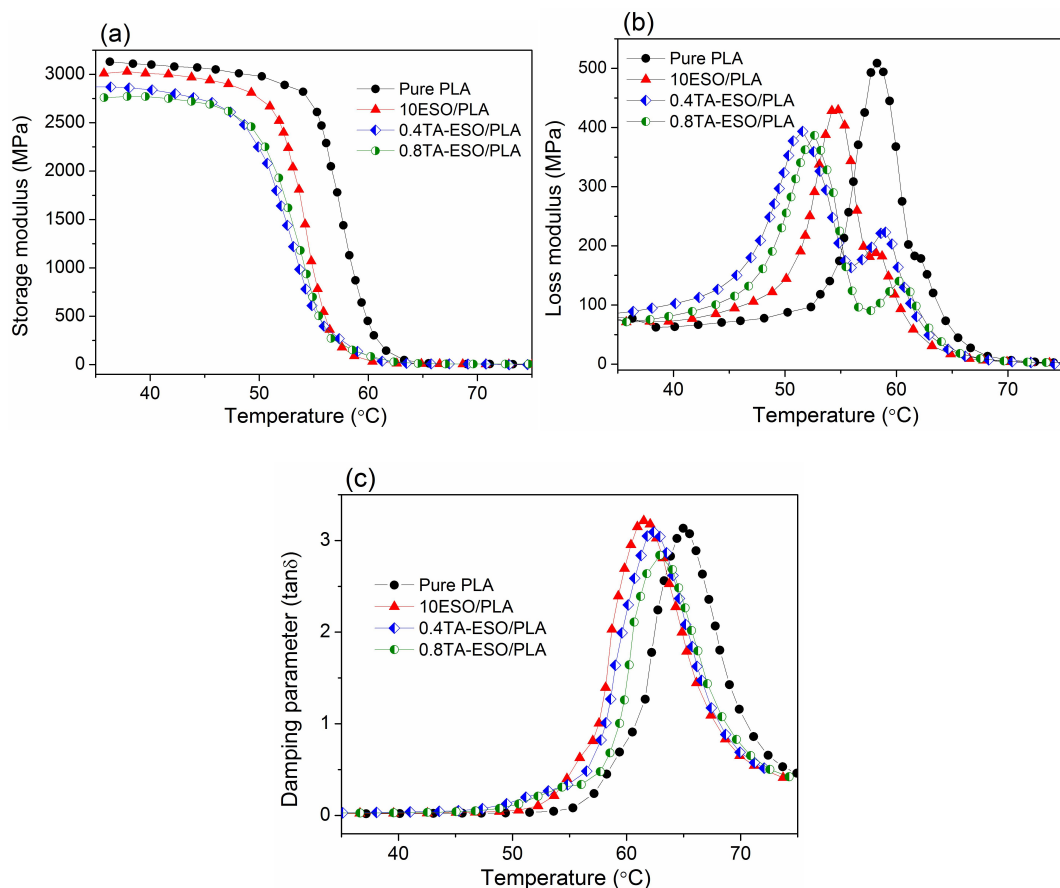


**Figure 4-5** DMA curves of TA-ESO/PLA blends. (a) Storage modulus; (b) loss modulus; (c) damping parameter

**Table 4-3** DMA results of TA-ESO/PLA blends

Reference	Storage modulus at 35 °C (GPa)	Peak temperatures from loss modulus (°C)		$T_g$ from $\tan \delta$ (°C)
		Peak 1	Peak 2	
Pure PLA	3.19	58.2	-	65.0
10ESO	3.03	54.5	58.2	61.5
0.4TA-ESO	2.86	51.6	58.8	62.1
0.8TA-ESO	2.77	52.6	60.5	62.9

increase of  $n_{\text{-OH/epoxy}}$  in the TA-ESO phase from 0.4 to 0.8. This is attributed to the improved interfacial adhesion between the TA-ESO phase and PLA matrix that might destroy the dense arrangement of PLA molecules in the amorphous region, hence resulting in reduced  $E'$ s of the blends [42].

The loss modulus ( $E''$ ) of pure PLA, indicating the ability of the material to dissipate energy, showed a loss modulus peak at 58.24°C due to the mobility of polymer molecules, which corresponds to the glass transition behavior of the polymer

from another perspective. The transition temperatures of the blends shifted to lower temperatures after the incorporation of ESO and TA-ESO phase due to their plasticizing effects, which is in agreement with the change in the  $T_g$  from DSC tests. A small shoulder in the  $E''$  curve at high temperature was observed for pure PLA, which is resulted from the chain rearrangement of oriented amorphous regions into crystalline phase [42]. The introduction of ESO into PLA blend led to an obvious  $E''$  peak at 58.17 °C after glass transition since the ESO could promote the segmental movements of mobile and amorphous regions. However, the second  $E''$  peak temperatures of the TA-ESO/PLA blends slightly increased when compared to that of 10ESO because of the restricted molecular motions by the crosslinking among TA, ESO and PLA.

The damping parameter ( $\tan \delta$ ), calculated from the ratio of  $E''$  to  $E'$ , indicates the ratio of energy loss to energy reserved in the loading cycle. The  $\tan \delta$  peak of pure PLA was sharp and intensive, while 10ESO blend has a higher width of the  $\tan \delta$  peak, indicative of an improved molecular mobility due to the diluting effect of ESO. The TA-ESO crosslinking slightly increased the peak area of  $\tan \delta$  curve of TA-ESO/PLA blends when compared to 10ESO, showing an improved ability of the material to dissipate energy. The temperature at the  $\tan \delta$  peak was usually defined as the  $T_g$  of a material from another perspective. The  $T_g$ s of all the PLA blends were slightly higher than their corresponding values determined by DSC scans due to the different basal theories of these two technologies. But the  $T_g$ s of the blends followed the order of PLA > 0.8TA-ESO > 0.4TA-ESO > 10ESO, which are associated with the molecular composition and structure of the blends as discussed in [Section 4.3.2](#).

#### 4.3.4 Thermal stability of TA-ESO/PLA blends

The thermal degradation of neat PLA and its blends with ESO and TA-ESO phase was presented in [Figure 4-6](#). The temperatures ( $T_5$  and  $T_{30}$ ) at a weight loss of 5% and 30%, respectively, and the maximum weight loss temperature ( $T_{max}$ ) were summarized in [Table 4-4](#). A heat-resistant index ( $T_s$ ), indicating the overall thermal stability of the blends, was determined based on the following [Equation 4-3](#) [43]:

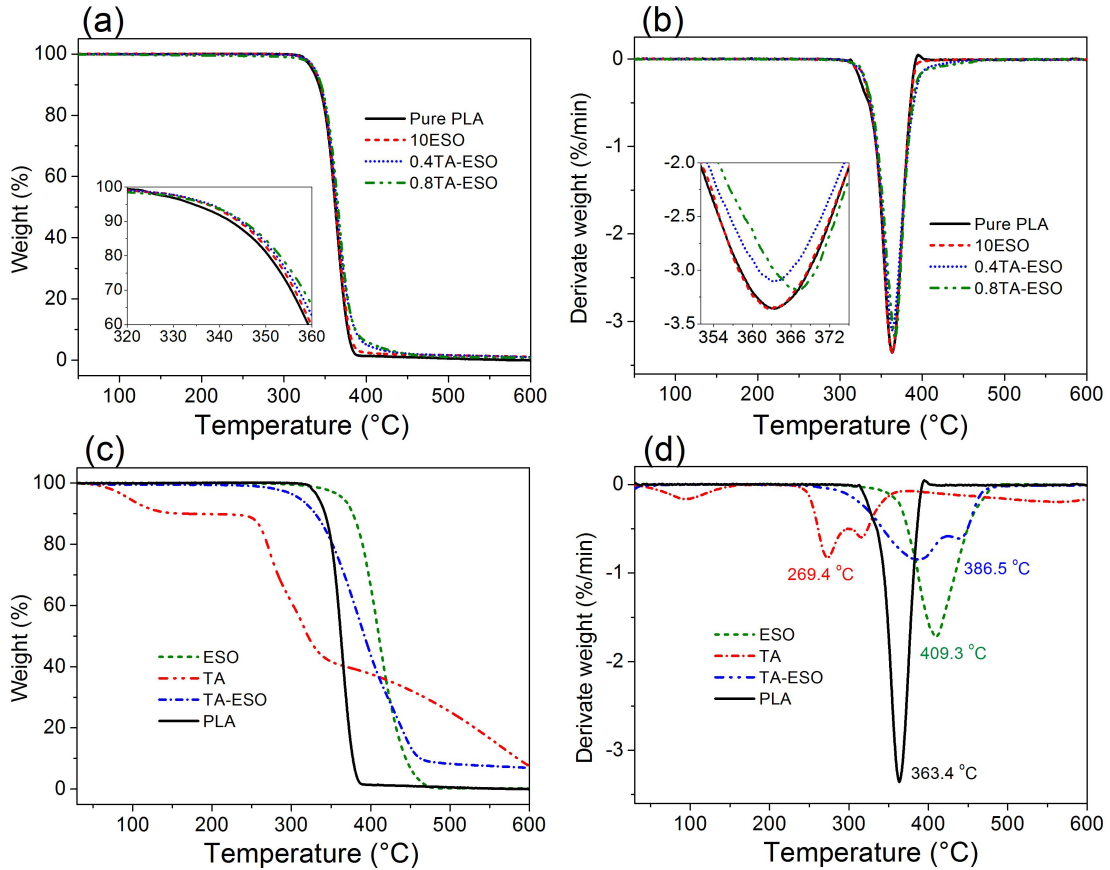


**Figure 4-6** Thermal degradation behavior of TA-ESO/PLA blends. (a) TG curves of TA-ESO/PLA blends; (b) DTG curves of TA-ESO/PLA blends; (c) TG curves of PLA, TA, ESO, and TA-ESO; (d) DTG curves of PLA, TA, ESO, and TA-ESO

**Table 4** Characteristic weight loss temperatures of TA-crosslinked-ESO/PLA blends

References	Characteristic weight loss temperature (°C)			$T_s$
	$T_{max}$	$T_5$	$T_{30}$	
	Pure PLA	363.4	334.3	
10ESO	362.8	337.2	356.2	170.8
0.4TA-ESO	363.3	337.9	357.1	171.2
0.8TA-ESO	366.9	337.3	358.1	171.4

$$T_s = 0.49[T_5 + 0.6(T_{30} - T_5)] \quad (4-3)$$

It is observed that the 10ESO exhibited an improved thermal stability relative to pure PLA because of its slightly higher  $T_s$ . This is in line with the fact that epoxidized vegetable oils have been normally used as thermal stabilizers [12,44]. As evidenced by Figure 4-6cd, the  $T_{max}$  of ESO was 409.3°C, which was greatly higher than that of PLA (363.4°C). The thermal decomposition of polymers involves the cleavage of

functional groups including C–C, C–O, and C=O bonds. The ESO molecules with aliphatic chains present higher thermal stability than the PLA chains featured by ester groups. Also, the oxirane rings of ESO could scavenge acid groups from PLA by thermal decomposition, which plays a positive role in increasing thermal stability [45].

As shown in Figure 4-6cd, with regard to ESO and PLA, TA exhibited an inferior thermal resistance with a  $T_{\max}$  of 269.4°C due to its large amount of –OH and ester groups. However, the crosslinking between ESO and TA consumes the –OH groups from TA, hence generating TA-ESO oligomers with higher thermal stability than TA. Especially, the incorporation of aromatic rings from TA endows TA-ESO oligomers a higher thermal degradation temperature as presented by the second  $T_{\max}$  in the DTG curve of TA-ESO. Hence, the 0.4TA-ESO and 0.8TA-ESO blends had higher  $T_{\max}$  and  $T_s$  than 10ESO, suggesting an improved thermal stability. Increases in  $T_s$  were observed with values of 171.2°C and 171.4°C for 0.4TA-ESO and 0.8TA-ESO when compared to pure PLA (170.0°C) and 10ESO (170.8°C). However, the effect of increment of  $n_{\text{-OH/epoxy}}$  from 0.4 to 0.8 on the thermal resistance of the blends was insignificant.

#### 4.3.5 Tensile properties of TA-ESO/PLA blends

The stress-strain curves of pure PLA, 10ESO, and TA-ESO/PLA blends are presented in Figure 4-7. Pure PLA exhibited a typical brittle fracture behavior, while

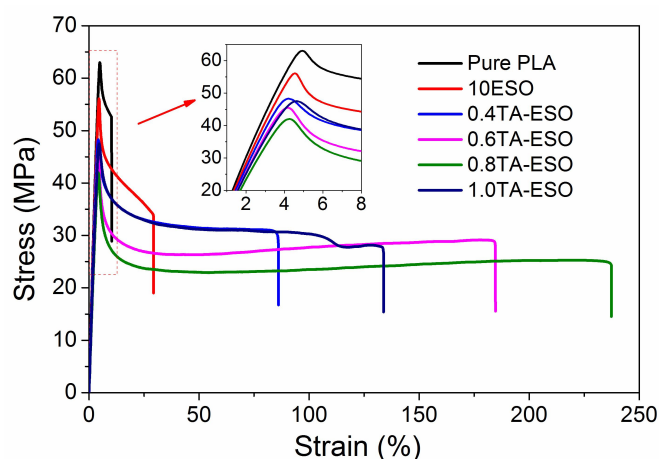


**Figure 4-7** Stress-strain curves of TA-ESO/PLA blends

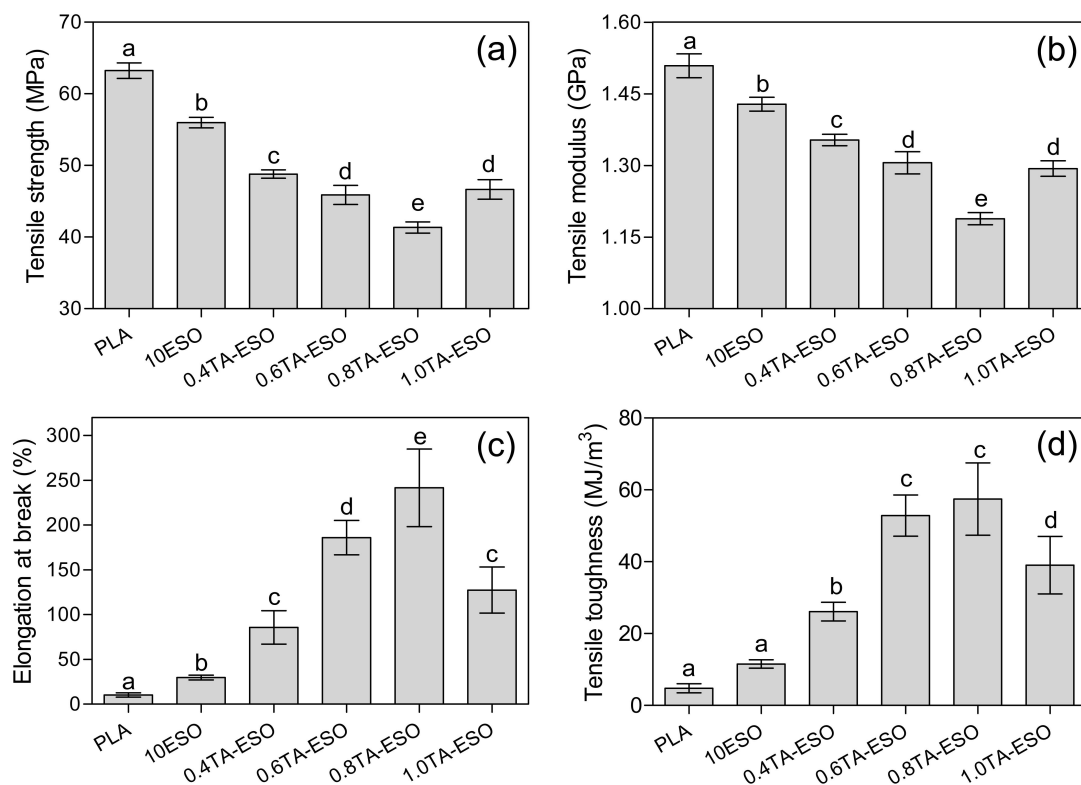


**Figure 4-8** Tensile properties of TA-ESO/PLA blends

Note: Data were analyzed with one-way ANOVA based on a 95% confidence interval; significant differences exist between any two groups when they do not share a common letter at the end of the data.

all ESO/PLA blends with or without TA as a vulcanizing agent showed ductile characteristics with clear yield point.

The tensile strength, tensile modulus, elongation at break, and tensile toughness (calculated from the area under the stress-strain curve) of the blends were summarized in Figure 4-8. Rigid PLA has high tensile strength of 63.2 MPa and tensile modulus of 1.5 GPa, as well as low elongation at break of 10.4% and tensile toughness of 4.8 MJ/m<sup>3</sup>. The introduction of 10 wt% ESO into PLA resulted in significant increases in elongation at break and tensile toughness to 29.6% and 11.5 MJ/m<sup>3</sup>, and subsequent decreases in tensile strength and tensile modulus with 56.0 MPa and 1.43 GPa, respectively. The elongation at break and tensile toughness of the TA-ESO/PLA blends considerably increased to 85.7–241.6% and 26.1–57.4 MJ/m<sup>3</sup> as the increase of TA concentration, which were significantly higher than those of pure PLA and 10ESO. However, much lower tensile strengths and moduli of 48.8–41.3 MPa and

1.4–1.2 GPa, respectively, were seen in the blends compared to pure PLA and 10ESO. This is attributed to the formation of stable TA-ESO rubbery phase in the PLA blends via dynamic vulcanization.

The toughening efficiency of TA-ESO on the PLA blends is closely correlated with the properties of the formed TA-ESO phase and its interfacial compatibility with PLA matrix. The crosslinking degree of the TA-ESO phase would increase with the increase in the amount of –OH groups in the systems, which facilitates the transformation of viscous ESO liquid into flexible TA-ESO rubber, and improves the interfacial adhesion between the TA-ESO phase with PLA. This contributes to continuous improvements in elongation at break and tensile toughness of the blends with the increase of  $n_{\text{-OH/epoxy}}$  from 0.4 to 0.8. However, a decrease case was observed in both tensile strength and modulus due to the improved ductility and thus reduced stiffness of the blends. The added ESO might diffuse into PLA amorphous area and interact with PLA molecular segments via possible covalent bonding, hydrogen bonding, and Van der Waals force [42]. This might destroy the interactions between PLA molecular chains and reduce the molecular density of PLA. This consequence was intensive by the improved interfacial bonding between TA-ESO phase and PLA matrix due to the increased TA concentration, hence leading to decreased tensile strength and modulus. It is reported that the TA-crosslinked-ESO had tensile strengths of 4.4 to 12.7 MPa and tensile moduli of 54 to 409 MPa, depending on the curing condition [34]. This also explains the decreased tensile strengths and moduli of the PLA blends after the introduction of TA-ESO phase, although the crystallinity of the blends were increased. However, further increase in the  $n_{\text{-OH/epoxy}}$  to 1.0 greatly reduced the elongation at break and tensile toughness while increasing the tensile strength and modulus of 1.0TA-ESO when compared to 0.8TA-ESO. The excess use of rigid TA into TA-ESO phase highly improves the crosslinking density and thus stiffness of the rubbery phase, resulting in improved strength and modulus as well as reduced toughness. In summary, the 0.8TA-ESO blend achieved the highest elongation at break and tensile toughness with values of 241.6% and 57.4 MJ/m<sup>3</sup>, respectively, which were about 22 and 11 times greater than those of pure PLA,

suggesting a considerable improvement in the flexibility of PLA.

### 4.3.6 Toughening mechanism

The SEM images of neat PLA, 10ESO, 0.4TA-ESO, and 0.8TA-ESO blends from the cryo-fractured specimen were given in Figure 4-9a-d. A smooth surface was seen for pure PLA, while rough surfaces with obvious phase separation were obtained for the ESO/PLA blends. Raised particles and voids were seen on the surface of the blends, indicating the pulling out of dispersed ESO or TA-ESO phase when the blends were cryo-fractured. The particle size distributions for the blends were measured and given in Figure 4-9e-g. For the 10ESO blend, the ESO particles with an average diameter of 0.41  $\mu\text{m}$  were uniformly dispersed in PLA matrix, suggesting an effective mixing for ESO and PLA via a twin-screw extruder. The distributed TA-ESO particle size in the TA-ESO/PLA blends mainly ranged from 0.2 to 0.8  $\mu\text{m}$ , with average values of 0.60 and 0.56  $\mu\text{m}$  for 0.4TA-ESO, and 0.8TA-ESO, respectively. When the TA monomers were added into ESO, the reaction between TA

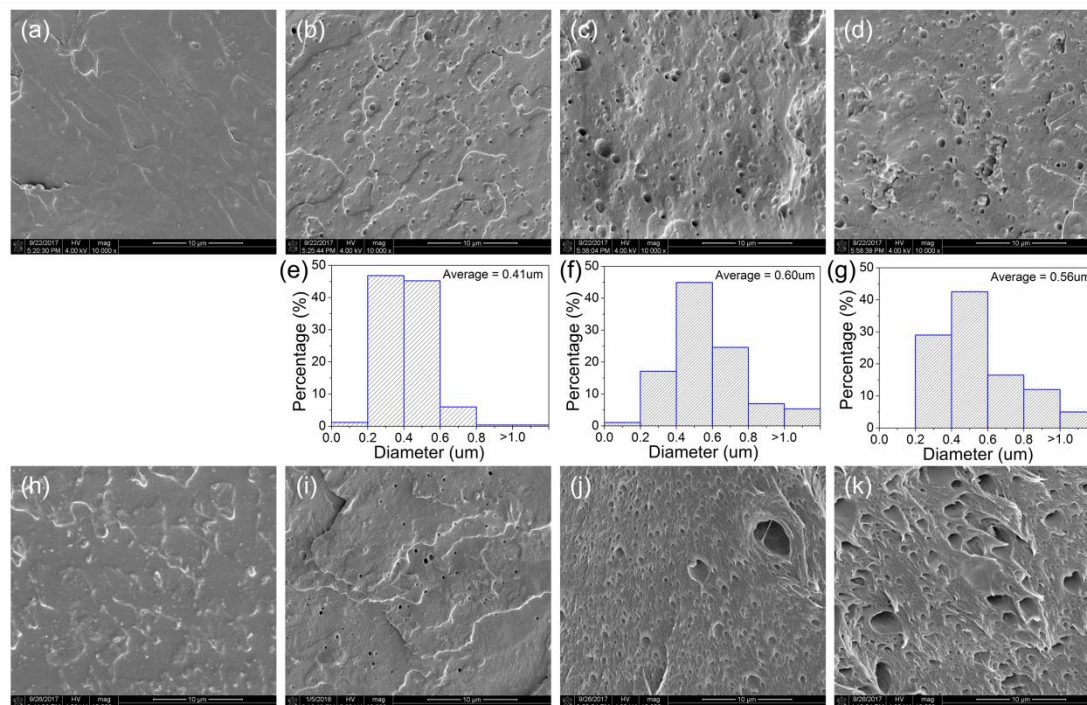


**Figure 4-9** SEM images of cryo-fractured surfaces of (a) pure PLA, (b) 10ESO, (c) 0.4TA-ESO, and (d) 0.8TA-ESO; Size distributions of TA-ESO particles on the cryo-fractured surfaces of (e) 10ESO, (f) 0.4TA-ESO, and (g) 0.8TA-ESO; SEM images of tensile-fractured surfaces of (h) pure PLA, (i) 10ESO, (j) 0.4TA-ESO, and (k) 0.8TA-ESO

and ESO would occur during the mixing process and hence preventing the breakage of TA-ESO phase into fine droplets. An increased viscosity in the system caused by the added TA monomers and their crosslinking with ESO and PLA also results in the formation of larger TA-ESO particles.

To further reveal the toughening mechanism of TA-ESO phase on the PLA blends, the morphology for the tensile-fractured surfaces of the blends were shown in [Figure 4-9h-k](#). A flat and smooth surface was observed on the fractured surfaces for brittle PLA, suggesting no evidence of plastic deformation. The fractured surfaces of the 10ESO showed clear voids generated from the pulling out of ESO particles, indicative of a weak interfacial adhesion between PLA and ESO. A higher spherical shapes was distinguished on the surface of 10ESO blend relative to pure PLA, which is responsible for its higher elongation at break and tensile toughness. Both 0.4TA-ESO and 0.8TA-ESO showed a large number of elongated cells with significantly plastic deformation occurred. When the blend was loaded under tension and the stress was higher than the interfacial adhesion between the two phases, the dispersed TA-ESO particles would be debonded from PLA matrix, hence generating cavities and causing large matrix plastic deformation due to the shear yielding caused by rubber particle debonding [32]. The average size of the elongated cells for 0.8TA-ESO was higher than that for 0.4TA-ESO, indicating an improved plastic deformation ability for the TA-ESO/PLA blends with a higher TA concentration. This is attributed to the simultaneously improved crosslinking density of TA-ESO phase and interfacial adhesion between the TA-ESO phase and PLA matrix.

#### **4.4 Conclusion**

Fully sustainable and highly tough PLA blends were successfully formulated by dynamic vulcanization of PLA with ESO by using TA as a green vulcanizing agent. Results indicated the incorporated TA carrying –OH groups could crosslink with ESO to form TA-ESO phase dispersed on the PLA matrix, and react with PLA to enhance the interfacial compatibility between the ESO phase and PLA matrix. The formation of stable TA-ESO phase and its improved interfacial adhesion with PLA contributed

to improving the toughening efficiency of TA-ESO phase on the PLA blends. The PLA blend containing 10 wt% TA-ESO phase with a molar ratio of –OH groups to epoxy rings of 0.8 achieved the highest elongation at break and tensile toughness with the values of 242% and 57.4 MJ/m<sup>3</sup>, respectively, which was correlated with the large-sized cavities formed during tension from the SEM images of the blend. The TA-ESO/PLA blends had slightly higher thermal stabilities and glass transition temperature than the ESO/PLA blend. In a word, dynamic vulcanization of PLA with ESO and TA was successfully performed to greatly improve the toughness of PLA products, which was a facile, cost-effective, and sustainable method to toughen PLA with biobased materials.

## References

- [1] Wang, L.; Gramlich, W.M.; Gardner, D.J. Improving the impact strength of poly(lactic acid) (PLA) in fused layer modeling (FLM). *Polymer* 2017, 114, 242-248.
- [2] Maroufkhani, M.; Katbab, A.; Liu, W.; Zhang, J. Polylactide (PLA) and acrylonitrile butadiene rubber (NBR) blends: The effect of ACN content on morphology, compatibility and mechanical properties. *Polymer* 2017, 115, 37-44.
- [3] Ma, P.; Lv, P.; Xu, P.; Du, M.; Zhu, H.; Dong, W.; Chen, M. Design of bio-based conductive and fast crystallizing nanocomposites with controllable distribution of multiwalled carbon nanotubes via interfacial stereocomplexation. *Chem. Eng. J.* 2018, 336, 223-232.
- [4] Zhang, K.; Yu, H.O.; Yu, K.X.; Gao, Y.; Wang, M.; Li, J.; Guo, S. A facile approach to constructing efficiently segregated conductive networks in poly(lactic acid)/silver nanocomposites via silver plating on microfibers for electromagnetic interference shielding. *Compos. Sci. Technol.* 2017, 156, 136-143.
- [5] Botlhoko, O.J.; Ramontja, J.; Ray, S.S. Morphological development and enhancement of thermal, mechanical, and electronic properties of thermally exfoliated graphene oxide-filled biodegradable polylactide/poly( $\epsilon$ -caprolactone) blend composites. *Polymer* 2018, 139, 188-200.
- [6] Zeng, J.B.; Li, K.A.; Du, A.K. Compatibilization strategies in poly(lactic acid)-based blends, *RSC Adv.* 2015, 5, 32546-32565.
- [7] Gandini, A. Polymers from renewable resources: A challenge for the future of macromolecular materials. *Macromolecules* 2008, 41, 9491-9504.
- [8] Meng, X.; Bocharova, V.; Tekinalp, H.; Cheng, S.; Kisliuk, A.; Sokolov, A.P.; Kunc, V.; Peter, W.H.; Ozcan, S. Toughening of nanocellulose/PLA composites via bio-epoxy interaction: Mechanistic study. *Mater. Des.* 2018, 139, 188-197.

- [9] Quiles-Carrillo, L.; Duart, S.; Montanes, N.; Torres-Giner, S.; Balart, R. Enhancement of the mechanical and thermal properties of injection-molded polylactide parts by the addition of acrylated epoxidized soybean oil. *Mater. Des.* 2018, 140, 54-63.
- [10] Xiong, Z.; Yang, Y.; Feng, J.; Zhang, X.; Zhang, C.; Tang, Z.; Zhu, J. Preparation and characterization of poly(lactic acid)/starch composites toughened with epoxidized soybean oil. *Carbohydr. Polym.* 2013, 92, 810-816.
- [11] Al-Mulla, E.A.J.; Yunus, W.M.Z.W.; Ibrahim, N.A.B.; Rahman, M.Z.A. Properties of epoxidized palm oil plasticized polylactic acid. *J. Mater. Sci.* 2010, 45, 1942-1946.
- [12] Ferri, J.; Garcia-Garcia, D.; Sánchez-Nacher, L.; Fenollar, O.; Balart, R. The effect of maleinized linseed oil (MLO) on mechanical performance of poly(lactic acid)-thermoplastic starch (PLA-TPS) blends. *Carbohydr. Polym.* 2016, 147, 60-68.
- [13] Carbonell-Verdu, A.; Garcia-Garcia, D.; Dominici, F.; Torre, L.; Sanchez-Nacher, L.; Balart, R. PLA films with improved flexibility properties by using maleinized cottonseed oil. *Eur. Polym. J.* 2017, 91, 248-259.
- [14] Carbonell-Verdu, A.; Samper, M.D.; Garcia-Garcia, D.; Sanchez-Nacher, L.; Balart, R. Plasticization effect of epoxidized cottonseed oil (ECSO) on poly(lactic acid). *Ind. Crop. Prod.* 2017, 104, 278-286.
- [15] Ferri, J.; Samper, M.; García-Sanoguera, D.; Reig, M.; Fenollar, O.; Balart, R. Plasticizing effect of biobased epoxidized fatty acid esters on mechanical and thermal properties of poly(lactic acid). *J. Mater. Sci.* 2016, 51, 5356-5366.
- [16] Mauck, S.C.; Wang, S.; Ding, W.; Rohde, B.J.; Fortune, C.K.; Yang, G.; Ahn, S.-K.; Robertson, M.L. Biorenewable tough blends of polylactide and acrylated epoxidized soybean oil compatibilized by a polylactide star polymer. *Macromolecules* 2016, 49, 1605-1615.
- [17] Robertson, M.L.; Chang, K.; Gramlich, W.M.; Hillmyer, M.A. Toughening of polylactide with polymerized soybean oil. *Macromolecules* 2010, 43, 1807-1814.
- [18] Chen, Y.; Yuan, D.; Xu, C. Dynamically vulcanized biobased polylactide/natural rubber blend material with continuous cross-linked rubber phase. *ACS Appl. Mater. Inter.* 2014, 6, 3811-3816.
- [19] Zhang, L.; Xiong, Z.; Shams, S.S.; Yu, R.; Huang, J.; Zhang, R.; Zhu, J. Free radical competitions in polylactide/bio-based thermoplastic polyurethane/free radical initiator ternary blends and their final properties. *Polymer* 2015, 64 69-75.
- [20] Lu, X.; Wei, X.; Huang, J.; Yang, L.; Zhang, G.; He, G.; Wang, M.; Qu, J. Supertoughened poly(lactic acid)/polyurethane blend material by in situ reactive interfacial compatibilization via dynamic vulcanization. *Ind. Eng. Chem. Res.* 2014, 53, 17386-17393.
- [21] Zhao, X.; Ding, Z.; Lin, Q.; Peng, S.; Fang, P. Toughening of polylactide via in situ formation of polyurethane crosslinked elastomer during reactive blending. *J. Appl. Polym. Sci.* 2016, 134, 44383.
- [22] Liu, G.C.; He, Y.S.; Zeng, J.B.; Li, Q.T.; Wang, Y.Z. Fully biobased and supertough

- polylactide-based thermoplastic vulcanizates fabricated by peroxide-induced dynamic vulcanization and interfacial compatibilization. *Biomacromolecules* 2014, 15, 4260-4271.
- [23] Valerio, O.; Pin, J.M.; Misra, M.; Mohanty, A.K. Synthesis of glycerol-based biopolyesters as toughness enhancers for polylactic acid bioplastic through reactive extrusion. *ACS Omega* 2016, 1, 1284-1295.
- [24] Kfoury, G.; Hassouna, F.; Raquez, J.M.; Toniazzo, V.; Ruch, D.; Dubois, P. Tunable and durable toughening of polylactide materials via reactive extrusion. *Macromol. Mater. Eng.* 2014, 299, 583-595.
- [25] Liu, H.; Chen, F.; Liu, B.; Estep, G.; Zhang, J. Super toughened poly(lactic acid) ternary blends by simultaneous dynamic vulcanization and interfacial compatibilization. *Macromolecules* 2010, 43, 6058-6066.
- [26] Ma, P.; Xu, P.; Liu, W.; Zhai, Y.; Dong, W.; Zhang, Y.; Chen, M. Bio-based poly(lactide)/ethylene-co-vinyl acetate thermoplastic vulcanizates by dynamic crosslinking: Structure vs. Property. *RSC Adv.* 2015, 5, 15962-15968.
- [27] Ma, P.; Xu, P.; Zhai, Y.; Dong, W.; Zhang, Y.; Chen, M. Biobased poly(lactide)/ethylene-co-vinyl acetate thermoplastic vulcanizates: Morphology evolution, superior properties, and partial degradability. *ACS Sustain. Chem. Eng.* 2015, 3, 2211-2219.
- [28] Yuan, D.; Chen, K.; Xu, C.; Chen, Z.; Chen, Y. Crosslinked bicontinuous biobased PLA/NR blends via dynamic vulcanization using different curing systems. *Carbohydr. Polym.* 2014, 113, 438-445.
- [29] Yuan, D.; Chen, Z.; Xu, C.; Chen, K.; Chen, Y. Fully biobased shape memory material based on novel cocontinuous structure in poly(lactic acid)/natural rubber TPVS fabricated via peroxide-induced dynamic vulcanization and in situ interfacial compatibilization, *ACS Sustain. Chem. Eng.* 2015, 3, 2856-2865.
- [30] Wu, N.; Zhang, H.; Fu, G. Super-tough poly(lactide) thermoplastic vulcanizates based on modified natural rubber. *ACS Sustain. Chem. Eng.* 2016, 5, 78-84.
- [31] Chen, Y.; Chen, K.; Wang, Y.; Xu, C. Biobased heat-triggered shape-memory polymers based on polylactide/epoxidized natural rubber blend system fabricated via peroxide-induced dynamic vulcanization: Co-continuous phase structure, shape memory behavior, and interfacial compatibilization. *Ind. Eng. Chem. Res.* 2015, 54, 8723-8731.
- [32] Zhao, T.H.; He, Y.; Li, Y.D.; Wang, M.; Zeng, J.B. Dynamic vulcanization of castor oil in a polylactide matrix for toughening. *RSC Adv.* 2016, 6, 79542-79553.
- [33] He, Y.; Zhao, T.H.; Li, Y.D.; Wang, M.; Zeng, J.B. Toughening polylactide by dynamic vulcanization with castor oil and different types of diisocyanates. *Polym. Test.* 2017, 59, 470-477.
- [34] Shibata, M.; Teramoto, N.; Makino, K. Preparation and properties of biocomposites composed of epoxidized soybean oil, tannic acid, and microfibrillated cellulose. *J. Appl. Polym. Sci.* 2011, 120, 273-278.

- [35] Shibata, M.; Nakai, K. Preparation and properties of biocomposites composed of bio-based epoxy resin, tannic acid, and microfibrillated cellulose. *J. Polym. Sci. Part B: Polym. Phys.* 2010, 48, 425-433.
- [36] Wang, L.; Lee, R.E.; Wang, G.; Chu, R.K.; Zhao, J.; Park, C.B. Use of stereocomplex crystallites for fully-biobased microcellular low-density poly(lactic acid) foams for green packaging. *Chem. Eng. J.* 2017, 327, 1151-1162.
- [37] Shechter, L.; Wynstra, J. Glycidyl ether reactions with alcohols, phenols, carboxylic acids, and acid anhydrides. *Ind. Eng. Chem.* 1956, 48, 86-93.
- [38] Zhao, T.H.; Yuan, W.Q.; Li, Y.D.; Weng, Y.X.; Zeng, J.B. Relating chemical structure to toughness via morphology control in fully sustainable sebacic acid cured epoxidized soybean oil toughened polylactide blends. *Macromolecules* 2018, 51, 2027-2037.
- [39] Vijayarajan, S.; Selke, S.E.M.; Matuana, L.M. Continuous blending approach in the manufacture of epoxidized soybean-plasticized poly(lactic acid) sheets and films. *Macromol. Mater. Eng.* 2014, 299, 622-630.
- [40] Liu, P.; Mullins, M.; Bremner, T.; Benner, N.; Sue, H.J. Interfacial phenomena and mechanical behavior of polyetheretherketone/polybenzimidazole blend under hygrothermal environment. *J. Phys. Chem. B* 2017, 121, 5396-5406.
- [41] Boyd, R.H. Relaxation processes in crystalline polymers: Experimental behaviour—a review. *Polymer* 1985, 26, 323-347.
- [42] Qian, S.; Zhang, H.; Yao, W.; Sheng, K. Effects of bamboo cellulose nanowhisker content on the morphology, crystallization, mechanical, and thermal properties of PLA matrix biocomposites. *Compos. Part B: Eng.* 2018, 133, 203-209.
- [43] Zhao, S.; Abu-Omar, M.M. Renewable epoxy networks derived from lignin-based monomers: effect of cross-linking density. *ACS Sustain. Chem. Eng.* 2016, 4, 6082-6089.
- [44] Johari, A.P.; Kurmvanshi, S.; Mohanty, S.; Nayak, S. Influence of surface modified cellulose microfibrils on the improved mechanical properties of poly(lactic acid). *Int. J. Biol. Macromol.* 2016, 84, 329-339.
- [45] Mohammed, F.S.; Conley, M.; Saunders, S.R.; Switzer, J.; Jha, R.; Cogen, J.M.; Chaudhary, B.I.; Pollet, P.; Eckert, C.A.; Liotta, C.L. Epoxidized linolenic acid salts as multifunctional additives for the thermal stability of plasticized PVC. *J. Appl. Polym. Sci.* 2015, 132, 41736.

# Chapter 5 Investigation on Carbon Nanotubes-Reinforced Epoxidized Soybean Oil /PLA Nanocomposites

## 5.1 Introduction

Biodegradable and biobased polymers have been widely developed to replace nonrenewable and petroleum-based counterparts to reduce plastics waste pollution. PLA is a linear aliphatic polyester that is derived from starch-rich products including corn and wheat via a fermentation process [1]. PLA possesses attractive properties such as high strength, easy processability, and non-toxicity to human beings and environment. Many studies have enabled the production of PLA products with a large-scale level and their various applications in packaging, textiles, automobiles, etc [2]. However, the intrinsic brittleness of PLA is the main bottleneck that inhibits its wider application.

Polymer blending is a convenient and efficient method to toughen PLA. Vegetable oils, containing flexible long-chain fatty acids, are cost-effective products due to their high availability and environmental credentials [3]. Vegetable oil derivatives, including epoxidized soybean oil (ESO) [4,5], epoxidized palm oil [6], maleinized linseed oil [7], maleinized and epoxidized cottonseed oils [8,9], and modified fatty acids [10], have been used as plasticizers for PLA. However, sufficient toughening efficiency is not achievable since these derivatives are immiscible with PLA. The interfacial adhesion between ESO and PLA was greatly increased by using a PLA star polymer with acrylated ESO core as compatibilizer, which contributed to significant increments in the tensile properties of the ESO/PLA blends [11]. The tensile toughness of the blends from polymerized soybean oil and PLA was considerably enhanced after the addition of poly(isoprene-*b*-L-lactide) block copolymers as a compatibilizer [12]. It is reported that dynamic vulcanization technique is effective in improving the interfacial compatibility of PLA-based blends and hence the toughening efficiency of the incorporated components on the blends [13]. The cationic polymerization of ESO was initiated during the blending of ESO

with PLA to produce fully biobased and highly toughly ESO/PLA blends (Chapter 3). A sustainable sebacic acid-cured ESO phase was introduced into PLA blends via dynamic vulcanization to increase the toughening efficiency of ESO on PLA [14]. The dynamic vulcanization of castor oil with PLA matrix induced by diisocyanates resulted in superior toughness and mechanical strength of the castor oil/PLA blends [15,16].

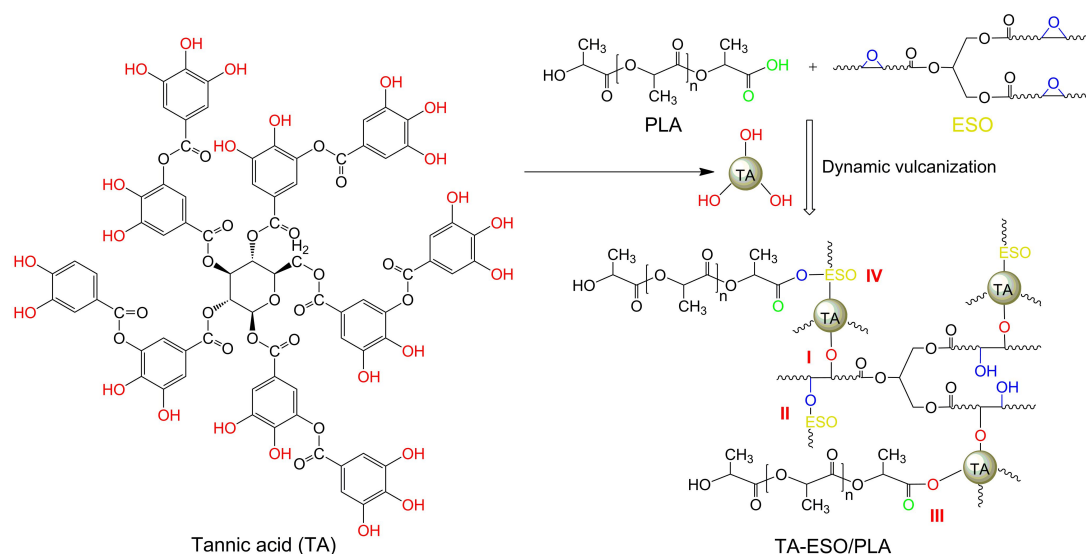


**Figure 5-1** Proposed reactions among TA, ESO and PLA during the preparation of TA-ESO/PLA blends

In Chapter 4, fully biobased ESO/PLA blends with high toughness were successfully developed via selecting a green monomer, i.e., tannic acid (TA), as a vulcanizing agent to crosslink ESO during dynamic vulcanization. As proposed in Figure 5-1, the possible reactions in the TA-ESO/PLA blends include 1) the phenolic  $-OH$  groups of TA with the epoxy rings of ESO (Reaction I), 2) the new generated  $-OH$  groups from Reaction I with other ESO epoxides (Reaction II), 3) the terminal  $-COOH$  groups of PLA with the  $-OH$  groups of TA (Reaction III), and 4) the terminal  $-COOH/-OH$  groups of PLA with the epoxy rings of ESO (Reaction IV). These result in the formation of a stable TA-crosslinked-ESO elastomer as a dispersed phase within PLA matrix and an improved interfacial adhesion between the TA-ESO phase and PLA matrix. Compared to the PLA blend with 10 wt% ESO, the PLA blend with 10 wt% TA-ESO (a molar ratio of  $-OH$  groups from TA to epoxy rings of ESO

was 0.6) achieved 5.3 and 3.6 times higher elongation at break and tensile toughness, respectively, while the tensile strength and tensile modulus dramatically reduced to 45.9 MPa and 1.3 GPa, respectively. Therefore, a significant compromise in mechanical strength and modulus is inevitable when using flexible polymers to toughen PLA.

Nanofillers, such as cellulose nanocrystals [17,18], graphene [19], montmorillonite [20], halloysite nanotubes [21], and carbon nanotubes (CNTs) [22], have been incorporated into PLA matrix for the preparation of PLA-based nanocomposites with significantly improved mechanical strength. CNT/PLA nanocomposites are particularly attractive due to the ability of CNTs to induce good mechanical strength and stiffness as well as superior thermal and electrical properties [23]. It was found that the PLA nanocomposite with 3 wt% CNTs obtained from twin-screw extrusion achieved significant improvements in tensile strength and modulus as well as electrical conductivity [24]. The key challenges for preparing CNT/PLA nanocomposites are the poor dispersion of CNTs in PLA matrix and filler-matrix interfacial adhesion, which could be alleviated by functionalization of CNTs [25]. However, incorporation of CNTs dramatically deteriorated the impact strength and elongation at break of the resulting PLA nanocomposites.

Investigations on the toughening of CNT/PLA nanocomposites have been addressed by blending with plasticizers, elastomers, and other flexible polymers. For example, novel electroactive shape memory polymer nanocomposites were prepared from CNTs and ESO or epoxidized linseed oil plasticized PLA [26, 27]. More importantly, the addition of CNTs into an immiscible polymer blends is an efficient strategy to improve the fracture toughness of the blends, and the toughening efficiency depends on the selective location of CNTs in the blend components [28]. The toughness of PLA blends was greatly improved by incorporation of pristine and functionalized CNTs, along with the addition of different toughening phases, such as thermoplastic polyurethane (TPU) [29,30], polycarbonate (PC) [31,32], poly(butylene adipate-co-terephthalate) [33], poly(3-hydroxybutyrate-co-4-hydroxy butyrate) [34], polystyrene [35], poly(ethylene-co-vinyl acetate) [36,37], and natural rubber [38]. The

mechanical properties and miscibility of PC/PLA blends were greatly improved by simultaneous addition of a compatibilizer and CNTs [39]. Highly conductive PLA/TPU/CNTs nanocomposites with a low percolation threshold and excellent stiffness-toughness balance were obtained via inducing the formation of co-continuous structure in the PLA/TPU blend matrix [40].

To further develop ESO/PLA-based nanocomposites with superior strength-toughness balance, TA and CNTs were simultaneously incorporated into the composite systems. The TA was used as a vulcanizing agent to induce the crosslinking of ESO and form highly tough ESO/PLA blend, while the CNTs was expected to impart the obtained CNT/TA-ESO/PLA nanocomposites with good mechanical strength and modulus as well as electrical properties. Fixed TA usage (10 wt% TA-ESO with a molar ratio of –OH to epoxy of 0.6) and various amounts of CNTs (0.5–10 wt %) were added into the ESO/PLA products to investigate the influence of CNTs content on the tensile properties, dynamic mechanical properties, crystallization behavior, thermal stabilities, electrical properties, and morphologies of the resulting CNT/ESO/PLA nanocomposites along with the synergistic effects of CNTs and TA-ESO on the reinforcing and toughening of the nanocomposites.

## **5.2 Experimental section**

### **5.2.1 Materials**

PLA (Ingeo 3001D) was obtained from NatureWorks Japan (Tokyo, Japan). ESO with an average molar ratio of epoxy group/ESO of 4 mol was purchased from Aladdin Industrial Corporation (Shanghai, China). Multi-walled CNTs (NANOCYL® NC7000™) (average diameter: 9.5 nm; average length: 1.5 μm; carbon purity: 90%; metal oxide: 10%; surface area: 250–300 m<sup>2</sup>/g) were obtained from Nanocyl Japan (Chiba, Japan). TA with a molar ratio of –OH group/TA of 25 mol and acetone were obtained from Nacalai Tesque, INC (Tokyo, Japan). All the chemicals were used without further purification.

### 5.2.2 Preparation of CNT/TA-ESO/PLA nanocomposites

TA (2.92 g) was dissolved in acetone (20 g) to generate a TA solution. ESO (17.08 g) was then mixed with the solution with a vigorous stirring for 5 min. The molar ratio of –OH groups from TA to epoxy groups from ESO was 0.6. Then, the obtained TA-ESO mixture was oven-dried at 80°C for 4 h to remove the acetone, and thus a ESO solution with dispersed TA was generated.

PLA pellets (180 g) were dried in an oven at 80°C for 12 h and then mixed with the TA-ESO mixture. The weight of the TA-ESO mixture was kept at 10 wt% based on the total weight of the resulting TA-ESO/PLA blend. The dynamic vulcanization process of PLA with TA-ESO was conducted on a twin-screw extruder (Technovel Corporation Japan, KZW25TW-60MG-NH(-1200)-AKT). The temperatures in six zones were set at 150, 160, 170, 170, 180, and 180°C from feeding zone to die section, respectively. The screw speed was constantly maintained at 50 r/min. The extruded TA-ESO/PLA blends were quenched in a water bath, chopped into pellets, and then oven-dried at 80°C for 12 h for composite preparation.

The obtained TA-ESO/PLA blends were mixed with CNTs at different weight ratios of 0.5, 1, 3, 5, 7, and 10 wt%, respectively, to fabricate the CNT/TA-ESO/PLA nanocomposites. The nanocomposites were abbreviated as  $x$ CNT/TA-ESO/PLA, where the  $x$  means the weight fraction of CNTs in the nanocomposites. The mixing process was carried out on the same twin-screw extruder as the procedure of TA-ESO/PLA blend preparation. Dumbbell and rectangular specimens were obtained on an injection molding machine (Nissei Plastic Industrial, Japan, NP7-1F). The nozzle temperature, injection speed, mold temperature, and cooling time were 170°C, 17.6 mm/s, 40°C, and 40 s, respectively. For comparison, TA-ESO/PLA blend and PLA nanocomposite with 5 wt% CNTs (5CNT/PLA) were also prepared under same conditions.

### 5.2.3 Characterization

Differential scanning calorimetry (DSC) analyses were conducted on a STA 449 F3 Jupiter Simultaneous Thermal Analyzer (NETZSCH, Selb, Germany). Samples

with a weight of 5–10 mg was placed in a standard porcelain crucible with a lid. The tests were conducted from 25 to 210°C with a heating rate of 10 °C/min under N<sub>2</sub> (flow rate: 30 mL/min). The glass transition temperature ( $T_g$ ), cold crystallization peak ( $T_{cc}$ ), and melt peak temperature ( $T_m$ ) of PLA phase in the nanocomposites were obtained from the DSC curves. The degree of crystallinity ( $X_c$ ) for PLA was calculated as the Equation 5-1 [41]:

$$X_c = \frac{\Delta H_m - H_{cc}}{\Delta H_{100} \times x_{PLA}} \times 100 \quad (5-1)$$

where  $\Delta H_m$  and  $\Delta H_m$  are melting and cold crystallization enthalpies, respectively;  $\Delta H_{100}$  is theoretical melting enthalpy of a completely crystalline PLA (93.6 J/g), and  $x_{PLA}$  is the weight fraction of PLA in the nanocomposites.

Dynamic mechanical analysis (DMA) tests were carried out on a RSA-G2 solids analyzer (TA Instrument, DE, USA) under three point bending mode with a strain of 0.1% according to ASTM D 7028-15. Rectangular samples (55 × 10 mm<sup>2</sup>) were prepared for the tests from 30 to 100°C at a heating rate of 2 °C/min and a frequency of 1Hz.

Thermogravimetric (TG) analyses were performed on a DTG-60 TG instrument (Shimadzu, Japan). Samples with a weight of 4–6 mg were placed in aluminum crucibles. The tests were conducted from room temperature to 600°C at a scan rate of 10 °C/min under N<sub>2</sub> atmosphere at a flow rate of 50 mL/min.

A Series 3360 universal testing machine (Instron, MA, USA) was used to evaluate the tensile properties of the nanocomposites according to ASTM D 638-10. Dumbbell specimens with 25 mm gauge length, 2 mm thickness, and 5 mm narrow section width were used for the test at a crosshead speed of 10 mm/s. Five replicates were conducted for each nanocomposite.

Morphologies of the nanocomposites were observed on a JSM-7500F scanning electron microscope (SEM) (JEOL, Tokyo, Japan) and a Tecnai G2 F30 transmission electron microscopy (TEM) (FEI, Oregon, USA). For SEM observation, the cryo-fractured and tensile-fractured surfaces of the samples were coated with a gold film (8 to 10 nm). For TEM analysis, ultrathin samples (~100 nm) were cryogenically

cut at a temperature of  $-80^{\circ}\text{C}$  using a Leica EM UC7 ultramicrotome (Leica Microsystems K.K., Tokyo, Japan).

The volume electrical conductivity of rectangular specimens was measured on a double loop resistance meter (UPMCP-HT450, Mitsubishi Chemical Cooperation, Tokyo, Japan). Five replicates were conducted for each nanocomposite.

## 5.3 Results and discussion

### 5.3.1 Morphological analysis

The distributions of TA-ESO phase and CNTs on the nanocomposites were observed by SEM and TEM. The SEM images of TA-ESO/PLA blend and its nanocomposites with 0.5, 3, and 5 wt% CNTs from their cryo-fractured specimens were shown in [Figure 5-2](#). The surface of TA-ESO/PLA blend exhibited a typical sea-island morphology as characterized by raised particles and voids due to the dispersed TA-ESO phase ([Figure 5-2a](#)). For the nanocomposite with 0.5 wt% CNTs, a small fraction of CNTs was observed as light spots in the major PLA continuous

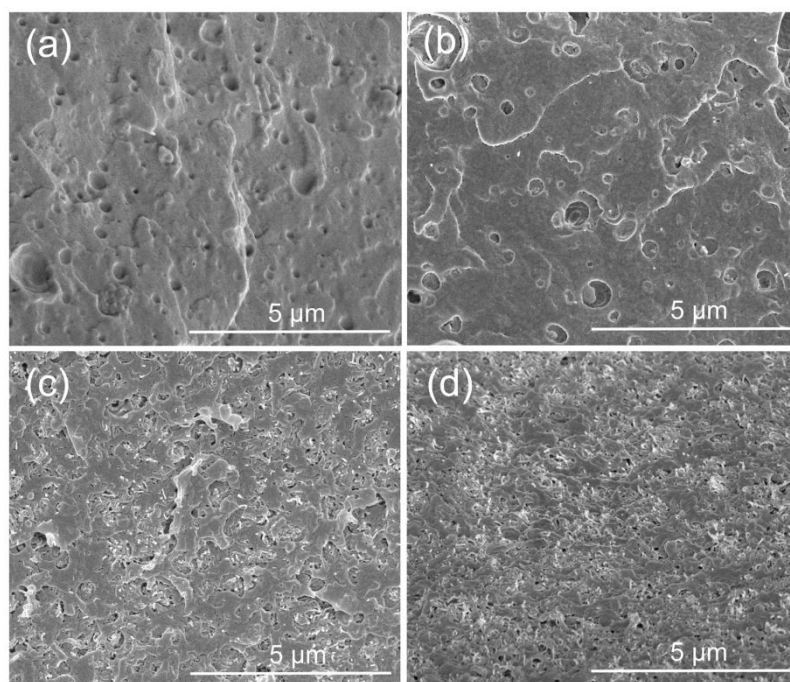


**Figure 5-2** SEM images of cryo-fractured surfaces of (a) TA-ESO/PLA blend, (b) 0.5CNT/TA-ESO/PLA, (c) 3CNT/TA-ESO/PLA, and (d) 5CNT/TA-ESO/PLA nanocomposites

phase (Figure 5-2b) because of the stronger affinity between CNTs and PLA than that between CNTs and TA-ESO phase. This can be confirmed by the matched solubility parameters of CNTs and PLA, which are approximately of 17.8 and 18.5 MPa<sup>1/2</sup>, respectively [24]. More importantly, the thermoset TA-ESO phase has a three dimensional network structure and hence can not be melted for the immersion of CNTs at high temperature. The size of the TA-ESO droplets was significantly reduced after the addition of CNTs. Especially, when the CNTs content increased up to 3 wt%, the TA-ESO phase was hardly observed due to its sharply decreased size (Figure 5-2cd). Meanwhile, large amount of CNTs were distributed and aggregated in the PLA phase. The selective distribution of CNTs in PLA phase tends to form a network structure as the increased CNTs content, which probably absorbs PLA phase around the CNTs networks and inhibits the breakup of PLA phase during processing. Also, the re-processing of the TA-ESO/PLA blend during nanocomposite preparation would reduce the particle size of the TA-ESO droplets because of the shear forces originated from the rotating screw.

The TEM images of TA-ESO/PLA blend exhibited number of broken cavities

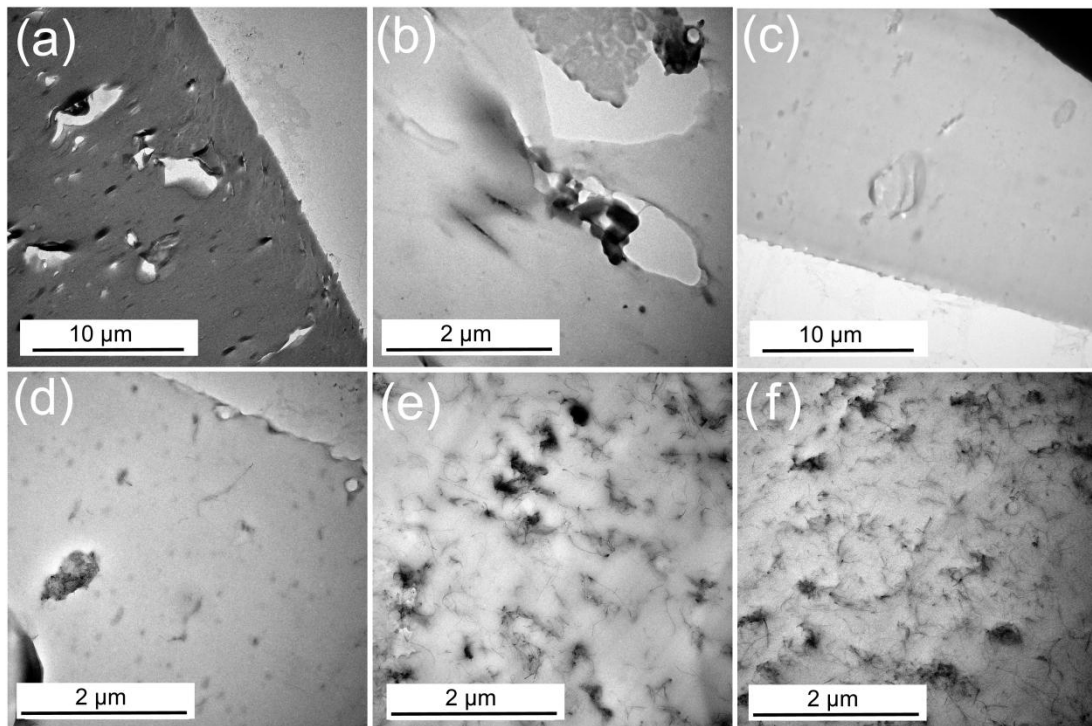


**Figure 5-3** TEM images of (a, b) TA-ESO/PLA blend, (c, d) 0.5CNT/TA-ESO/PLA, (e) 3CNT/TA-ESO/PLA, and (f) 5CNT/TA-ESO/PLA nanocomposites.

resulted from the TA-ESO droplets since the size of the droplets was much higher than the thickness of the prepared sample for TEM analysis (Figure 5-3ab). This phenomenon was largely eliminated for the 0.5CNT/TA-ESO/PLA nanocomposite due to the decreased particle size of the droplets (Figure 5-3c); a small part of CNTs was evenly distributed in the the nanocomposite (Figure 5-3d). In agreement with the information from SEM images, more CNTs were distributed and aggregated in the nanocomposites when the CNTs content increased to 3 and 5 wt% (Figure 5-3ef). The aggregation of CNTs in the nanocomposites was observed because of the poor interfacial adhesion between the pristine CNTs and PLA matrix, indicating that further functionalization for CNTs is desired for the nanocomposites to achieve higher performance.

### 5.3.2 Crystallization behavior of CNT/TA-ESO/PLA nanocomposites

The thermal transition and crystallization behavior of TA-ESO/PLA blend and its nanocomposites with CNTs were revealed by DSC analysis (Figure 5-4 and Table 5-1). TA-ESO/PLA blend showed significantly reduced glass transition temperature ( $T_g$ ) and cold crystallization temperature ( $T_{cc}$ ) as well as improved crystallinity ( $X_c$ ) when compared to neat PLA. The reduced  $T_g$  and  $T_{cc}$  are attributed to the plasticizing effect of TA-ESO phase, which would diffuse inside the PLA matrix and exist between the PLA molecular chains, hence increasing the free volume that makes the molecular chains move at lower temperatures [9]. The increased  $X_c$  is likely due to the nucleation effect of the added TA-ESO that provides additional heterogeneous nucleation sites for the crystallization of PLA. The addition of CNTs into TA-ESO/PLA blend slightly increased the  $T_g$  of the resulting nanocomposites, indicating the reinforcing effect of CNTs on PLA resin. Slight decreases in  $T_{cc}$  and cold crystallization enthalpy ( $\Delta H_{cc}$ ) were observed from the nanocomposites compared to TA-ESO/PLA blend because the added CNTs could act as a nucleating agent and induce crystallization. This also explains the lightly increased  $X_c$  of the nanocomposite from 28.51% to 31.41% after the introduction of 0.5 wt% CNTs. However, the agglomeration of excess CNTs would prevent the growth of the crystal

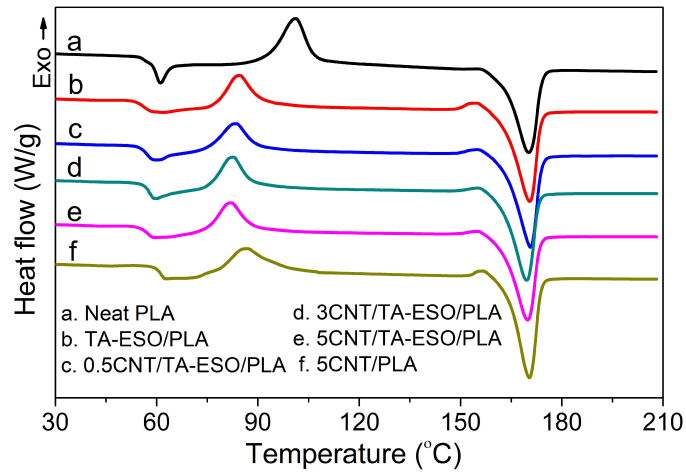


**Figure 5-4** DSC curves of neat PLA, TA-ESO/PLA, CNT/PLA and CNT/TA-ESO/PLA nanocomposites

**Table 5-1** DSC results of neat PLA, TA-ESO/PLA, CNT/PLA and CNT/TA-ESO/PLA nanocomposites

References	$T_g$ (°C)	$T_{cc}$ (°C)	$T_m$ (°C)	$\Delta H_{cc}$ (J/g)	$\Delta H_m$ (J/g)	$X_c$ (%)
Neat PLA	61.15	101.07	170.18	23.73	37.81	14.93
TA-ESO/PLA	58.37	84.29	170.48	17.33	41.19	28.33
0.5CNT/TA-ESO/PLA	58.74	83.60	170.84	14.28	40.44	31.21
3CNT/TA-ESO/PLA	59.47	82.49	169.38	14.74	37.92	28.37
5CNT/TA-ESO/PLA	59.10	81.76	169.75	14.62	37.46	28.54
5CNT/PLA	63.14	86.49	170.11	19.06	40.61	24.23

nucleus and hence reduce the ability of inducing crystallization, which was confirmed by the decreased  $X_c$  of the nanocomposites when increasing CNTs usage up to 3 wt%. The melting process of the crystalline phase in PLA showed a single melting peak around 170°C (melting temperature,  $T_m$ ) for all the blends and nanocomposites, which was not significantly affected by the addition of TA-ESO phase and CNTs. The melting enthalpy ( $\Delta H_m$ ) of TA-ESO/PLA was higher than that of neat PLA because of the increased  $X_c$ . However, the incorporation of CNTs led to slight reduction in  $\Delta H_m$  due to the reduced relatively amount of crystalline PLA phase in the nanocomposites.

As for the 5CNT/PLA nanocomposite, increases in  $T_g$  and  $X_c$  were observed along with decreases in  $T_{cc}$ ,  $\Delta H_{cc}$ , and  $\Delta H_m$  when compared to neat PLA due to the reinforcing and heterogeneous nucleation effects of CNTs on PLA. These effects are in agreement with the influence of CNTs on TA-ESO/PLA blend with a diminished

degree. This confirms that the flexible TA-ESO rubbery phase has a significant effect on the crystallization behavior of nanocomposites.

### 5.3.3 Dynamic mechanical properties of CNT/TA-ESO/PLA nanocomposites

DMA curves and their characteristic results of the nanocomposites were presented in Figure 5-5 and Table 5-2. The storage modulus ( $E'$ ) curves for all the

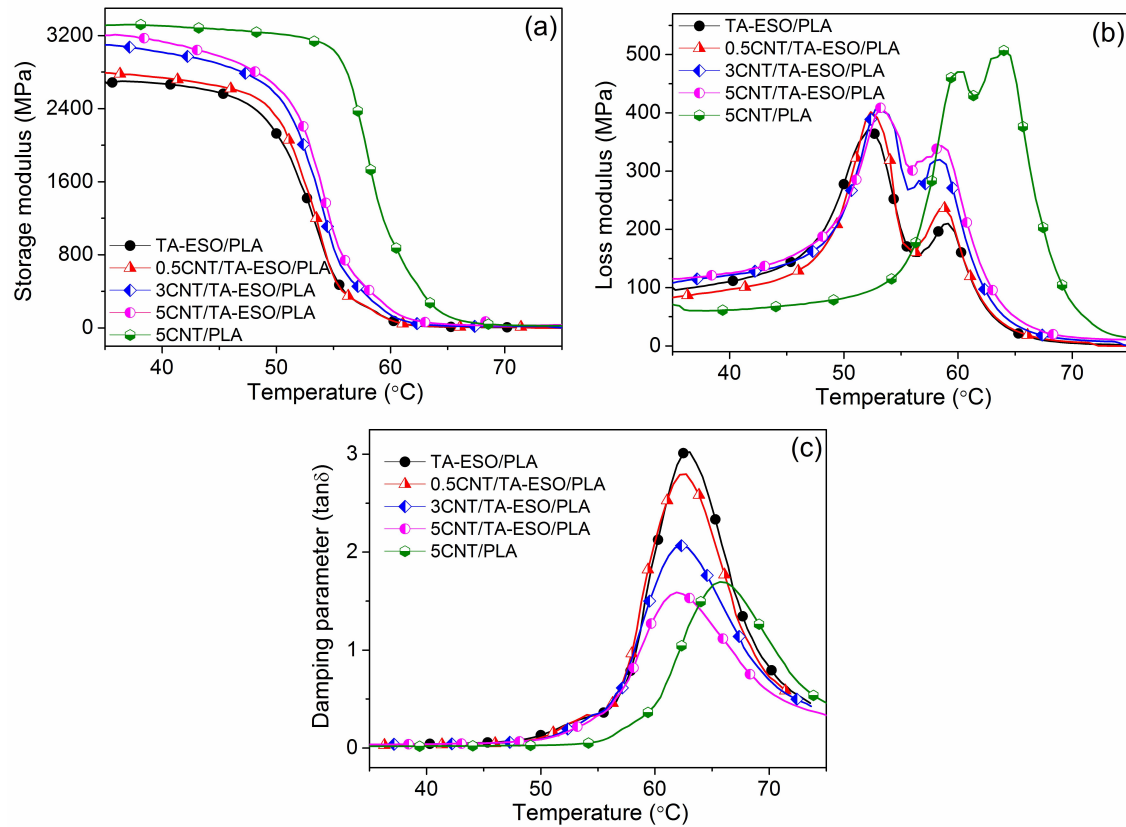


**Figure 5-5** DMA curves of TA-ESO/PLA, CNT/PLA and CNT/TA-ESO/PLA nanocomposites. (a) Storage modulus; (b) loss modulus; (c) damping parameter.

**Table 5-2** DMA results of TA-ESO/PLA, CNT/PLA and CNT/TA-ESO/PLA nanocomposites

Reference	Storage modulus at 35°C (GPa)	Peak temperatures from loss modulus (°C)		$T_g$ from $\tan \delta$ (°C)
		Peak 1	Peak 2	
TA-ESO/PLA	2.67	52.22	59.11	62.76
0.5CNT/TA-ESO/PLA	2.79	52.44	58.75	62.43
3CNT/TA-ESO/PLA	3.10	52.93	58.36	62.32
5CNT/TA-ESO/PLA	3.20	53.32	58.55	61.99
5CNT/PLA	3.31	60.18	64.06	65.86

nanocomposites had a platform from room temperature to 50°C and then experienced a dramatic drop at temperatures of 50–65°C, which is resulted from glass transition behavior. The  $E'$  of TA-ESO/PLA blend in the initial stage was 2.67 GPa, much lower than that of neat PLA (3.19 GPa) due to the plasticization effect of TA-ESO phase (Chapter 4). The addition of CNTs into the blend resulted in significant increments in the  $E'$ s of the resulting nanocomposites. The  $E'$ s of the nanocomposites at room temperature increased from 2.79 to 3.20 GPa as the increase of CNTs usage from 0.5 to 5 wt%. This is attributed to the strengthening effect of CNTs that has extremely high strength and modulus. Further, the 5CNT/TA-ESO/PLA nanocomposite has a slightly lower  $E'$  than 5CNT/PLA nanocomposite because of the added TA-ESO rubbery phase that reduces the stiffness of the nanocomposite.

The loss modulus ( $E''$ ) of TA-ESO/PLA blend showed two modulus peaks due to the mobility of polymer molecules, which corresponds to the glass transition behavior of the polymer and the chain rearrangement of oriented amorphous regions into crystalline phase [42], respectively. The incorporation of CNTs did not significantly change the transition temperatures of the nanocomposites, but increased the intensity of the second transition peak at high temperature region. This indicates that the added CNTs could promote the segmental movements of mobile and amorphous regions due to its heterogeneous nucleation effect, which is in agreement with the reduced  $T_{cc}$  obtained from DSC analyses as the increase of CNTs usage.

The damping parameter ( $\tan \delta$ ), calculated from the ratio of  $E''$  to  $E'$ , indicates the ratio of energy loss to energy reserved in the loading cycle, i.e., the ability of the material to dissipate energy. The  $\tan \delta$  peak of TA-ESO/PLA blend was sharp and intensive, which has higher height and peak area than those of the nanocomposites, indicating a superior molecular mobility due to the toughening effect of TA-ESO phase. The peak height and area of the nanocomposites significantly decreased with the increase of CNTs content, indicative of a reduced damping capacity due to the improved stiffness. The temperature at the  $\tan \delta$  peak was usually defined as the  $T_g$  of a material. The  $T_g$ s of all the CNT/TA-ESO/PLA nanocomposites were comparable with that of TA-ESO/PLA blend, but significantly lower than that of 5CNT/PLA

nanocomposite. This demonstrates that the ability of CNTs in improving the  $T_g$  of PLA nanocomposites is completely overlapped by the weakening effect of the ductile TA-ESO phase. The results are in accordance with that from DSC scans, although their  $T_g$ s were slightly higher than those from DSC tests because of the different basal theories of these two technologies.

### 5.3.4 Thermal stability of CNT/TA-ESO/PLA nanocomposites

The thermal degradation of TA-ESO/PLA blend and its nanocomposites with CNTs was presented in Figure 5-6. The temperatures ( $T_5$  and  $T_{30}$ ) at which a weight loss of 5% and 30%, and the maximum weight loss temperature ( $T_{max}$ ) were summarized in Table 5-3. A heat-resistant index ( $T_s$ ), indicating the overall thermal stability of the nanocomposites, was determined based on the following equation [43]:

$$T_s = 0.49[T_5 + 0.6(T_{30} - T_5)] \quad (5-2)$$

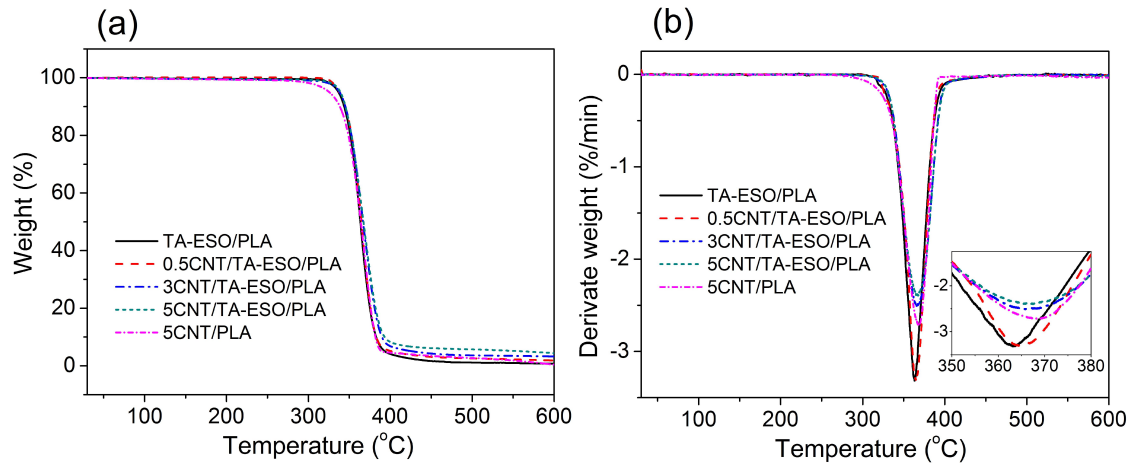


**Figure 5-6** Thermal degradation behaviors of TA-ESO/PLA, CNT/PLA and CNT/TA-ESO/PLA nanocomposites. (a) TG curves; (b) DTG curves

**Table 5-3** Characteristic weight loss temperatures of TA-ESO/PLA, CNT/PLA and CNT/TA-ESO/PLA nanocomposites

References	Characteristic weight loss temperature (°C)			$T_s$
	$T_{max}$	$T_5$	$T_{30}$	
TA-ESO/PLA	363.4	336.6	356.1	170.7
0.5CNT/TA-ESO/PLA	364.9	338.4	357.8	171.5
3CNT/TA-ESO/PLA	367.6	338.1	357.9	171.5
5CNT/TA-ESO/PLA	367.4	339.1	358.1	171.7
5CNT/PLA	368.8	325.5	335.0	162.3

It is observed that the thermal stability of the nanocomposites was slightly improved after the addition of CNTs. The  $T_{max}$ s of the nanocomposites increased from 364.9 to 367.4°C with the increase of CNTs from 0.5 to 5 wt%, although the  $T_s$ s of the nanocomposites were not significantly affected by the CNTs content. It is reported that the added CNTs would provide tortuous paths and barrier effects against the volatile pyrolysis products of PLA, which effectively prevents the diffusion of oxygen into the polymer matrix and thus the thermal degradation of the nanocomposites [38,44]. Furthermore, compared to 5CNT/PLA nanocomposite, 5CNT/TA-ESO/PLA nanocomposite exhibited an improved thermal stability because of its significantly higher  $T_{max}$  and  $T_s$ . The thermal decomposition of polymers involves the cleavage of functional groups including C–C, C–O, and C=O bonds. Both ESO molecules with aliphatic chains and TA monomers with aromatic rings have higher thermal stability than PLA chains featured by ester groups, which is responsible for the increased thermal resistance of the nanocomposites in the presence of TA-ESO phase.

### 5.3.5 Tensile properties of CNT/TA-ESO/PLA nanocomposites

The stress-strain curves of TA-ESO/PLA blend and its nanocomposites with 0.5, 3, and 5 wt% CNTs are presented in Figure 5-7. TA-ESO/PLA blend exhibited ductile characters with clear yield point and cold-drawing region, while the characters for the nanocomposites gradually mitigated with the increase of CNTs content. 5CNT/PLA

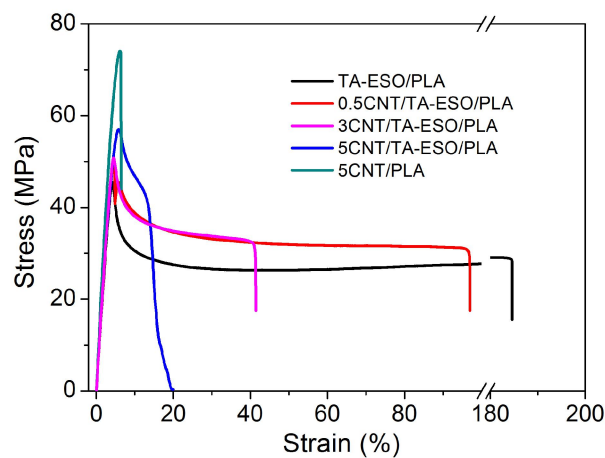


**Figure 5-7** Stress-strain curves of TA-ESO/PLA, CNT/PLA and CNT/TA-ESO/PLA nanocomposites

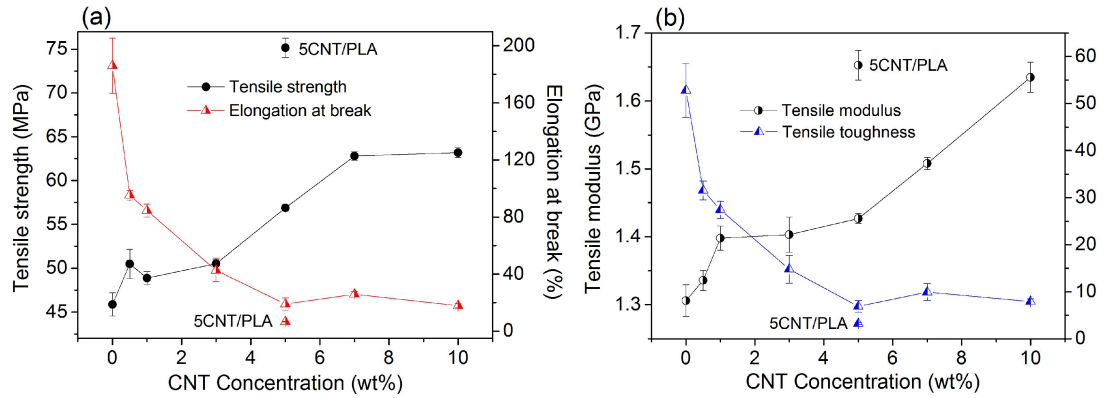


**Figure 5-8** Tensile properties of TA-ESO/PLA, CNT/PLA and CNT/TA-ESO/PLA nanocomposites

nanocomposite showed a typical brittle fracture behavior due to the brittleness nature of PLA and reinforcing effect of CNTs. However, the TA-ESO/PLA nanocomposite with 5 wt% CNTs presented obvious yield point and subsequent stress drop region due to the toughening effect of TA-ESO rubbery phase.

The tensile strength, tensile modulus, elongation at break, and tensile toughness (calculated from the area under the stress-strain curve) of the nanocomposites are shown in Figure 5-8. TA-ESO/PLA blend had high elongation at break of 186.1% and tensile toughness of 52.8 MJ/m<sup>3</sup>, but low tensile strength of 45.9 MPa and tensile modulus of 1.3 GPa. The presence of TA-ESO phase induced the deterioration of strength and modulus of the blend when compared to neat PLA. The strength and modulus can be compensated by the addition of CNTs due to its good strengthening effect. The tensile strength and modulus of the nanocomposites greatly increased from 50.5 to 63.2 MPa and 1.34 to 1.65 GPa, respectively, when the CNTs usage raised from 0.5 to 10 wt%. However, the addition of CNTs resulted in dramatic decrease in tensile ductility of the nanocomposites. The elongation at break and tensile toughness of the nanocomposites dramatically reduced from 95.4 to 19.0 % and 31.6 to 6.9 MJ/m<sup>3</sup>, respectively, as the increase of CNTs content from 0.5 to 5 wt%; further increase in CNTs usage from 5 to 10 wt% did not significantly affect the elongation at break and tensile toughness of the nanocomposites. This can be explained by the following two reasons: 1) The agglomerates of large CNTs function as the stress concentrator and thus lead to the failure of the nanocomposites during the tensile

process; 2) The formation of a dense CNTs network structure in the composites inhibits the plastic flow of PLA macromolecules along the tensile direction [39]. Although the introduction of CNTs into TA-ESO/PLA blend causes significant deterioration in toughness, the tensile ductility of 5CNT/TA-ESO/PLA nanocomposite still keeps at a relatively high level when compared to that of 5CNT/PLA nanocomposite. In summary, the 5CNT/TA-ESO/PLA nanocomposite achieved balanced tensile properties with higher elongation at break and tensile toughness as well as lower tensile strength and modulus in comparison to 5CNT/PLA nanocomposite, which is resulted from the synergistic effects of CNTs reinforcement and TA-ESO phase induced toughening.

### 5.3.6 Reinforcing and toughening mechanism

To reveal the influence of CNTs on the toughening mechanism of TA-ESO phase on the PLA blends, the morphology for the tensile-fractured surfaces of the nanocomposites were shown in Figure 5-9. Briefly, the SEM image of TA-ESO/PLA blend was not given. The dispersed TA-ESO particles would be debonded from PLA

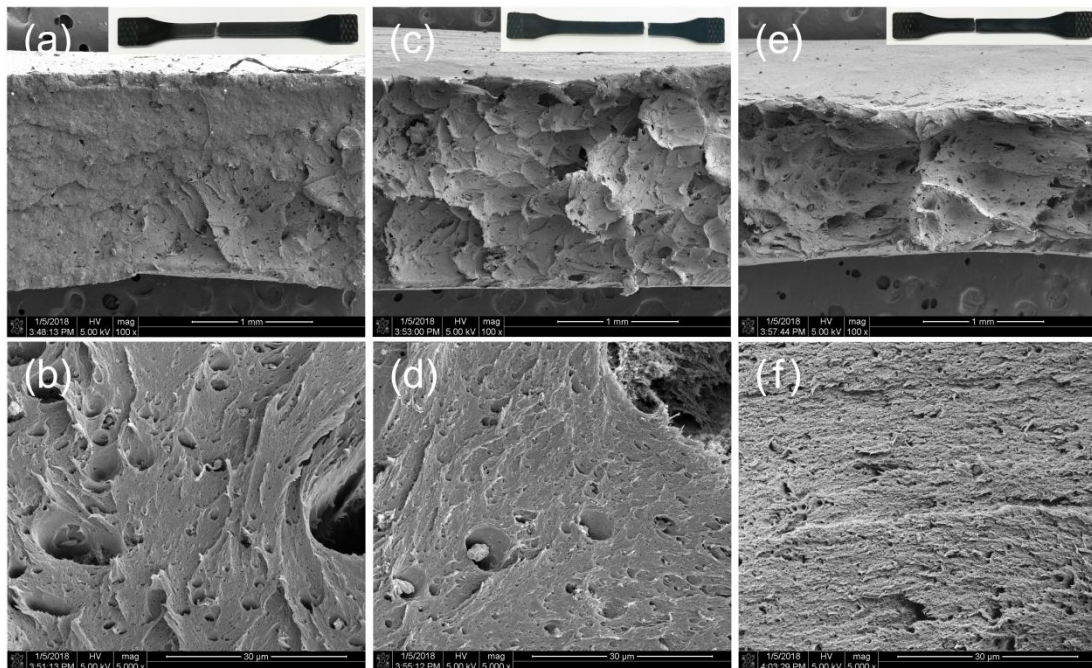


**Figure 5-9** SEM images of tensile-fractured surfaces of (a, b) 0.5CNT/TA-ESO/PLA, (c, d) 3CNT/TA-ESO/PLA, and (e, f) 5CNT/TA-ESO/PLA nanocomposites

matrix when the blend was loaded under tension, and hence the shear yielding caused by TA-ESO rubber particle debonding would result in forming cavities and large matrix plastic deformation [13, 45]. Similar to TA-ESO/PLA blend, the nanocomposite with 0.5 wt% CNTs still showed a large number of elongated cells with significant plastic deformation occurred (Figure 5-9ab). From the SEM images with low magnifications (Figure 5-9ace), it is clearly observed that the fractured surface of the nanocomposites changed from smooth morphology to coarse surface with the increase of CNTs usage, and obvious and huge holes were seen on the nanocomposites with high CNTs content. These indicate that the aggregation of CNTs at a high content in PLA phase would act directly on the stress concentration region, hence retarding the toughening effect of TA-ESO phase on PLA blends. Therefore, the shear yielding phenomenon caused by TA-ESO phase are inhibited during the loading process, which can be confirmed by the SEM images with high magnifications for the flat surface region of the nanocomposites (Figure 5-9bdf). The average size of the elongated cells and cavities reduced with the increase of CNTs usage from 0.5 to 5 wt%, indicating a decreased degree of plastic deformation. This is in agreement with the decreased elongation at break of the nanocomposites as the increase of CNTs usage.

### 5.3.7 Electrical properties of CNT/TA-ESO/PLA nanocomposites

The electrical conductivity of the CNT/TA-ESO/PLA nanocomposites increased exponentially with the increase of CNTs concentration (Figure 5-10). For the formation of an electrical conductive pathway constructed in the polymer composites, the distance between CNTs should be very close such that electron can be activated by thermal vibration, goes across the polymer barrier, and thus transfers to the adjacent CNTs to form a tunnelling current [34]. The percolation threshold ( $p_c$ ) was calculated by fitting the dependence of the measured electrical conductivity ( $\rho$ ) on CNTs content ( $p$ ) according to classical percolation theory [34, 46]:

$$\rho = \sigma_0(p-p_c)^t \quad (5-3)$$

where  $\sigma_0$  is a scaling factor, and  $t$  is a percolation exponent that represents the

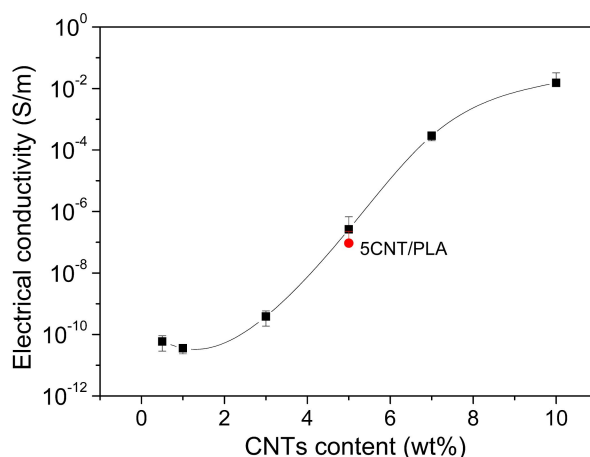


**Figure 5-10** Electrical conductivity of CNT/TA-ESO/PLA nanocomposites

dimensionality of percolation network with values around 1.3 and 2 for two and three-dimensions, respectively. The  $p_c$  and  $t$  values of the CNT/TA-ESO/PLA nanocomposites were estimated to be 6.38 wt% and 2.25, respectively, which confirms the formation of an approximate three-dimensional conductive network in the nanocomposites. Moreover, the electrical conductivity of 5CNT/TA-ESO/PLA nanocomposite was slightly higher than that of 5CNT/PLA nanocomposite. As revealed by SEM images, the morphology of TA-ESO/PLA blend was a typical sea-island structure with PLA as a continuous phase and TA-ESO as a dispersed phase; the added CNTs were mostly distributed in the PLA phase for the CNT/TA-ESO/PLA nanocomposites. Therefore, the CNTs is slightly easier to connect to each other and form a conductive network in the CNT/TA-ESO/PLA nanocomposite via continuous PLA phase relative to the CNT/PLA nanocomposite when the same loading of CNTs was incorporated.

## 5.4 Conclusion

High biobased content, strength-toughness balanced, and electrically conductive CNT/TA-ESO/PLA nanocomposites were successfully fabricated by dynamic vulcanization of PLA with ESO, by using TA as a green vulcanizing agent and CNTs as reinforcement. Results indicated that the obtained TA-ESO/PLA blend presented a typical sea-island structure and the incorporated CNTs were majorly dispersed in the continuous PLA phase. The combination of TA-ESO phase and CNTs resulted in an

improved crystallinity of PLA phase due to their heterogeneous nucleation effects. The tensile strength, tensile modulus, storage modulus, and thermal stability of the nanocomposites were increased with the addition of CNTs; however, the added CNTs led to significant decreases in elongation at break, tensile toughness, and damping ability of the nanocomposites. This indicated that the toughening effect of TA-ESO phase was reduced by the addition of stiff CNTs. The formed sea-island structure in TA-ESO/PLA blends contributed to improving the electrical conductivity of the nanocomposites. The PLA nanocomposites containing 10 wt% TA-ESO phase and 10 wt% CNTs achieved the optimum strength-toughness balance with a tensile strength of 63.2 MPa and a tensile toughness of 7.9 MJ/m<sup>3</sup> as well as good electrical conductivity ( $1.5 \times 10^{-2}$  S/m). In a word, a facial and cost-effective method to toughen and strengthen PLA products was provided by using TA to induce crosslinking of ESO and CNTs as reinforcing fillers.

## References

- [1] Nagarajan, V.; Mohanty, A.K.; Misra, M. Perspective on polylactic acid (PLA) based sustainable materials for durable applications: Focus on toughness and heat resistance. *ACS Sustain. Chem. Eng.* 2016, 4, 2899-2916.
- [2] Wang, M.; Wu, Y.; Li, Y.D.; Zeng, J.B. Progress in toughening poly(lactic acid) with renewable polymers. *Polym. Rev.* 2017, 57, 557-593.
- [3] Gandini, A. Polymers from renewable resources: A challenge for the future of macromolecular materials. *Macromolecules* 2008, 41, 9491-9504.
- [4] Vijayarajan, S; Selke, S.E.; Matuana, L.M. Continuous blending approach in the manufacture of epoxidized soybean-plasticized poly(lactic acid) sheets and films. *Macromol. Mater. Eng.* 2014, 299, 622-630.
- [5] Xiong, Z.; Yang, Y; Feng, J; Zhang, X; Zhang, C; Tang, Z.; Zhu, J. Preparation and characterization of poly(lactic acid)/starch composites toughened with epoxidized soybean oil. *Carbohydr. Polym.* 2013, 92, 810-816.
- [6] Al-Mulla, E.A.J.; Yunus, W.M.Z.W.; Ibrahim, N.A.B.; Rahman, M.Z.A. Properties of epoxidized palm oil plasticized polylactic acid. *J. Mater. Sci.* 2010, 45, 1942-1946.
- [7] Ferri, J.; Garcia-Garcia, D.; Sánchez-Nacher, L.; Fenollar, O.; Balart, R. The effect of maleinized linseed oil (MLO) on mechanical performance of poly(lactic acid)-thermoplastic starch (PLA-TPS) blends. *Carbohydr. Polym.* 2016, 147, 60-68.
- [8] Carbonell-Verdu, A.; Garcia-Garcia, D.; Dominici, F.; Torre, L.; Sanchez-Nacher, L.; Balart R.

- PLA films with improved flexibility properties by using maleinized cottonseed oil. *Eur. Polym. J.* 2017, 91, 248-259.
- [9] Carbonell-Verdu, A.; Samper, M.D.; Garcia-Garcia, D.; Sanchez-Nacher, L.; Balart, R. Plasticization effect of epoxidized cottonseed oil (ECSO) on poly(lactic acid). *Ind. Crop. Prod.* 2017, 104, 278-286.
- [10] Ferri, J.; Samper, M.; García-Sanoguera, D.; Reig, M.; Fenollar, O.; Balart, R. Plasticizing effect of biobased epoxidized fatty acid esters on mechanical and thermal properties of poly(lactic acid). *J. Mater. Sci.* 2016, 51(11), 5356-5366.
- [11] Mauck, S.C.; Wang, S.; Ding, W.; Rohde, B.J.; Fortune, C.K.; Yang, G.; Ahn, S.K.; Robertson, M.L. Biorenewable tough blends of polylactide and acrylated epoxidized soybean oil compatibilized by a polylactide star polymer. *Macromolecules* 2016, 49, 1605-1615.
- [12] Robertson, M.L.; Chang, K.; Gramlich, W.M.; Hillmyer, M.A. Toughening of polylactide with polymerized soybean oil. *Macromolecules* 2010, 43, 1807-1814.
- [13] Chen, Y.; Yuan, D.; Xu, C. Dynamically vulcanized biobased polylactide/natural rubber blend material with continuous cross-linked rubber phase. *ACS Appl. Mater. Inter.* 2014, 6, 3811-3816.
- [14] Zhao, T.; Yuan, W.; Li, Y.; Weng, Y.; Zeng, J. Relating chemical structure to toughness via morphology control in fully sustainable sebacic acid cured epoxidized soybean oil toughened polylactide blends. *Macromolecules* 2018, 51, 2027-2037.
- [15] Zhao, T.; He, Y.; Li, Y.; Wang, M.; Zeng, J. Dynamic vulcanization of castor oil in a polylactide matrix for toughening. *RSC Adv.* 2016, 6, 79542-79553.
- [16] He, Y.; Zhao, T.; Li, Y.; Wang, M.; Zeng, J. Toughening polylactide by dynamic vulcanization with castor oil and different types of diisocyanates. *Polym. Test.* 2017, 59, 470-477.
- [17] Singh, A.A.; Geng, S.; Herrera, N.; Oksman, K. Aligned plasticized polylactic acid cellulose nanocomposite tapes: Effect of drawing conditions. *Part A Appl. Sci. Manuf.* 2018, 104, 101-107.
- [18] Barmouz, M.; Behraves, A.H. Shape memory behaviors in cylindrical shell PLA/TPU-cellulose nanofiber bio-nanocomposites: Analytical and experimental assessment. *Part A Appl. Sci. Manuf.* 2017, 101, 160-172.
- [19] Kuang, T.; Mi, H.; Fu, D.; Jing, X.; Chen, B.; Mou, W.; Peng, X. Fabrication of poly(lactic acid)/graphene oxide foams with highly oriented and elongated cell structure via unidirectional foaming using supercritical carbon dioxide. *Ind. Eng. Chem. Res.* 2015, 54, 758-768.
- [20] Piekarska, K.; Sowinski, P.; Piorkowska, E.; Haque M.M.U.; Pracella, M. Structure and properties of hybrid PLA nanocomposites with inorganic nanofillers and cellulose fibers. *Part A Appl. Sci. Manuf.* 2016, 82, 34-41.
- [21] Dong, Y.; Marshall, J.; Haroosh, H.J.; Mohammadzadehmoghadam, S.; Liu, D.; Qi, X.; Lau,

- K.T. Polylactic acid (PLA)/halloysite nanotube (HNT) composite mats: Influence of HNT content and modification. *Part A Appl. Sci. Manuf.* 2015, 76, 28-36.
- [22] Rivière, P.; Nypelö, T.E.; Obersriebnig, M.; Bock, H.; Müller, M.; Mundigler, N.; Wimmer, R. Unmodified multi-wall carbon nanotubes in polylactic acid for electrically conductive injection-moulded composites. *J. Thermoplast. Compos.* 2017, 30, 1615-1638.
- [23] Mittal, G.; Dhand, V.; Rhee, K.Y.; Park S.J.; Lee, W.R. A review on carbon nanotubes and graphene as fillers in reinforced polymer nanocomposites. *J. Ind. Eng. Chem.* 2015, 21, 11-25.
- [24] Wang, L.; Qiu, J.; Sakai, E.; Wei, X. The relationship between microstructure and mechanical properties of carbon nanotubes/polylactic acid nanocomposites prepared by twin-screw extrusion. *Part A Appl. Sci. Manuf.* 2016, 89, 18-25.
- [25] Brzeziński, M.; Biela, T. Polylactide nanocomposites with functionalized carbon nanotubes and their stereocomplexes: A focused review. *Mater. Lett.* 2014, 121, 244-250.
- [26] Alam, J.; Alam, M.; Raja, M.; Abduljaleel, Z.; Dass, L.A. MWCNTs-reinforced epoxidized linseed oil plasticized polylactic acid nanocomposite and its electroactive shape memory behaviour. *Int. J. Mol. Sci.* 2014, 15, 19924-19937.
- [27] Alam, J.; Khan, A.; Alam, M.; Mohan, R. Electroactive shape memory property of a Cu-decorated CNT dispersed PLA/ESO nanocomposite. *Materials* 2015, 8, 6391-6400.
- [28] Yang, J.; Qi, X.; Zhang, N.; Huang, T.; Wang, Y. Carbon nanotubes toughened immiscible polymer blends. *Compos. Commun.* 2018, 7, 51-64.
- [29] Raja, M.; Ryu, S.H.; Shanmugaraj, A. Thermal, mechanical and electroactive shape memory properties of polyurethane (PU)/poly(lactic acid)(PLA)/CNT nanocomposites. *Eur. Polym. J.* 2013, 49, 3492-3500.
- [30] Shi, Y.; Zhang, W.; Yang, J.; Huang, T.; Zhang, N.; Wang, Y.; Yuan, G.; Zhang, C. Super toughening of the poly(L-lactide)/thermoplastic polyurethane blends by carbon nanotubes. *RSC Adv.* 2013, 3, 26271-26282.
- [31] Wu, D.; Zhang, Y.; Zhang, M.; Yu, W. Selective localization of multiwalled carbon nanotubes in poly( $\epsilon$ -caprolactone)/polylactide blend. *Biomacromolecules* 2009, 10, 417-424.
- [32] Huang, J.; Mao, C.; Zhu, Y.; Jiang, W.; Yang, X. Control of carbon nanotubes at the interface of a co-continuous immiscible polymer blend to fabricate conductive composites with ultralow percolation thresholds. *Carbon* 2014, 73, 267-274.
- [33] Nasti, G.; Gentile, G.; Cerruti, P.; Carfagna, C.; Ambrogio, V. Double percolation of multiwalled carbon nanotubes in polystyrene/polylactic acid blends. *Polymer* 2016, 99, 193-203.
- [34] Urquijo, J.; Aranburu, N.; Dagréou, S.; Guerrica-Echevarría, G.; Eguiazábal, J. CNT-induced morphology and its effect on properties in PLA/PBAT-based nanocomposites. *Eur. Polym. J.* 2017, 93, 545-555.
- [35] Gao, T.; Li, Y.; Bao, R.; Liu, Z.; Xie, B.; Yang, M.; Yang, W. Tailoring co-continuous like

- morphology in blends with highly asymmetric composition by MWCNTs: Towards biodegradable high-performance electrical conductive poly(l-lactide)/poly(3-hydroxybutyrate-co-4-hydroxybutyrate) blends. *Compos. Sci. Technol.* 2017, 152, 111-119.
- [36] Shi, Y.; Li, Y.; Xiang, F.; Huang, T.; Chen, C.; Peng, Y.; Wang, Y. Carbon nanotubes induced microstructure and mechanical properties changes in cocontinuous poly(L-lactide)/ethylene-co-vinyl acetate blends. *Polym. Adv. Technol.* 2012, 23, 783-790.
- [37] Wang, X.; He, Z.; Yang, J.; Zhang, N.; Huang, T.; Wang, Y.; Zhou, Z. Super toughened immiscible poly(l-lactide)/poly(ethylene vinyl acetate)(PLLA/EVA) blend achieved by in situ cross-linking reaction and carbon nanotubes. *Part A Appl. Sci. Manuf.* 2016, 91, 105-116.
- [38] Desa, M.; Zaidi, M.S.; Hassan, A.; Arsad, A.; Arjmandi, R.; Mohammad, N.N.B. Influence of rubber content on mechanical, thermal, and morphological behavior of natural rubber toughened poly(lactic acid)-multiwalled carbon nanotube nanocomposites. *J. Appl. Polym. Sci.* 2016, 133, 44344.
- [39] Wang, Y.; Xu, X.; Dai, J.; Yang, J.; Huang, T.; Zhang, N.; Wang, Y.; Zhou, Z.; Zhang, J. Super toughened immiscible polycarbonate/poly(L-lactide) blend achieved by simultaneous addition of compatibilizer and carbon nanotubes. *RSC Adv.* 2014, 4, 59194-59203.
- [40] Liu, Z.; Bai, H.; Luo, Y.; Zhang, Q.; Fu, Q. Achieving a low electrical percolation threshold and superior mechanical performance in poly(l-lactide)/thermoplastic polyurethane/carbon nanotubes composites via tailoring phase morphology with the aid of stereocomplex crystallites. *RSC Adv.* 2017, 7, 11076-11084.
- [41] Wang, L.; Lee, R.E.; Wang, G.; Chu, R.K.; Zhao, J.; Park, C.B. Use of stereocomplex crystallites for fully-biobased microcellular low-density poly(lactic acid) foams for green packaging. *Chem. Eng. J.* 2017, 327, 1151-1162.
- [42] Radjabian, M.; Kish, M.; Mohammadi, N. Structure-property relationship for poly(lactic acid) (PLA) filaments: Physical, thermomechanical and shape memory characterization. *J. Polym. Res.* 2012, 19, 9870.
- [43] Zhao, S.; Abu-Omar, M.M. Renewable epoxy networks derived from lignin-based monomers: Effect of cross-linking density. *ACS Sustain. Chem. Eng.* 2016, 4, 6082-6089.
- [44] Arjmandi, R.; Hassan, A.; Haafiz, M.; Zakaria, Z.; Islam, M.S. Effect of hydrolysed cellulose nanowhiskers on properties of montmorillonite/poly(lactic acid) nanocomposites. *Int. J. Biol. Macromol.* 2016, 82, 998-1010.
- [45] Hu, X.; Li, Y.; Li, M.; Kang, H.; Zhang, L. Renewable and supertoughened polylactide-based composites: Morphology, interfacial compatibilization, and toughening mechanism. *Ind. Eng. Chem. Res.* 2016, 55, 9195-9204.
- [46] Liu, H.; Bai, H.; Bai, D.; Liu, Z.; Zhang, Q.; Fu, Q. Design of high-performance poly(l-lactide)/elastomer blends through anchoring carbon nanotubes at the interface with the aid of stereocomplex crystallization. *Polymer* 2017, 108, 38-49.

# **Chapter 6 Modification of Bamboo Fibers-Reinforced PLA Biocomposites with Tannic Acid-Crosslinked Epoxidized Soybean Oil**

## **6.1 Introduction**

PLA is a renewable and biodegradable polyester that is derived from starch-rich materials including corn and wheat. PLA has been extensively applied to replace petroleum-based and non-degradable counterparts due to its merits including renewability, biodegradability, good processability, and high strength [1]. However, the main bottleneck of PLA is high brittleness, which largely restricts its practical application. The introduction of reinforcing fibers to fabricate PLA composites is an effective strategy to endow PLA products with specific use characteristics and improved performance. Natural fibers (NFs) are particularly attractive for their application in the preparation of NF/PLA biocomposites due to their intrinsic advantages such as low-cost, renewability, and high specific strength and stiffness [2]. Commonly used NFs in PLA biocomposites are normally extracted from hemp [3], jute [4], bamboo [5], flax [6], sisal [7], etc. The most intractable challenge for NF/PLA biocomposites is the poor interfacial adhesion as a result of the highly hydrophilic NFs in contrast to the hydrophobic PLA matrix. Surface chemical treatment for NFs aims at altering the surface characteristics of the fibers into more intimate with PLA matrix, thereby increasing the interfacial bonding of the biocomposites [8]. Concerning the improvement of interfacial adhesion of NF/PLA biocomposites, many chemical strategies including alkali treatment [9], acetylation [10], silane [11], and anhydride [12] have been carried out for modifying NFs. Nevertheless, the modification for NFs normally refers to a rigorous reaction condition that uses organic solvents, elevated temperature, and/or organometal catalysts, which undoubtedly increases the production cost of composites. During the processing of NFs and PLA at high temperature, the addition of

compatibilizers could induce the in-situ generation of grafted-polymers at the interface of the composites, which is usually considered as reactive compatibilization. Therefore, functionalized oligomers including maleic anhydride (MA)-grafted PLA [13,14] and epoxy-contained terpolymer [15], and reactive monomers such as MA [16], maleinized linseed oil [17] and epoxidized citric acid [18] have been incorporated into NF/PLA biocomposites to increase their interfacial compatibility.

Triglyceride-based vegetable oils (VOs), consisting of glycerol esters with three long fatty acid chains, are ideal renewable feedstocks for formulating biobased polymers. VOs contain functional groups including esters and C=C bonds, which provides the reactive sites for chemical modification to develop various VO-based polymers [19]. As a commercialized VO-based derivative, epoxidized soybean oil (ESO) is synthesized from soybean oil through epoxidation of C=C bonds from the fatty acid chains [20]. The blending of ESO with petroleum-based epoxy monomers could increase the sustainability of the resulting epoxy resins [21]. Fully sustainable thermosets were prepared by curing ESO with biobased crosslinkers such as tannic acid and citric acid, while the resulting ESO resins showed low mechanical strength, toughness and thermal resistance [22-24]. Furthermore, these ESO-based thermosets are all three-dimensional network structure and thus are not thermally reprocessable.

ESO has been incorporated into PLA as plasticizers to increase the toughness of PLA, while the uncured ESO monomers are immiscible with PLA and hence is easy to leach or migrate to the surface of PLA [25,26]. Dynamic vulcanization involves the melt-compounding of PLA with the blended components and the formation of a crosslinked rubbery phase within PLA matrix. The dynamic vulcanization of PLA with ESO in the presence of vulcanizing agents is an efficient method to prepare crosslinked-ESO/PLA blends with thermal processability and improved toughness. The dynamic vulcanization of ESO with sebacic acid (SA) and PLA generated SA-ESO/PLA blends with thermoplasticity and high performance; compared to pure SA-ESO resins, the incorporation of 20 wt% PLA into the blends significantly increased the tensile strength and modulus by around 11 and 16 times, respectively [27]. Similar works were addressed on the blending of ESO with PLA [28],

poly(butylene succinate) [29], and castor oil-based polyamide [30], which significantly improved the mechanical and thermal properties of the blends. In [Chapter 3](#), the crosslinking of ESO was induced by cationic initiator during dynamical vulcanization, which resulted in the formation of a stable polymerized ESO (PESO) rubbery phase dispersed within PLA matrix and improvement of the interfacial compatibility between the PESO phase and PLA. Moreover, completely biobased and highly tough ESO/PLA blends were fabricated by using tannic acid (TA) as a green vulcanizing agent to crosslink ESO ([Chapter 4](#)). As proposed in [Figure 6-1](#), in the course of dynamic vulcanization, the phenolic –OH groups of TA mainly react with the epoxy rings of ESO to form TA-crosslinked ESO (TA-ESO) phase; meanwhile, the secondary reaction between the TA-ESO phase and PLA also could occur for achieving an improved interfacial adhesion. This resulted in significantly improved elongation at break and tensile toughness of the PLA blends with decreased tensile strength and modulus.

In this work, bamboo fibers (BFs) is selected as reinforcing fibers for the TA-ESO/PLA blends to develop fully biobased BF/TA-ESO/PLA ternary biocomposites with tailorable performance via reactive blending. TA-ESO oligomer

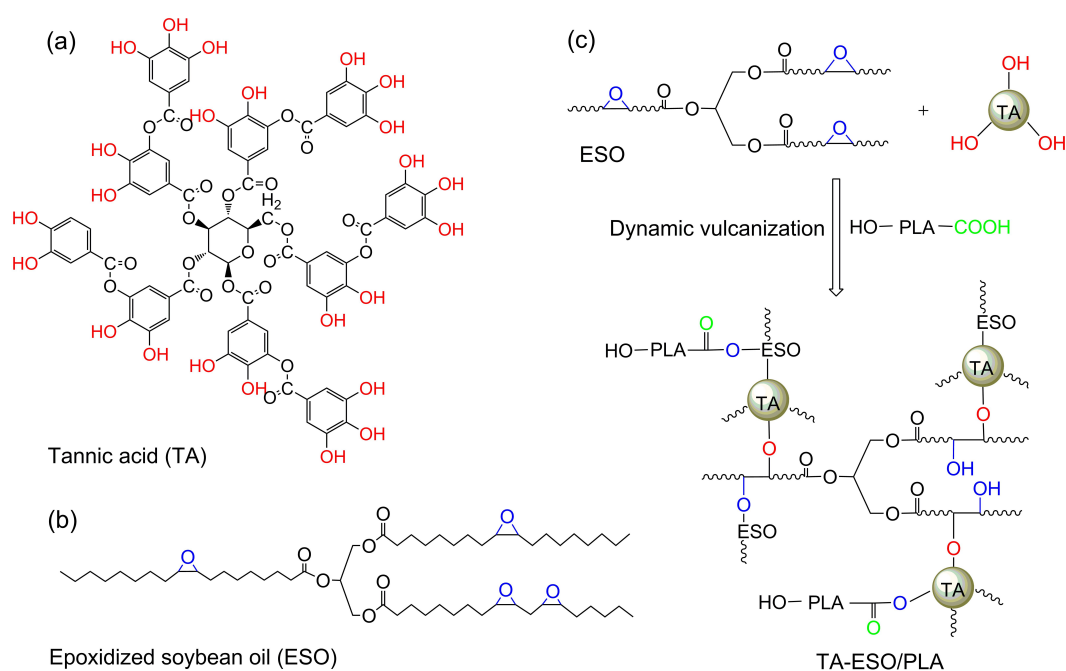


**Figure 6-1** Possible reaction among TA, ESO and PLA

is regulated to localize at the interface between BFs and PLA matrix via surface coating of BFs with TA-ESO solution to improve the interfacial adhesion of the composites. The TA-ESO oligomer is expected to have strong interactions with BFs via natural polyphenol-inspired chemistry and then form a flexible interfacial layer between fibers and matrix. Further, high content of TA-ESO is incorporated into the composites to facilitate the formation of a stable phase-separated structure in PLA matrix and hence to toughen the composites, which simultaneously endows ESO-based polymers with thermal malleability and PLA-based products with favorable toughness. The strengthening and toughening mechanism of TA-ESO phase on the interphase and PLA matrix of the composites will be fully studied along with their synergistic effects on the composites properties through numerous powerful methods.

## **6.2 Experimental section**

### **6.2.1 Materials**

BFs with an average particle size of 126  $\mu\text{m}$  were given by Fujian HBS Chemical Technology (Fujian, China). PLA (Ingeo 3001D) was provided by NatureWorks (Tokyo, Japan). ESO ( $\geq 99.5\%$ ) with an average epoxy groups of 4 per molecule was purchased from Aladdin Industrial Corporation (Shanghai, China). TA with an average  $-\text{OH}$  groups of 25 per molecule, acetone, and chloroform were purchased from Nacalai Tesque, INC (Tokyo, Japan).

### **6.2.2 Preparation of BF/TA-ESO/PLA biocomposites**

TA and ESO were successively dissolved in acetone (40 mL) with a vigorous stirring for 5 min to form a TA-ESO solution. The solution was evenly sprayed on the surface of the oven-dried BFs (80°C, 12 h), and the resulting TA-ESO-coated BFs were further dried in an oven at 80°C for 4 h to evaporate acetone.

The TA-ESO-coated BFs were mixed with the oven-dried PLA pellets (80°C, 12 h) for melt-compounding in a KZW25TW-60MG-NH(-1200)-AKT twin-screw

extruder (Technovel Corporation, Osaka, Japan). The blending condition was as follows: the temperatures ranged from 150 to 180°C from feeding zone to die section; the screw speed was fixed at 50 r/min. The extruded BF/TA-ESO/PLA blends were quenched in a water bath and chopped into pellets for specimen preparation.

After being oven-dried at 80°C for 12 h, the BF/TA-ESO/PLA pellets were injected into dumbbell and rectangular specimens for characterization by an NP7-1F injection molding machine (Nissei Plastic Industrial, Nagano, Japan). The condition for molding was as follows: nozzle temperature of 170°C, injection speed of 17.6 mm/s, injection time of 6 s, mold temperature of 40°C, and cooling time of 40 s. To tailor the distribution of TA-ESO, different TA-ESO concentration ranging from 0.5 to 20 wt% were coated on the BFs surface for the preparation of BF/TA-ESO/PLA composites with a BF content of 20 wt%. To investigate the effect of BFs content on the properties of the composites, different BFs contents, i.e., 10, 20, 30, and 40 wt%, were added into PLA and TA-ESO/PLA blends (15 wt% TA-ESO), respectively. The main compositions of the composites were given in [Table 6-1](#). The composites were abbreviated as  $x$ BF/ $y$ TA-ESO, where the  $x$  and  $y$  represent the weight fractions of BFs and TA-ESO phase in the composites, respectively. The weight ratio of TA to ESO in the TA-ESO oligomer was calculated from the optimized molar ratio (0.8) of –OH

**Table 6-1** Compositions of BF/TA-ESO/PLA biocomposites

References	Compositions (wt%)				
	BFs	TA-ESO	TA	ESO	PLA
10BF	10	/	/	/	90
20BF	20	/	/	/	80
30BF	30	/	/	/	70
40BF	40	/	/	/	60
20BF/0.5TA-ESO	20	0.5	0.45	0.05	79.5
20BF/1TA-ESO	20	1	0.90	0.10	79
20BF/5TA-ESO	20	5	4.48	0.52	75
20BF/10TA-ESO	20	10	8.97	1.03	70
20BF/15TA-ESO	20	15	13.46	1.54	65
20BF/20TA-ESO	20	20	17.94	2.06	60
10BF/15TA-ESO	10	15	13.46	1.54	75
30BF/15TA-ESO	30	15	13.46	1.54	55
40BF/15TA-ESO	40	15	13.46	1.54	45

groups from TA to epoxy groups from ESO according to [Chapter 4](#).

### 6.2.3 Characterization

To characterize the surface chemistry of BFs, the BFs were extracted by dissolving the composites (2 g) in chloroform (40 mL) for 24 h. The uncrosslinked ESO molecules and PLA were dissolved in chloroform. The TA-ESO phase could not dissolve in chloroform but suspended on the surface of the solution, while the BFs precipitated at the bottom. Thus, the BFs were isolated by repeating the procedure for 3 times and then extracted with chloroform in a Soxhlet extractor at 80°C for 8 h. The obtained BFs were oven-dried (80°C, 24 h) for Fourier transform infrared spectroscopy (FTIR) analysis on a Nicolet iN10 FTIR spectrometer (Thermo Fisher Scientific, MA, USA). The spectra were collected from 4000 to 400 cm<sup>-1</sup> at a spectral resolution of 4 cm<sup>-1</sup>. For comparison, the FTIR spectrum of a TA-ESO oligomer that was cured in an oven at 180°C for 10 min was also obtained. X-ray photoelectron spectroscopy (XPS) experiments were performed on a PHI 5000 Series XPS instrument (ULVAC-PHI, Kanagawa, Japan) equipped with Al K $\alpha$  radiation source. Atomic high-resolution spectra were run with pass energy of 70.0 eV and an increment of 0.2 eV. The obtained C1s spectra were resolved with the software of XPS Peak 4.0 (The Chinese University of Hong Kong, Hong Kong, China).

Crystallization behavior was tested on an X-DSC7000 differential scanning calorimetry (DSC) analyzer (SII Nano Technology Inc., Chiba, Japan). About 10 mg samples were sealed into an aluminum pan with a lid, and an empty hermetic pan was used as reference. The scans were performed under liquid nitrogen (flow rate: 50 mL/min) from 25 to 210°C at a heating rate of 10°C/min. Based on the DSC results, the crystallinity ( $X_c$ ) of PLA was calculated according to the following equation [31]:

$$X_c = \frac{\Delta H_m - H_{cc}}{\Delta H_{100} \times x_{PLA}} \times 100 \quad (6-1)$$

where  $\Delta H_m$  is melting enthalpy,  $\Delta H_{cc}$  is cold crystallization enthalpy,  $\Delta H_{100}$  is the theoretical enthalpy of crystalline PLA to melt (93.6 J/g), and  $x_{PLA}$  is the weight ratio of PLA in the composites.

Thermal-mechanical properties were evaluated on a RSA-G2 dynamic mechanical analysis (DMA) solids analyzer (TA Instrument, DE, USA). Rectangular samples ( $55 \times 10 \times 4 \text{ mm}^2$ ) were tested under three-point bending mode with a strain of 0.1% from 30 to 100°C at a heating rate of 2°C/min and a frequency of 1 Hz.

Tensile properties were obtained from a Series 3360 universal testing machine (Instron, MA, USA) using dumbbell specimens (25 mm gauge length, 2 mm thickness, and 5 mm narrow section width) in accordance with ASTM D 638-10. The tests were conducted at room temperature, and the crosshead speed was 10 mm/s. Notched Izod impact strength was measured using rectangular samples ( $80 \times 10 \times 4 \text{ mm}^3$ ) on a Toyoseiki IT impact tester (Tokyo, Japan) at room temperature according to ASTM D 256-10. For the tensile and impact tests, five measurements were conducted for each composite.

The tensile-fractured and cryo-fractured samples were used for scanning electron microscope (SEM) observation. To observe the internal structure of the tensile-fractured samples, the samples were dealt with liquid nitrogen and then cut at different directions using a Leica RM2135 rotary microtome (Leica Microsystems K.K., Tokyo, Japan). Before testing, the testing surfaces were sputtered with a gold film. SEM images were taken from a JEOL JSM-7500F SEM (JEOL, Tokyo, Japan) at an accelerating voltage of 4.0 kV.

## **6.3 Results and discussion**

### **6.3.1 Reaction mechanism of TA-ESO in BF/PLA biocomposites**

The surface coating of BFs with TA-ESO solution aims at forming a flexible interfacial layer between the BFs and PLA matrix and hence improving the interfacial bonding of the BF/PLA composites (Figure 6-2). According to the reported work that used epoxy-contained chemicals as compatibilizers for sisal fibers/PLA biocomposites [7, 32], the reaction between the –OH groups of fibers and the epoxy groups of the compatibilizers could occur at high temperature. However, the epoxy

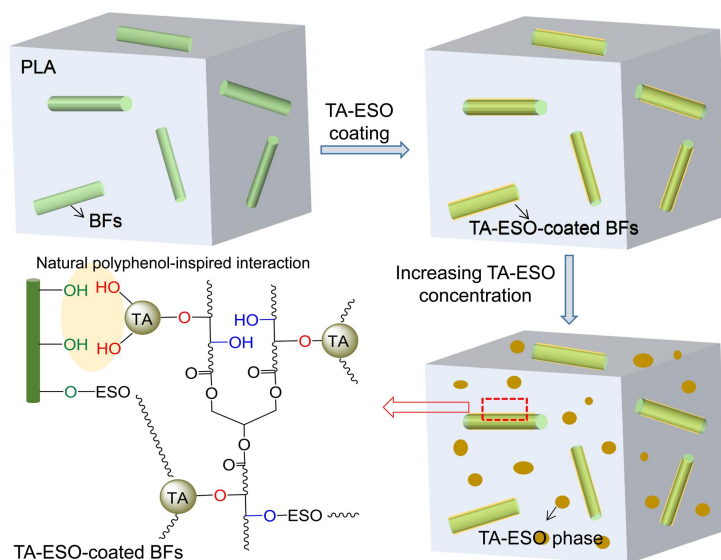


**Figure 6-2** Proposed reaction mechanism of TA-ESO in BF/PLA biocomposites

groups in ESO molecules are positioned in the middle of fatty acid chains, which largely restricts its reactivity towards BFs due to steric effect. The addition of TA into ESO could induce the epoxy-ring opening reaction of ESO caused by the abundant phenolic  $-OH$  groups from TA and thus promote the generation of a crosslinked ESO oligomer layer on the BFs surface. The TA-ESO layer is expected to form strong interactions with BFs via natural polyphenol-inspired chemistry such as hydrogen bonding and  $\pi-\pi$  interaction [33]. It was reported that TA could deposit onto different substrates, such as cellulose [34] and graphene oxide [35], via the formation of new covalent bonds and/or strong intermolecular interaction, although the exact coating mechanism is not fully clear.

The interaction between BFs and TA-ESO can be verified by FTIR and XPS analyses. The FTIR spectrum of the BFs from 20BF composite presented a shoulder peak at  $1750\text{ cm}^{-1}$  (Figure 6-3a), which is attributed to the  $C=O$  stretching vibration resulted from carboxylic acid in lignin or ester group in hemicellulose [36]. As shown in Figure 6-3bcd, an increased intensity of the shoulder peak was observed after the surface coating of BFs with TA-ESO; the peak position shifted from  $1750$  to  $1740\text{ cm}^{-1}$  as the increase of TA-ESO concentration from 0.5 to 15 wt%. These demonstrate that the BFs surfaces are wrapped by the introduced TA-ESO oligomer that has

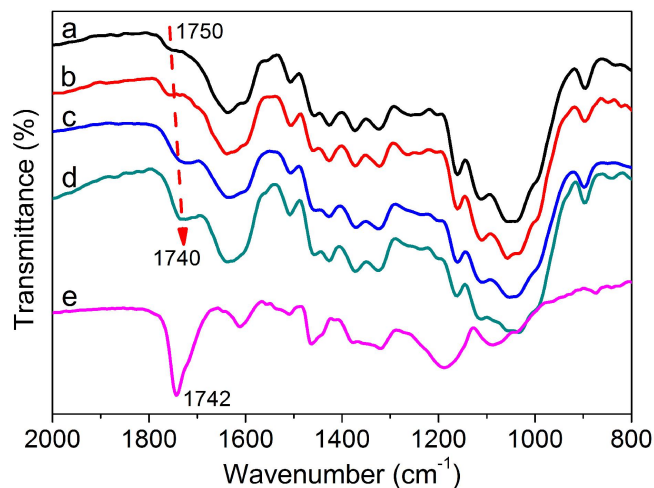


**Figure 6-3** FTIR spectra of BFs extracted from (a) 20BF, (b) 20BF/0.5TA-ESO, (c) 20BF/5TA-ESO, and (d) 20BF/15TA-ESO composites and (e) TA-cured ESO polymer.

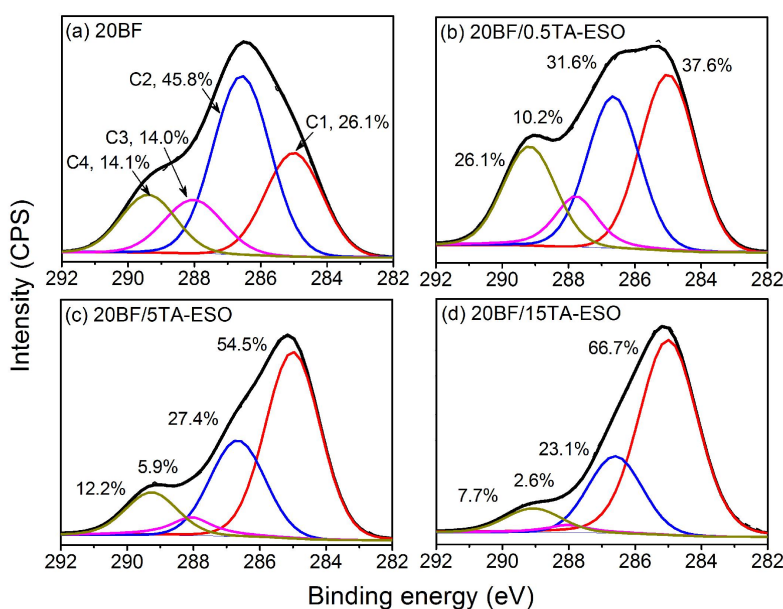


**Figure 6-4** Curve-resolved spectra of XPS C1s peak of the extracted BFs.

characteristic C=O peak at  $1742\text{ cm}^{-1}$  corresponding to the ester groups from TA and ESO (Figure 6-3e).

The surface components of the extracted BFs were revealed by the high-resolution C1s spectra (Figure 6-4). The BFs from 20BF composite showed four characteristic functional groups of natural fibers, i.e., C1 (C–C/C=C), C2 (C–O), C3 (O–C–O/C=O), and C4 (O–C=O) [37]. After the coating of BFs with 0.5 wt% TA-ESO, the C1 and C4 contents on the fiber surface increased from 26.1 to 37.6% and 14.1 to 26.1%, respectively, which is owing to the coated TA-ESO oligomer that

contains benzene rings from TA, aliphatic chains from ESO, and ester groups from TA and ESO. Especially, the benzene rings and aliphatic chains belong to the C1 component, which resulted in the fact that the C1 fraction of the fibers greatly increased from 37.6 to 66.7% as the increase of TA-ESO concentration. Meanwhile, the C3 component gradually disappeared as the increased TA-ESO usage due to the absence of C=O/O–C–O groups in the TA-ESO oligomer. Although there might be some unreacted –OH groups remaining in the TA-ESO, the relative content of C2 was significantly reduced because the increase in C1 content. Therefore, it is confirmed that strong interactions between BFs and TA-ESO are generated since the TA-ESO phase that was not bonded onto BFs would be removed by chloroform extraction during purification.

Moreover, when a high content of TA-ESO solution was coated on BFs, the TA-ESO would diffuse inside PLA matrix and form a stable rubbery phase dispersed within continuous PLA matrix (Figure 6-2), which is envisaged to provide a toughening effect on the BF/PLA composites. The possible chemical linkages between TA-ESO and PLA and toughening mechanism of TA-ESO on PLA matrix were fully investigated in Chapter 4.

### 6.3.2 Morphological analysis of BF/TA-ESO/PLA biocomposites

The cryo-fractured surfaces of 20BF, 40BF, 20BF/0.5TA-ESO, 20BF/5TA-ESO, 20BF/15TA-ESO, and 40BF/15TA-ESO composites were observed by SEM analysis. The PLA matrix in 20BF composite exhibited a relatively smooth surface with a small number of holes due to the pull-out of fine fibers (Figure 6-5a). As shown in Figure 6-5c, the coating of BFs did not have significant influence on the morphology of PLA matrix in 20BF/0.5TA-ESO composite, indicating that the TA-ESO oligomer was majorly localized at the interface between BFs and PLA. However, when the TA-ESO concentration increased to 5 wt%, many raised particles and voids were observed on the surface of PLA matrix from 20BF/5TA-ESO composite (Figure 6-5d). This indicates that excess TA-ESO oligomer diffuses from the BFs surface to PLA matrix

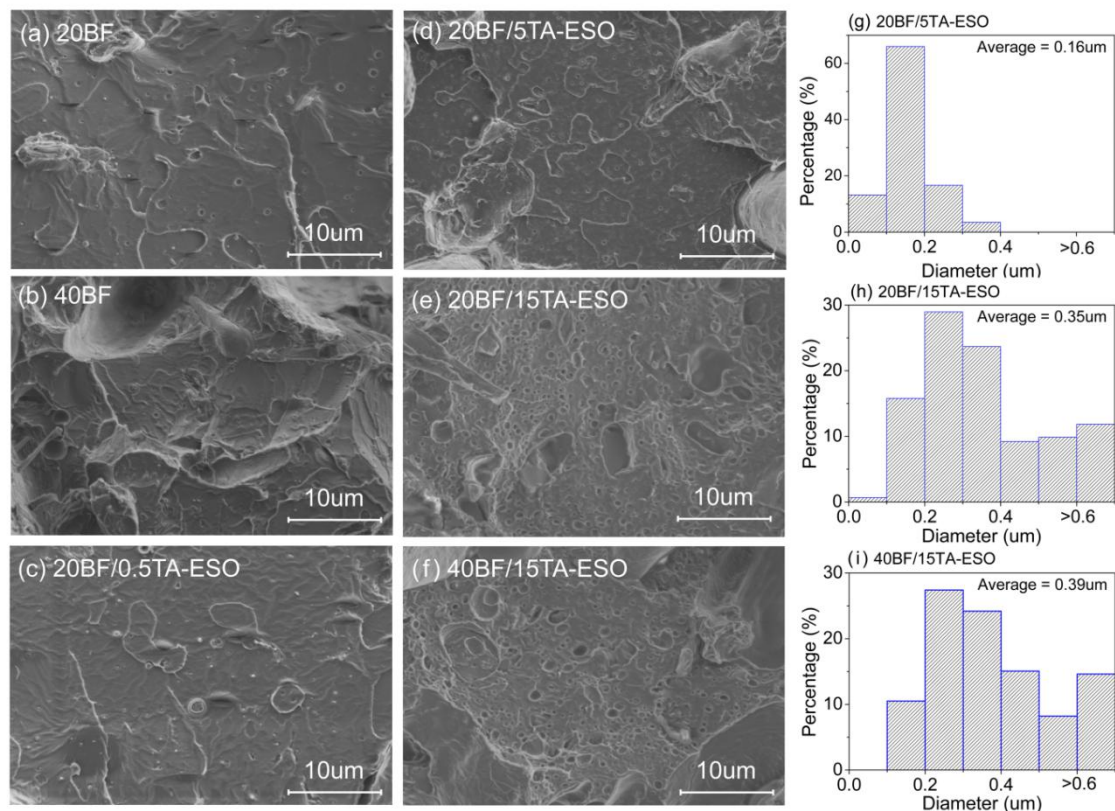


**Figure 6-5** SEM images of cryo-fractured surfaces of (a) 20BF, (b) 40BF, (c) 20BF/0.5TA-ESO, (d) 20BF/5TA-ESO, (e) 20BF/15TA-ESO, and (f) 40BF/15TA-ESO composites; Calculated size distribution of TA-ESO particles from (g) 20BF/5TA-ESO, (h) 20BF/15TA-ESO, and (i) 40BF/15TA-ESO.

and functions as a toughening agent on PLA. The particle size of dispersed TA-ESO phase in 20BF/5TA-ESO composite was lower than 0.4 μm and averaged at 0.16 μm (Figure 6-5g), which shows a uniform dispersion of TA-ESO particles within PLA matrix as a result of superior interfacial adhesion between the TA-ESO and PLA. The average diameter of the TA-ESO particles increased to 0.35 μm for 20BF/15TA-ESO composite, where a large number of raised voids due to the pull-out of TA-ESO particles were seen in PLA matrix (Figure 6-5eh). The TA-ESO particles of 20BF/15TA-ESO composite had a much lower size than that of TA-ESO/PLA polymer blends (0.56 μm) (Chapter 4), indicating an improved dispersing efficiency of TA-ESO in the presence of BFs. This is likely because the added BFs would increase the shearing stress of the blends during the preparation of composites, which effectively retards the coalescence of TA-ESO phase. Therefore, a typical sea-island structure with a stable TA-ESO as dispersed phase and PLA matrix as continuous

phase was achieved in the BF/TA-ESO/PLA ternary composites with a high content of TA-ESO.

A smooth matrix surface was seen in 40BF composite (Figure 6-5b), while 40BF/15TA-ESO composite had a PLA matrix with a large amount of obvious holes originated from TA-ESO phase (Figure 6-5f). The average size of TA-ESO particles in 40BF/15TA-ESO composite was 0.39  $\mu\text{m}$  (Figure 6-5i), which was slightly higher than that in 20BF/15TA-ESO composite. When maintaining an unchanged concentration of TA-ESO in the composites, the increase in the BFs usage decreases the PLA content in the composites, i.e., increases the relative concentration of TA-ESO in PLA matrix, which facilitates the aggregation of TA-ESO phase.

### 6.3.3 Crystallization behavior of BF/TA-ESO/PLA biocomposites

The thermal transition behavior of the composites was investigated by DSC scans (Figure 6-6 and Table 6-2). The glass transition temperature ( $T_g$ ) of 20BF composite was 61.0°C, which slightly decreased to 58.4 and 58.3°C for the composites after incorporation of 0.5 and 1 wt% TA-ESO. For 20BF/0.5TA-ESO and 20BF/1TA-ESO composites, the formed chemical connections between BFs and PLA via TA-ESO oligomer would restrict the molecular chain mobility and thus reduce the crystallization ability of PLA. This is in agreement with the slightly decreased crystallinity ( $X_c$ ) of PLA. When the TA-ESO content increased to 5 and 10 wt%, a shoulder peak gradually appeared around the glass transition zone at higher temperature, which is attributed to the  $T_g$  of the cured TA-ESO phase existing within PLA matrix. This is confirmed by the reported  $T_g$  of the TA-ESO thermoset (54–63°C) [24]. The two glass transitions of the composites gradually transferred into only one  $T_g$  with the further increased TA-ESO concentration from 10 to 20 wt%. That is, the glass transition behavior of PLA is overlapped by that of TA-ESO phase because a large amount of TA-ESO diffuses into PLA molecular chains and form superior interfacial adhesion with PLA molecules.

A cold crystallization peak was observed for all the composites. The cold crystallization temperature ( $T_{cc}$ ) of the composites was not significantly changed after

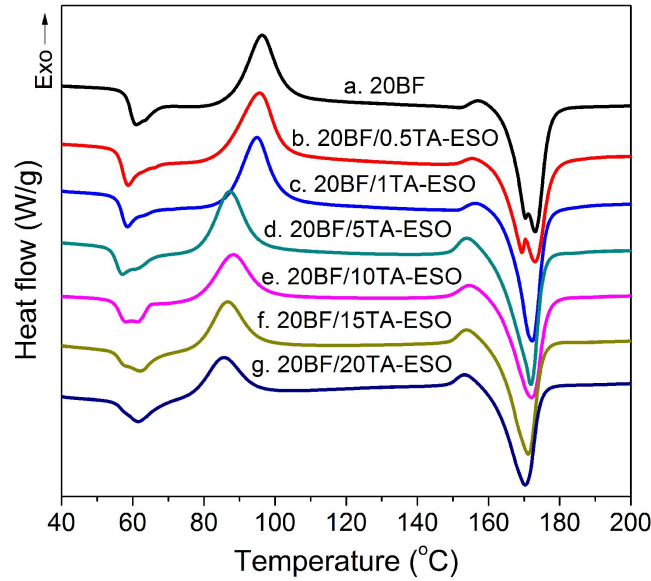


**Figure 6-7** DSC curves of BF/TA-ESO/PLA biocomposites

**Table 6-2** DSC and DMA results of BF/TA-ESO/PLA biocomposites

References	$T_g$ (°C)	$T_{cc}$ (°C)	$T_m$ (°C)	$\Delta H_{cc}$ (J/g)	$\Delta H_m$ (J/g)	$X$ (%)	$E'$ at 35°C (GPa)	$T_g$ from $\tan \delta$ (°C)
20BF	61.0	96.4	173.1	21.3	32.6	15.1	2.41	63.9
20BF/0.5TA-ESO	58.4	95.7	172.9	23.3	32.3	12.1	2.73	62.4
20BF/1TA-ESO	58.3	94.7	172.4	20.8	31.2	14.0	2.59	63.6
20BF/5TA-ESO	57.0	87.6	171.7	18.7	33.9	21.6	2.38	62.9
20BF/10TA-ESO	57.9 61.8	88.3	172.1	16.4	29.9	20.6	2.07	62.9
20BF/15TA-ESO	61.7	86.5	171.2	15.9	30.8	24.5	2.04	63.2
20BF/20TA-ESO	61.6	85.8	170.3	11.1	28.2	30.3	1.67	62.5

the addition of 0.5 or 1 wt% TA-ESO. When the TA-ESO usage was higher than 5 wt%, the TA-ESO polymer started to disperse within PLA matrix, which significantly decreased the  $T_{cc}$ s of the composites due to its plasticizing effect. The presence of TA-ESO within PLA would increase the molecular distance between PLA polymer chains and thereby improve the free volume that facilitates the mobility of molecular chains at lower temperature [38]. Moreover, this contributed to significantly improved  $X_c$ s of PLA from 14.0 to 30.3 % when increasing TA-ESO content from 5 to 20 wt%. The nucleating effect of TA-ESO particles, i.e., additional heterogeneous nucleating site, also promotes the crystallization of PLA.

The melting process of crystalline PLA for 20BF and 20BF/0.5TA-ESO

composites presented a melting peak at around 173°C with a shoulder peak on the left. This is related to some poor crystalline regions of PLA with different crystalline structures [15]. The shoulder peak disappeared for the composites with the increased TA-ESO content due to the improved  $X_c$ s of PLA. The melting temperatures ( $T_m$ s) of the composites gradually reduced with the increase of TA-ESO usage, which is explained by the improved molecular mobility of PLA chains due to the presence of TA-ESO phase.

### 6.3.4 Dynamic mechanical properties of BF/TA-ESO/PLA biocomposites

The thermal-mechanical properties of the composites were obtained from DMA analysis (Figure 6-7 and Table 6-2). For briefly, the DMA curves of 20BF/10TA-ESO and 20BF/20TA-ESO composites were not given in Figure 6-7. The storage modulus ( $E'$ ) curves of all the composites experienced a flat plot from 30 to 50°C and then a significant reduction at temperatures of 50–65°C resulted from the improved mobility of polymer chains with elevated temperature. The  $E'$  of 20BF/0.5TA-ESO composite was much higher than that of 20BF composite at the measured temperature due to the improved interfacial adhesion between BFs and PLA. Further increase in TA-ESO usage significantly decreased the  $E'$ s of the composites; the  $E'$ s of the composites at 30°C reduced from 2.73 to 1.67 GPa as the increase of TA-ESO content from 0.5 to 20 wt%. This is due to the toughening effect of TA-ESO phase, where the incorporated TA-ESO phase forming covalent bonds with PLA molecular chains

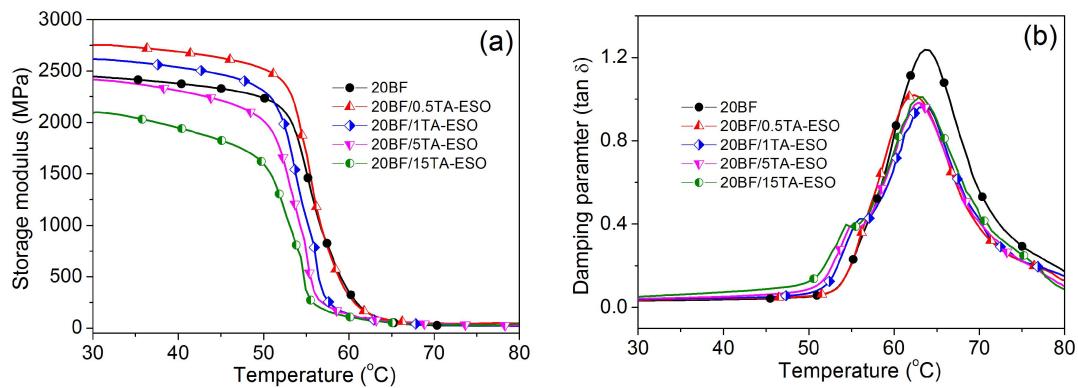


**Figure 6-7** DMA curves of BF/TA-ESO/PLA biocomposites. (a) Storage modulus; (b) damping parameter

might destroy the dense structure of PLA molecules in the amorphous area and hence decrease the modulus of PLA matrix [39]. The TA-ESO phase with a much lower modulus than PLA is also responsible for the reduced  $E$ 's of the composites.

The damping parameter ( $\tan \delta$ ) of all the composites, indicating the energy dissipation capacity, showed a peak at around 60°C corresponding to the glass transition behavior. Thus, the peak temperature of the  $\tan \delta$  curve is defined as the glass transition temperature ( $T_g$ ) of the composites. The  $T_g$ s of the composites were not significantly affected by the introduction of TA-ESO phase, which contradicts with the  $T_g$ s from DSC tests. This is probably because of the different basic principles in determining  $T_g$  of a material between DMA and DSC analyses. Actually, the  $T_g$  from DSC is based on the endothermic process of glass transition of PLA matrix, while the  $T_g$  from DMA is resulted from the modulus change of composites during glass transition. The introduced BFs greatly increase the modulus of the composites, which might be the main reason for the insignificant change in  $T_g$  from DMA. Nevertheless, a small shoulder on the left of the  $\tan \delta$  curve was seen in the composites with TA-ESO content higher than 1 wt%. The transfer of TA-ESO from the interface to PLA matrix results in the formation of ternary composites, where the TA-ESO phase inside PLA matrix increases the segmental movements of polymer chains of the composites at lower temperature.

### 6.3.5 Mechanical properties of BF/TA-ESO/PLA biocomposites

As given in [Figure 6-8ab](#), the tensile strength (TS) and tensile modulus (TM) of 20BF/0.5TA-ESO composite were much higher than those of 20BF composite, which proves the improved fiber-matrix interfacial adhesion due to the formation of TA-ESO interfacial layer between BFs and PLA. Further increase in TA-ESO concentration from 0.5 to 20 wt% significantly reduced the TS and TM of the composites. This is reasonable because the incorporated TA-ESO phase had much lower strength and modulus than PLA. It was reported that the TS and TM of TA-crosslinked ESO thermoset were around 14–23 MPa and 180–450 MPa, respectively, depending on the molar ratio of TA to ESO [24]. The diffusion of

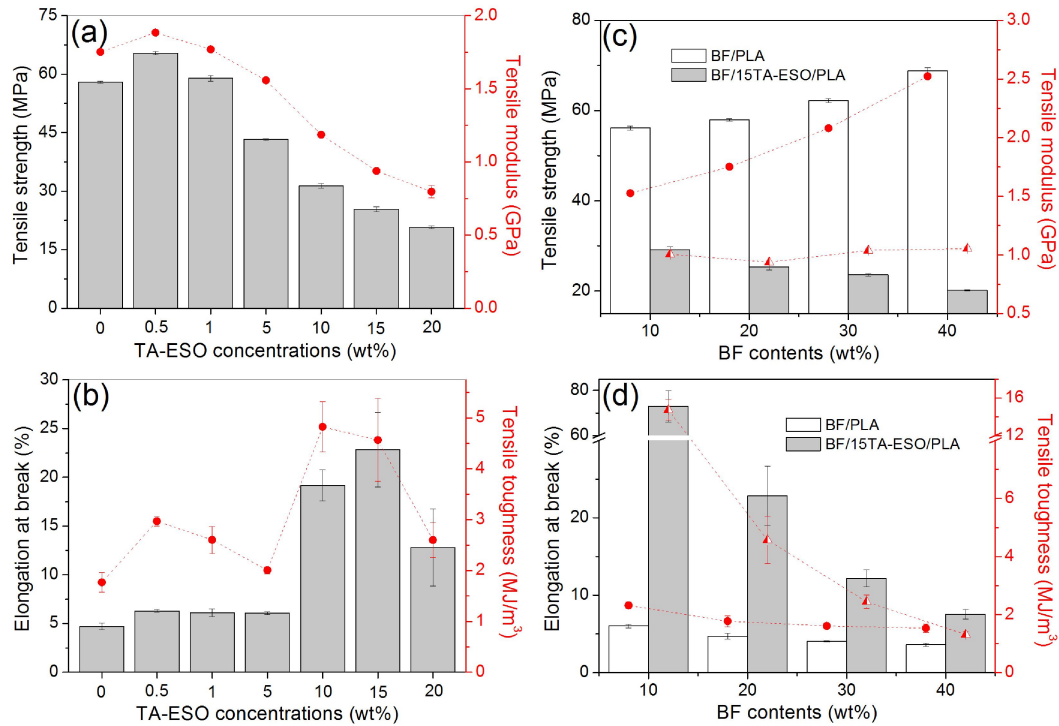


**Figure 6-8** Tensile properties of BF/TA-ESO/PLA biocomposites. (a, b) Effect of TA-ESO concentrations; (c, d) Effect of BF contents.

TA-ESO phase inside PLA matrix might destroy the integrity of PLA molecular structure via superior interaction between TA-ESO and PLA molecular chains [40], especially when high concentration of TA-ESO was incorporated into the composites. This would reduce the strength and modulus of the PLA matrix and hence the composites. Furthermore, significant improvements in elongation at break (EAB) and tensile toughness (TT) were achieved in 20BF/0.5TA-ESO composite relative to 20BF composite. As proposed in Figure 6-2, the coating of 0.5 wt% TA-ESO on the surface of BFs resulted in the formation of a flexible interfacial layer at the interface of the composites, which is conducive to avoiding stress concentration at the fiber/matrix interface when the composites are loaded. When the TA-ESO content increased from 0.5 to 5 wt%, the EAB of the composites were statistically comparable with that of 20BF/0.5TA-ESO composite, while their TT decreased with the reduced TS. When the TA-ESO content is excessive for forming a strong interfacial layer, a weak and “thick” interfacial layer would be generated and firstly broken under a tension loading. However, considerable increases in the EAB and TS of the

composites were achieved when the TA-ESO usage further increased to 10 and 15 wt%, which is contributed by the toughening effect of TA-ESO phase on PLA matrix. As evidenced by SEM images, for the dynamic vulcanization of BF/PLA blends with high content of TA-ESO, the TA-ESO polymer was dispersed as a stable rubbery phase within PLA matrix, leading to a high toughening efficiency on PLA matrix and hence the composites. But the toughening efficiency was reduced when excessive TA-ESO phase (20 wt%) was generated in the PLA matrix since TA-ESO polymer was a relatively brittle material (EAB of 6~35%) [24]. The aggregation of brittle and weak TA-ESO would deteriorate the properties including toughness of the composites.

As shown in [Figure 6-8cd](#), the TT and TM of BF/PLA composites greatly increased with the increase of BF contents from 10 to 40 wt%, indicating a reinforcing effect of BFs. However, after the incorporation of 15 wt% TA-ESO into the composites, the TS slightly decreased with the increasing BF contents, while the TM was not significantly affected. With a constant TA-ESO concentration in the composites, the increased BF content means a decreased percentage of PLA. PLA majorly provides mechanical strength for the TA-ESO/PLA matrix; when the reduced matrix strength exceeds the reinforcing effect of BFs, a reduced TS would take place in the composites. For both BF/PLA and BF/15TA-ESO/PLA composites, the increased BF contents led to significant reductions in the EAB and TT, although both EAB and TT of BF/15TA-ESO/PLA composites were much higher than those of their corresponding BF/PLA composites with a same BF loading. This indicates that the toughening effect of TA-ESO on the composites are gradually eliminated by the increase of BFs loading.

The dependence of impact strength (IS) of the composites on the TA-ESO content presented a similar trend to the situation for the TT ([Figure 6-9a](#)). The 20BF/0.5TA-ESO composite had the highest IS among all the composites due to the formation of a flexible layer at the interface of the composite. As the TA-ESO content increased from 0.5 to 5 wt%, both TT and IS of the composites dramatically reduced. The TA-ESO with a relatively high content would form a “thick” interfacial layer at

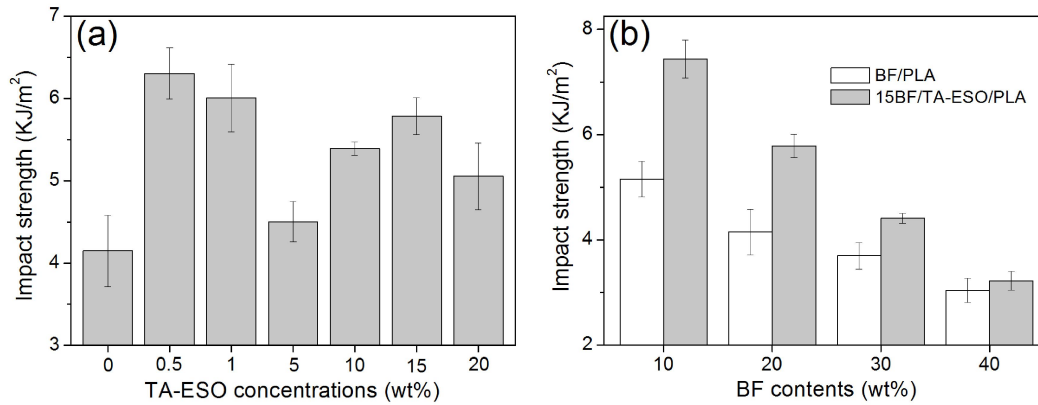


**Figure 6-9** Impact strength of BF/TA-ESO/PLA biocomposites. (a) Effect of TA-ESO concentrations; (b) Effect of BF contents.

the composites, where the layer is brittle and easy to be broken. Further increasing TA-ESO content from 5 to 15 wt% conversely resulted in an increased IS of the composites thanks to the toughening of TA-ESO on PLA matrix. However, excessive TA-ESO usage (20 wt%) for the PLA matrix also reduced the IS of the composites. Regarding the effect of BF content, the IS of both BF/PLA and BF/15TA-ESO/PLA composites significantly decreased with the increased BF content, while the composites with 15 wt% TA-ESO had much higher IS than their corresponding BF/PLA composites (Figure 6-9b).

### 6.3.6 Reinforcing and toughening mechanism

The tensile-fractured surfaces of the composites were revealed by SEM scans (Figure 6-10). Both 20BF and 40BF composites showed amounts of deep grooves generated from fiber pull-out (Figure 6-10ab), indicating a weak interfacial adhesion between BFs and PLA. Most of fibers were broken at the root and an indistinguishable fiber-matrix interface was seen on the surface of 20BF/0.5TA-ESO composite (Figure 6-10c), which confirms an improved interfacial bonding of the composite caused by the formed TA-ESO interface layer. A relatively superior interfacial bonding was also achieved for 20BF/5TA-ESO composite as the SEM image of the composite showed ambiguous fiber-matrix interface (Figure 6-10d). As shown in Figure 6-10abc, the matrix of 20BF, 40BF and 20BF/0.5TA-ESO composites were broken with a number of exfoliated blocks, indicative of a brittle

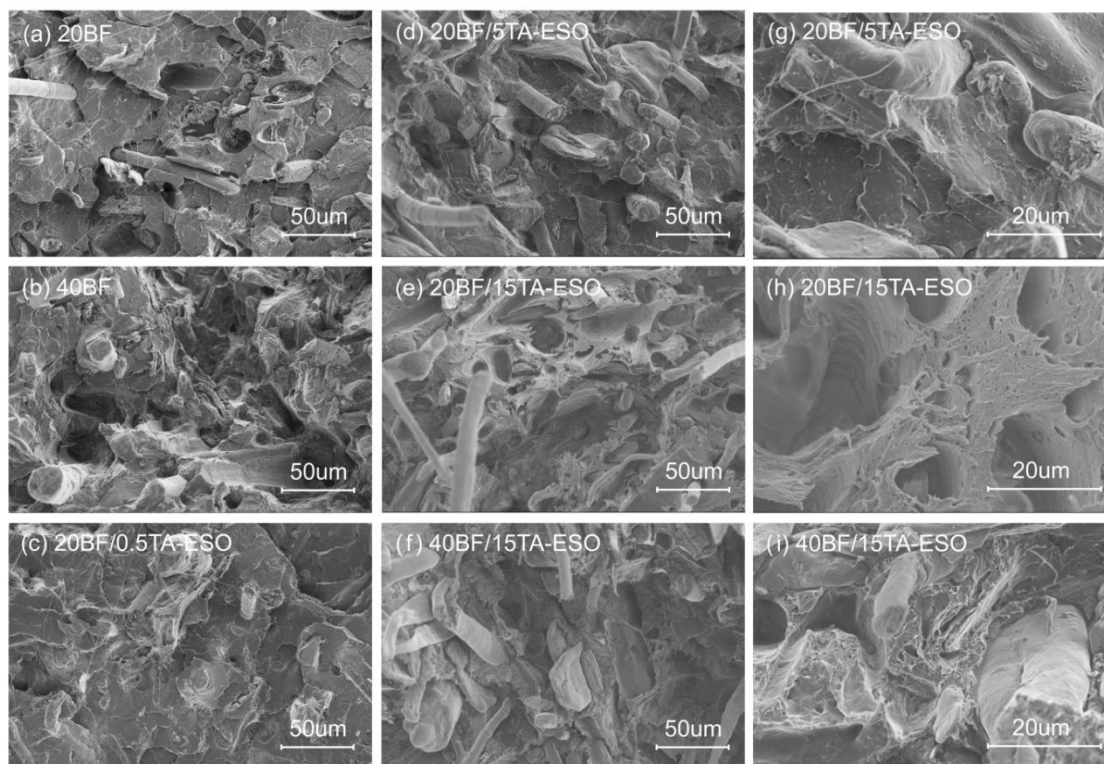


**Figure 6-10** SEM images of tensile-fractured surfaces of (a) 20BF, (b) 40BF, (c) 20BF/0.5TA-ESO, (d, g) 20BF/5TA-ESO, (e, h) 20BF/15TA-ESO, and (f, i) 40BF/15TA-ESO composites

fracture mode. As shown in [Figure 6-4dg](#), there was part of TA-ESO phase dispersed within PLA matrix when the TA-ESO content was increased to 5 wt%, but no obvious tough characteristic was seen in the matrix of 20BF/5TA-ESO composite ([Figure 6-10d](#)). This might be because the toughening effect of TA-ESO was overlapped by the reinforcing capacity of BFs. However, concerning 20BF/15TA-ESO composite, the fibers were pulled out and the matrix was torn apart ([Figure 6-10e](#)); a large amount of elongated cells with significantly plastic deformation was observed on the matrix surface ([Figure 6-10h](#)). With a high content of TA-ESO, a relatively “thick” interfacial layer is formed between BFs and PLA matrix; when the composite is loaded under tension, the TA-ESO flexible layer is firstly broken, and hence the fibers are debonded and pulled out from PLA matrix before breakage; meanwhile, the TA-ESO/PLA matrix also occurs a plastic deformation because of the toughening effect of TA-ESO phase. For 40BF/15TA-ESO composite, a rough surface was observed with a plastic fracture feature; however, the plastic deformation of the

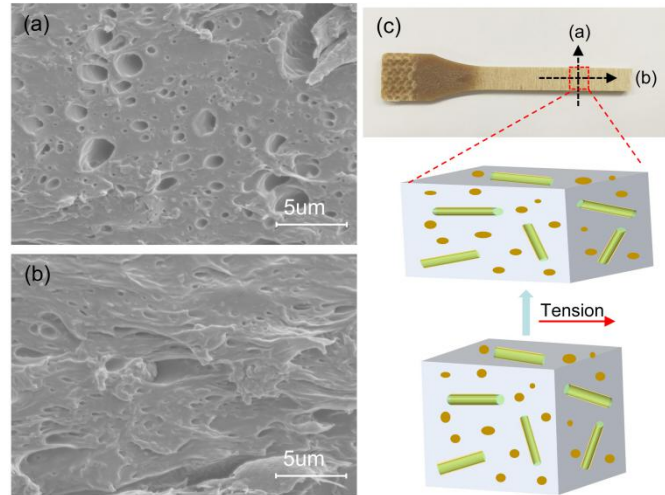


**Figure 6-11** SEM images of stretched samples of 20BF/15TA-ESO composite from different perspectives and proposed toughening mechanism during tension

matrix was restricted by the high content of BFs (Figure 6-10fi).

For further studying the toughening mechanism of TA-ESO phase on the biocomposites, the internal morphology for the stretched sample is given in Figure 6-11. The vertical direction of the sample presented randomly orientated TA-ESO cavities since the observed cavities is perpendicular to the stretching direction Figure 6-11a). From the stretching direction, a large number of highly orientated and elliptical cells with high aspect ratio were observed (Figure 6-11b). As proposed in Figure 6-11c, with a tension loading, the randomly distributed TA-ESO particles in original composites start to deform and array orderly along the stretching direction; meanwhile, the matrix around TA-ESO phase would orientate and then debond from TA-ESO phase when the stress is higher than their interfacial adhesion. This facilitates the generation of cavities and large matrix plastic deformation due to the shear yielding. The plastic deformation of matrix and TA-ESO phase contributes to effective energy dissipation to obtain high toughness. However, for the composites with a high content of BFs, the maximum plastic deformation of TA-ESO/PLA matrix could not be reached because the incorporated BFs cause stress concentration that leads to the fracture of the composites.

## 6.4 Conclusion

Fully biobased biocomposites with tailorable performance were successfully produced from renewable materials including BFs, TA-ESO and PLA via reactive blending technique. The properties of the composites were regulated by changing the TA-ESO concentration on the BFs surface, where the TA-ESO phase was designed to function as two roles in BF/PLA biocomposites, i.e., coupling agent and toughening agent. At a low content of TA-ESO, the TA-ESO was localized at the fiber-matrix interface via the formation of a flexible interfacial layer between BFs and PLA. This resulted in significant increases in tensile strength, tensile modulus, elongation at break, tensile toughness, impact strength, and storage modulus of the composites. When a high content of TA-ESO was used, the TA-ESO oligomer acted as a toughening phase inside PLA. The formation of phase-separated structure in TA-ESO/PLA matrix contributed to significantly increased elongation at break, tensile toughness, and impact strength of the composites. The TA-ESO rubbery phase induced cavity growth and matrix plastic deformation are proposed as the main toughening mechanism of TA-ESO on PLA matrix and composites.

## References

- [1] Gu, J.; Xiao, P.; Chen, P.; Zhang, L.; Wang, H.; Dai, L.; Song, L.; Huang, Y.; Zhang, J.; Chen, T. Functionalization of biodegradable PLA nonwoven fabric as superoleophilic and superhydrophobic material for efficient oil absorption and oil/water separation. *ACS Appl. Mater. Inter.* 2017, 9, 5968-5973.
- [2] Siakeng, R.; Jawaid, M.; Ariffin, H.; Sapuan, S.; Asim, M.; Saba, N. Natural fiber reinforced polylactic acid composites: A review. *Polym. Compos.* 2018/01/26, <https://doi.org/10.1002/pc.24747>.
- [3] Baghaei, B.; Skrifvars, M. Characterisation of polylactic acid biocomposites made from preregs composed of woven polylactic acid/hemp–lyocell hybrid yarn fabrics. *Compos. Part A Appl. Sci. Manuf.* 2016, 81, 139-144.
- [4] Arao, Y.; Fujiura, T.; Itani, S.; Tanaka, T. Strength improvement in injection-molded jute-fiber-reinforced polylactide green-composites. *Compos. Part B Eng.* 2015, 68, 200-206.

- [5] Pozo Morales, A.; Güemes, A.; Fernandez-Lopez, A.; Carcelen Valero, V.; De La Rosa Llano, S. Bamboo–polylactic acid (PLA) composite material for structural applications. *Materials* 2017, 10, 1286.
- [6] Couture, A.; Lebrun, G.; Laperrière, L. Mechanical properties of polylactic acid (PLA) composites reinforced with unidirectional flax and flax-paper layers. *Compos. Struct.* 2016, 154, 286-295.
- [7] Hao, M.; Wu, H.; Qiu, F.; Wang, X. In-situ reactive interfacial compatibilization and properties of polylactide/sisal fiber biocomposites via melt-blending with epoxy-functionalized oligomer. *Materials* 2018, 11, 398.
- [8] Pickering, K.L.; Efendy, M.A.; Le, T.M. A review of recent developments in natural fibre composites and their mechanical performance. *Compos. Part A Appl. Sci. Manuf.* 2016, 83, 98-112.
- [9] Liu, X.; Lv, S.; Jiang, Y.; Shi, J.; Tan, H.; Gu, J.; Zhang, Y. Effects of alkali treatment on the properties of wf/PLA composites. *J. Adhes. Sci. Technol.* 2017, 31, 1151-1161.
- [10] Chung, T.-J.; Park, J.-W.; Lee, H.-J.; Kwon, H.-J.; Kim, H.-J.; Lee, Y.-K.; Tai Yin Tze, W. The improvement of mechanical properties, thermal stability, and water absorption resistance of an eco-friendly PLA/kenaf biocomposite using acetylation. *Appl. Sci.* 2018, 8, 376.
- [11] Qian, S.; Sheng, K. PLA toughened by bamboo cellulose nanowhiskers: Role of silane compatibilization on the PLA bionanocomposite properties. *Compos. Sci. Technol.* 2017, 148, 59-69.
- [12] Lv, S.; Gu, J.; Tan, H.; Zhang, Y. Modification of wood flour/PLA composites by reactive extrusion with maleic anhydride. *J. Appl. Polym. Sci.* 2016, 133, 43295.
- [13] Zhang, L.; Lv, S.; Sun, C.; Wan, L.; Tan, H.; Zhang, Y. Effect of mah-g-PLA on the properties of wood fiber/polylactic acid composites. *Polymers* 2017, 9, 591.
- [14] Ghasemi, S.; Behrooz, R.; Ghasemi, I.; Yassar, R.S.; Long, F. Development of nanocellulose-reinforced PLA nanocomposite by using maleated PLA (PLA-g-MA). *J. Thermoplast. Compos.* 2018, 31, 1090-1101.
- [15] Hao, M.; Wu, H.; Zhu, Z. In situ reactive interfacial compatibilization of polylactide/sisal fiber biocomposites via meltblending with an epoxy-functionalized terpolymer elastomer. *RSC Adv.* 2018, 7, 32399.
- [16] Yatigala, N.S.; Bajwa, D.S.; Bajwa, S.G. Compatibilization improves physico-mechanical properties of biodegradable biobased polymer composites. *Compos. Part A Appl. Sci. Manuf.* 2018, 107, 315-325.
- [17] Quiles-Carrillo, L.; Montanes, N.; Sammon, C.; Balart, R.; Torres-Giner, S. Compatibilization of highly sustainable polylactide/almond shell flour composites by reactive extrusion with maleinized linseed oil. *Ind. Crop. Prod.* 2018, 111, 878-888.

- [18] Dai, X.; Xiong, Z.; Ma, S.; Li, C.; Wang, J.; Na, H.; Zhu, J. Fabricating highly reactive bio-based compatibilizers of epoxidized citric acid to improve the flexural properties of polylactide/microcrystalline cellulose blends. *Ind. Eng. Chem. Res.* 2015, 54, 3806-3812.
- [19] Zhang, C.; Garrison, T.F.; Madbouly, S.A.; Kessler, M.R. Recent advances in vegetable oil-based polymers and their composites. *Prog. Polym. Sci.* 2017, 71, 91-143.
- [20] Gandini, A. Polymers from renewable resources: A challenge for the future of macromolecular materials. *Macromolecules* 2008, 41, 9491-9504.
- [21] Kumar, S.; Samal, S.K.; Mohanty, S.; Nayak, S.K. Epoxidized soybean oil based epoxy blend cured with anhydride based crosslinker: Thermal and mechanical characterization. *Ind. Eng. Chem. Res.* 2017, 56, 687-698.
- [22] Altuna, F.I.; Pettarin, V.; Williams, R.J. Self-healable polymer networks based on the cross-linking of epoxidised soybean oil by an aqueous citric acid solution. *Green Chem.* 2013, 15, 3360-3366.
- [23] Li, A.; Li, K. Pressure-sensitive adhesives based on epoxidized soybean oil and dicarboxylic acids. *ACS Sus. Chem. Eng.* 2014, 2, 2090-2096.
- [24] Qi, M.; Xu, Y.; Rao, W.; Luo, X.; Chen, L.; Wang, Y. Epoxidized soybean oil cured with tannic acid for fully bio-based epoxy resin. *RSC Adv.* 2018, 8, 26948-26958.
- [25] Tee, Y.B.; Talib, R.A.; Abdan, K.; Chin, N.L.; Basha, R.K.; Yunus, K.F.M. Comparative study of chemical, mechanical, thermal, and barrier properties of poly(lactic acid) plasticized with epoxidized soybean oil and epoxidized palm oil. *BioResources* 2015, 11, 1518-1540.
- [26] Vijayarajan, S.; Selke, S.E.; Matuana, L.M. Continuous blending approach in the manufacture of epoxidized soybean oil-plasticized poly(lactic acid) sheets and films. *Macromol. Mater. Eng.* 2014, 299, 622-630.
- [27] Zhao, T.-H.; Wu, Y.; Li, Y.-D.; Wang, M.; Zeng, J.-B. High performance and thermal processable dicarboxylic acid cured epoxidized plant oil resins through dynamic vulcanization with poly(lactic acid). *ACS Sustain. Chem. Eng.* 2017, 5, 1938-1947.
- [28] Tsujimoto, T.; Uyama, H. Full biobased polymeric material from plant oil and poly(lactic acid) with a shape memory property. *ACS Sustain. Chem. Eng.* 2014, 2, 2057-2062.
- [29] Jian, X.-Y.; He, Y.; Li, Y.-D.; Wang, M.; Zeng, J.-B. Curing of epoxidized soybean oil with crystalline oligomeric poly(butylene succinate) towards high performance and sustainable epoxy resins. *Chem. Eng. J.* 2017, 326, 875-885.
- [30] Jian, X.-Y.; An, X.-P.; Li, Y.-D.; Chen, J.-H.; Wang, M.; Zeng, J.-B. All plant oil derived epoxy thermosets with excellent comprehensive properties. *Macromolecules* 2017, 50, 5729-5738.
- [31] Wang, L.; Lee, R.E.; Wang, G.; Chu, R.K.; Zhao, J.; Park, C.B. Use of stereocomplex crystallites for fully-biobased microcellular low-density poly(lactic acid) foams for green packaging. *Chem. Eng. J.* 2017, 327, 1151-1162.

- [32] Hao, M.; Wu, H.; Qiu, F.; Wang, X. Interface bond improvement of sisal fibre reinforced polylactide composites with added epoxy oligomer. *Materials* 2018, 11, 398.
- [33] Lee, H.; Dellatore, S.M.; Miller, W.M.; Messersmith, P.B. Mussel-inspired surface chemistry for multifunctional coatings. *Science* 2007, 318, 426-430.
- [34] Hu, Z.; Berry, R.M.; Pelton, R.; Cranston, E.D. One-pot water-based hydrophobic surface modification of cellulose nanocrystals using plant polyphenols. *ACS Sustain. Chem. Eng.* 2017, 5, 5018-5026.
- [35] Wang, J.; Jin, X.; Zhang, X.; Xia, L.; Li, C.; Wu, H.; Guo, S. Achieving high-performance poly(styrene-*b*-ethylene-ranbutylene-*b*-styrene) nanocomposites with tannic acid functionalized graphene oxide. *Compos. Sci. Technol.* 2018, 158, 137-146.
- [36] Liu, W.; Chen, T.; Wen, X.; Qiu, R.; Zhang, X. Enhanced mechanical properties and water resistance of bamboo fiber–unsaturated polyester composites coupled by isocyanatoethyl methacrylate. *Wood Sci. Technol.* 2014, 48, 1241-1255.
- [37] Liu, W.; Xie, T.; Qiu, R. Bamboo fibers grafted with a soybean-oil-based monomer for its unsaturated polyester composites. *Cellulose* 2016, 23, 2501-2523.
- [38] Ferri, J.; Samper, M.; García-Sanoguera, D.; Reig, M.; Fenollar, O.; Balart, R. PLAsticizing effect of biobased epoxidized fatty acid esters on mechanical and thermal properties of poly(lactic acid). *J. Mater. Sci.* 2016, 51, 5356-5366.
- [39] Meng, X.; Bocharova, V.; Tekinalp, H.; Cheng, S.; Kisliuk, A.; Sokolov, A.P.; Kunc, V.; Peter, W.H.; Ozcan, S. Toughening of nanocellulose/PLA composites via bio-epoxy interaction: Mechanistic study. *Mater. Design* 2018, 139, 188-197.
- [40] Qian, S.; Zhang, H.; Yao, W.; Sheng, K. Effects of bamboo cellulose nanowhisker content on the morphology, crystallization, mechanical, and thermal properties of PLA matrix biocomposites. *Compos. Part B Eng.* 2018, 133, 203-209.

## Chapter 7 Summary

Fully biobased, thermally remoldable, and highly tough blends were successfully formulated from ESO and PLA via dynamic vulcanization. Two vulcanizing agents, i.e., cationic initiator and tannic acid (TA), were utilized to induce the crosslinking of ESO and its reaction with PLA matrix for performing dynamic vulcanization. The achieved TA-ESO/PLA blends with high toughness were further used as matrices for the development of nanocomposites and biocomposites. The main conclusions are as follows.

(1) Thermally processable and highly tough PESO/PLA blends were prepared by melt-blending of PLA with ESO using  $\text{BF}_3\text{NH}_2\text{Et}$  as a cationic initiator for the self-polymerization ESO. The weight ratios of ESO to PLA ranging from 1:9 to 4:6 were designed to tailor the properties of the formed PESO/PLA blends. Results indicated the incorporated ESO could form a PESO phase dispersed on the PLA matrix and a superior interfacial compatibility with PLA matrix, which contributed to an improved toughening efficiency of PESO phase on the PLA blends. The PESO/PLA blends exhibited significantly increased elongation at break, tensile toughness, crystallinity, and complex viscosity when compared to pure PLA due to the formation of a two-phase separated structure in the blends; however, significant decreases in tensile strength, tensile modulus, storage modulus, and glass transition temperature of the blends were observed after the addition of ESO.

(2) Highly tough and biobased ESO/PLA blends were formulated through in-situ formation of TA-crosslinked ESO (TA-ESO) oligomer as a dispersed phase with PLA matrix by dynamic vulcanization technique. The crosslinking degree of ESO molecules and the interfacial compatibility between the ESO phase and PLA matrix were thus improved. The properties of the TA-ESO phase and its interfacial adhesion with PLA matrix were tailored by changing the molar ratio of TA to ESO, which significantly influenced the crystallization behavior, mechanical properties, thermal stabilities, and morphologies of the TA-ESO/PLA blends. After the incorporation of 10 wt% TA-ESO (based on the final blend) with a  $-\text{OH}$  groups to

epoxy rings molar ratio of 0.8 into PLA system, the elongation at break (242%) and tensile toughness ( $57.4 \text{ MJ/m}^3$ ) of the resulting PLA blend were 7 and 4 times higher than those of the blend with 10 wt% ESO, respectively. Compared to the 10 wt% ESO/PLA blend, the glass transition temperatures and thermal stabilities of the TA-ESO/PLA blends were slightly enhanced due to the increased crosslinking density of the TA-ESO phase; however, a slightly decreased crystallinity was observed for PLA after the addition of TA into ESO phase.

(3) To repair the sacrificial strength of the TA-ESO/PLA blends and impart the composites with electrical conductivity, different concentrations of CNTs, i.e., 0.5 to 10 wt%, were incorporated into the TA-ESO/PLA blends to prepare CNT/TA-ESO/PLA nanocomposites. The added CNTs selectively localized within the PLA matrix, leading to a reduced size of TA-ESO phase. The synergistic effects of CNTs and TA-ESO phase on the properties of the nanocomposites were fully investigated along with the understanding of CNT reinforcing and TA-ESO toughening mechanism. The formation of TA-ESO phase significantly increased the fracture elongation and tensile toughness of the blends, while the incorporation of CNTs resulted in increased tensile strength, tensile modulus, and storage modulus of the nanocomposites; the combination of this two effects contributed to the obtained ternary composites with balanced mechanical properties and favorable electrical conductivity.

(4) Fully biobased biocomposites with tailorable performance were successfully produced from renewable materials including BFs, TA-ESO and PLA via reactive blending technique. The properties of the composites were regulated by changing the TA-ESO concentration on the BFs surface, where the TA-ESO phase was designed to function as two roles in BF/PLA biocomposites, i.e., coupling agent and toughening agent. At a low content of TA-ESO, the TA-ESO was localized at the fiber-matrix interface via the formation of a flexible interfacial layer between BFs and PLA. This resulted in significant increases in tensile strength, tensile modulus, elongation at break, tensile toughness, impact strength, and storage modulus of the composites. When a high content of TA-ESO was used, the TA-ESO oligomer acted as a

toughening phase inside PLA. The formation of phase-separated structure in TA-ESO/PLA matrix contributed to significantly increased elongation at break, tensile toughness, and impact strength of the composites. The TA-ESO rubbery phase induced cavity growth and matrix plastic deformation are proposed as the main toughening mechanism of TA-ESO on PLA matrix and composites.

## Publications

### I. 審查付投稿論文

- \*[1] **Wendi Liu**, Jianhui Qiu, Ming-en Fei, Renhui Qiu, Eiichi Sakai, Min Zhang. Balancing performance of epoxidized soybean oil (ESO)/poly(lactic acid) composites: Synergistic effects of carbon nanotubes and tannic acid-induced crosslinking of ESO. *Express Polymer Letter*, 2019, 13(2), 109-122. (IF=3.064)
- \*[2] **Wendi Liu**, Jianhui Qiu, Longxiang Zhu, Ming-en Fei, Renhui Qiu, Eiichi Sakai, Kazushi Ito, Guolin Song, Guoyi Tang. Tannic acid-induced crosslinking of epoxidized soybean oil for toughening poly(lactic acid) via dynamic vulcanization. *Polymer*, 2018, 148, 109-118. (IF=3.483)
- \*[3] **Wendi Liu**, Jianhui Qiu, Ming-en Fei, Renhui Qiu, Eiichi Sakai. Manufacturing of thermally remoldable blends from epoxidized soybean oil and poly(lactic acid) via dynamic cross-linking in a twin-screw extruder. *Industrial & Engineering Chemistry Research*, 2018, 57(22), 7516-7524. (IF=3.141)
- [4] **Wendi Liu**, Ming-en Fei, Yang Ban, Anming Jia, Renhui Qiu, Jianhui Qiu. Concurrent improvements in crosslinking degree and interfacial adhesion of hemp fibers reinforced acrylated epoxidized soybean oil composites. *Composites Science and Technology*, 2018, 160, 60-68. (IF=5.160)
- [5] **Wendi Liu**, Ming-en Fei, Yang Ban, Anming Jia, Renhui Qiu. Preparation and evaluation of green composites from microcrystalline cellulose and a soybean-oil derivative. *Polymers*, 2017, 9(10), 541. (IF=2.935)
- [6] Ming-en Fei, **Wendi Liu**, Anming Jia, Yang Ban, Renhui Qiu. Bamboo fibers composites based on styrene-free soybean-oil thermosets using methacrylates as reactive diluents. *Composites Part A: Applied Science and Manufacturing*, 2018, 114, 40-48. (IF=4.514)
- [7] Ming-en Fei, Tianshun Xie, **Wendi Liu**, Renhui Qiu. Toughening of bamboo fibers/unsaturated polyester composites with 2-acetoacetoxyethyl methacrylate. *Polymer Composites*, 2018.05.06, published online. (IF=1.943)

- [8] Ming-en Fei, Tianshun Xie, **Wendi Liu**, Han Chen, Renhui Qiu. Surface grafting of bamboo fibers with 1, 2-epoxy-4-vinylcyclohexane for reinforcing unsaturated polyester. *Cellulose*, 2017, 24(12), 5505-5514. (IF=3.809)
- [9] **Wendi Liu**, Tingting Chen, Ming-en Fei, Renhui Qiu, Demei Yu, Jianhui Qiu. Tailoring properties of biocomposites from natural fibers and biobased thermosets: Effects of fiber type and resin composition. Submitted to *Composites Part B: Engineering*, 2018, Under review. (IF=4.920)
- [10] Hongjian Huang, Jianhui Qiu, Manxi Sun, **Wendi Liu**, Xiaowei Wei, Eiichi Sakai, Kazushi Ito. A new hard coating with MAO/AAO double layers prepared on aluminum in etidronic acid by DC oxidation. *Surface and Coatings Technology*, 2019, 360, 307-317. (IF=2.906)

注：博士論文研究関連：3編（（1）～（3））、その他：7編（（4）～（10））

\* 提出要件となる原著論文(3編)：(1)～(3)

## II. 国際会議論文・発表

- [1] **Wendi Liu**, Jianhui Qiu, Renhui Qiu, Eiichi Sakai, Kazushi Ito. Development and evaluation of highly tough epoxidized soybean oil/poly(lactic acid) blends via reactive extrusion. The 13<sup>th</sup> China-Japan Joint Conference on Composite Materials (CJJCC-13), Lanzhou, October 20<sup>th</sup> to 25<sup>th</sup>, 2018.
- [2] **Wendi Liu**, Jianhui Qiu, Renhui Qiu, Eiichi Sakai, Kazushi Ito. Improvement in interfacial adhesion of bamboo fibers reinforced poly(lactic acid) composites via reactive extrusion. The 13<sup>th</sup> China-Japan Joint Conference on Composite Materials (CJJCC-13), Lanzhou, October 20<sup>th</sup> to 25<sup>th</sup>, 2018.
- [3] **Wendi Liu**, Ming-en Fei, Renhui, Qiu. Green composites from hemp fibers and acrylated epoxidized soybean oil-based resins. The 21<sup>st</sup> International Conference on Composite Materials, Xi'an, China, August 21<sup>st</sup> to 25<sup>th</sup>, 2017.

注：博士論文研究関連：2編（（1）～（2））、その他：1編（（3））

## III. 国内学会

- [1] 劉 文地、邱 建輝、邱 仁輝、境 英一、伊藤 一志. In-situ polymerization of epoxidized soybean oil (ESO) for manufacturing highly tough ESO/poly(lactic acid) blends in a twin-screw extruder. 平成 30 年度化学系学協会東北大会，秋田，2018 年 9 月 15~16 日.
- [2] 劉 文地、邱 建輝、邱 仁輝、朱 龍祥、境 英一、伊藤 一志. 改質した大豆油仁よるポリ乳酸強靱化および性能評価. 日本複合材料学会第 42 回複合材料シンポジウム，仙台，2017 年 9 月 14~15 日.

注：博士論文研究関連：2 件 （ (1) ～ (2) ）

## **Acknowledgements**

I would like to express my sincere gratitude to to my major supervisor Prof. Jianhui Qiu for his guidance and support through the course of my PhD study. I deeply appreciate his consistent and illuminating instruction. He has been and always be my inspiration scientist and human decency.

I would like to appreciate Prof. Qingqing Ni from Department of Mechanical Engineering & Robotics, Shinshu University, and Prof. Teruo Bitoh and Prof. Nobuhiro Kanazawa from Department of Mechanical Engineering, Faculty of Systems Science and Technology, Akita Prefectural University, for being my committee members and their time in reviewing my thesis.

I deeply appreciate Prof. Renhui Qiu from Fujian Agriculture and Forestry University (FAFU) for his kind support and comments on my thesis documents. I would also like to expend my thank to Mr. Ming-en Fei from FAFU for his experimental support.

My sincere appreciation goes to the members of Prof. Jianhui Qiu's Composites Laboratory, Dr. Eiichi Sakai, Dr. Kazushi Ito, Dr. Shuping Jin, Dr. Longxiang Zhu, Dr. Jiao Chen, Mr. Haodao Mo, Mr. Hongjian Huang, Ms Manxi Sun, and Mr. Pengpeng Wang for their advice and kindly help in completing my PhD program.

Most important appreciation goes to my wife Ms Tingting Chen and my beloved parents for their moral support and warm encouragements.

Wendi Liu

2018.11, Yurihonjo, Japan